

A MODULAR, TUNABLE TACTILE ANTENNA FOR
EXPLORING THE MECHANICS OF SENSING

by
Alican Demir

A thesis submitted to Johns Hopkins University in conformity with the requirements for
the degree of Master of Science in Engineering

Baltimore, Maryland
September, 2009

©Alican Demir 2009
All rights reserved

Abstract

Arthropods, which by some estimates comprise the vast majority of animal species, use their antennae for multimodal sensory acquisition in order to perform a wide variety of tasks. A particularly remarkable antenna-mediated behavior is rapid wall following by cockroaches. Many biologists and roboticists investigate the individual mechanisms facilitating this tactile function. Isolating and repeatedly testing the roles of each mechanosensory feature of the highly complex natural antennal structure is challenging, so an analogous artificial antenna can be a powerful experimental platform for testing hypotheses regarding wall following and the mechanics of sensing in general.

The work presented in this essay fills the need for such a robotic model of biological antennae. Specifically, this document describes the design of a small, highly tunable, tactile antenna prototype. The assembled flexible artificial antenna consist of 40mm long, modular, stand-alone segments with embedded computing, each capable of detecting external contacts and measuring angular position with respect to the next segment. The user can independently vary the stiffness of each joint or modify the antennal hairs that enable touch sensing. A metric of angular sensitivity has been employed to gauge the main performance of individual segments and the entire antenna.

The next step will be to use this new experimental platform to facilitate testing of a wide variety of other hypotheses regarding the mechanics of sensing.

Advisor: Noah J. Cowan, Ph.D

Acknowledgements

I give my deepest and most sincere gratitude to my supervisor, teacher, and advisor Professor Noah Cowan. Suffice it to say, there is no other person, who is more pivotal in my academic and professional career, in the western hemisphere. It is a true privilege to be his student.

I cannot thank enough to the wonderful professors and mentors who thought and guided me throughout the difficult but rewarding path of Hopkins Engineering for six years. Besides Professor Noah Cowan, I exclusively would like to acknowledge Professor Allison Okamura, Professor K.T. Ramesh, Professor Sharpe, Lester ¹, Professor Dan Stoianovici, Professor Rene Vidal and Professor Louis Whitcomb for without their lectures and teachings this project wouldn't be realized by me.

A special gratitude goes to the valuable past and current members of the LIMBS Lab for always being there to answer, comment, suggest and share on the spot to help me solve the random issues I encountered during the long course of the project. In particular I would like to thank Jusuk Lee for leading the research with such inspiration, enthusiasm and willingness to help even in the most busy times; Brett Kutcher, Owen Loh and Andrew Lamperski for laying all the early foundations of my work; Kelly Canfield and Nicholas Keller for their various contributions to the project; Eatai Roth for his precision in explaining concepts and John Swensen for his ever-constructive criticism and ideas.

I would like to thank to several individuals for their specific contributions: My friend, lab and roommate Terrence Jao for giving me the valuable discussions, comments and feedback

¹Professor Lester Su

about the project in general and help in implementing Garcia's high-level controller; my friend Ali Üneri for introducing me with all the tools, scripts, templates and methods that considerably boosted my productivity; Dr. Anton Deguet for showing me the trick to solve Cmake issues with libraries in object-file format; Joe Riley for his C++ network socket routines and finally Doug Karlsberg and Ned Samson for setting up the linear repeatable testing platform for my antenna. I would also like to thank Ned Samson for helping me to collect data as well.

I would like to acknowledge the ME and LCSR staff, especially Katy Sanderson and Jamie Meehan for doing an excellent job in handling and tracking the endless requests for this research projects' shipments, returns and purchases; and of course Mike Bernard for his first rate managing skills to keep us away from all the administrative and bureaucratic issues we do not know about.

I would also like to thank all the people that made and make the powerful LCSR environment with all its constituent labs. Without their combined facilities and utilities, the research processes would have been considerably slower.

A special thanks goes to Bob Blakely, who among many other things keeps the laser cutter working.

Finally I dedicate this work to my parents. It is their unwavering love and support that keeps me on track towards my dreams.

Contents

Abstract	ii
Acknowledgements	iv
Contents	ix
1 Introduction	1
1.1 Bioinspiration: Antennae and The American Cockroach	2
1.2 Earlier Related Work	4
2 Antennal Tactile Sensing	10
2.1 Biological Antennae	10
2.1.1 At a Glance	10
2.1.2 Cockroach Antennae and Tactile Sensing	12
2.2 Tactile Sensing Technology	18
2.3 Artificial Antennal Sensing and Perception	19
2.3.1 Classifying Antennae	19
2.3.2 What is an artificial “tactile” antenna?	23
2.3.3 Sensing curvature	26
2.3.4 Contact Sensing	27
3 Antenna Design	28
3.1 General Statement of Goal	28
3.2 Intended Market	28

3.3	Design Constraints and Requirements	29
3.4	Engineering Design Criteria	30
3.5	Evolution of Design	32
3.5.1	Brainstorming	32
3.5.2	Evolution	34
3.6	Final Design	38
3.6.1	Overview	38
3.7	Design Features	40
3.7.1	Embedded computing	40
3.7.2	I ² C communication backbone	41
3.7.3	Variable parameters	42
3.7.4	Non-Sagging structure	43
3.7.5	Circuit protection	43
3.7.6	Frictionless angle sensing	44
3.7.7	Symmetric structure	45
3.7.8	In system programming	47
3.7.9	Contact sensing	48
3.7.10	The indicator LED	51
4	Antenna Performance	54
4.1	Angle measurement performance	54
4.1.1	Setup & Procedure	55
4.1.2	Analysis & Discussion	56
4.2	Angular Error Propagation	61
4.2.1	Setup & Procedure	61
4.2.2	Trial 1	62
4.2.3	Trial 2	63
4.2.4	Trial 3	64
4.2.5	Trial 4	65
4.2.6	Trial 5	66

4.2.7	Analysis	66
4.3	Communication Performance	68
4.3.1	Procedure	68
4.3.2	Analysis	71
5	Conclusions and Future Work	73
	Bibliography	80
A	Notes	81
B	Segment Part Models	82
C	Segment - Engineering Drawings	90
D	Segment - Circuit Diagram	94
E	Segment - PCB Layouts	97
E.1	Vertical Section	97
E.2	Horizontal Section	97
F	Segment - Firmware	99
G	Segment - Bill of Materials	111
H	Segment - Component Datasheets	113
I	Antenna - Accessories	142
I.1	Power+I ² C Dongle	142
I.2	Programming Dongle	142
J	Antenna - Users Manual	145
J.1	Assembling antenna	145
J.2	Firmware update	162
K	Technology Readiness Levels	175

List of Figures

1.1	Antennae on insects (Paul Beckmann) (Image credit: [2])	3
1.2	Biomimetic lobster antenna (Barnes, et al.)(Image credit: [3])	4
1.3	Artificial antenna (Cowan et al.)(Image credit: [8])	5
1.4	Artificial antenna (Kutcher and Loh)(Image credit: [23])	6
1.5	Artificial antenna (Lamperski et al.)(Image credit: [24])	7
1.6	The pre-bent, continuously flexible artificial antenna (Lee et al.)(Image credit: [26])	8
2.1	Different antenna forms in different insects (Image credit: [7])	11
2.2	Proximal regions of the segmented and annulated antennae (Image credit: [7])	11
2.3	Surface view of antennae of <i>P. americana</i> (Image credit: [38])	13
2.4	Scanning Electron Microscope view of the of the <i>P. americana</i> flagellum (Image credit: [36])	14
2.5	Flagellar segment of American Cockroach antenna. Thick-walled contact chemoreceptors (sensilla Chaetica B) and thin-walled olfactory sensilla (sen- silla trichodea) cover the segment [42].	14
2.6	Surface view of antennae of <i>P. americana</i> (Image credit: [42])	16
2.7	Scanning Electron Microscope view of the <i>Marginal Sensillum</i> of <i>P. ameri-</i> <i>cana</i> (x10000 magnification)(Image credit: [42])	16
2.8	Macro view of the <i>P. americana</i> flagellum (Image credit: [21])	17
2.9	Different types of antennae in nature (Image credit: [46], Copyright©2007 L. Shyamal)	24
2.10	Features that do not violate the definition of being an antenna	25

3.1	The earliest proof of concept platform for the new antenna.	34
3.2	The next step in evolution. Modularity and embedded computing on an antenna superstructure was tested first time.	35
3.3	The third iteration in antenna design. This is the first antenna design with a custom PCB and touch sensor incorporation.	36
3.4	Figure depicts how this antenna version cannot detect contacts at the flexible section. Also it shows that a single flex sensor can bend in different locations.	37
3.5	The fourth iteration of the tactile antenna. This version incorporated haired touch sensors, flexibility via NiTi, Angle sensing via Hall-effect sensors and modularity.	38
3.6	The fourth iteration of the tactile antenna.	39
3.7	Angular motion range of a segment.	39
3.8	Using a bus architecture prevents the accumulation of wires as new sensors are added.	41
3.9	The top piece of the designed aluminum shell.	44
3.10	The Hall-effect sensor can measure the angular orientation of a rotating diametrically magnetized magnet (Image credit: [33]).	45
3.11	Symmetric nature of the segment design.	46
3.12	Coupling cable may pose a problem if it interferes with the touch sensing hairs.	46
3.13	Coupling cable can be bent such that it does not interfere with the contact sensors.	47
3.14	The three pins on the side of the segments.	48
3.15	In System Programming of the segments.	49
3.16	In System Programming of the segments.	49
3.17	Touch sensors on the electronic sub-assembly.	50
3.18	Passive and active hairs.	51
3.19	Hair and the contact sensors.	51
3.20	Segments with lit LED indicators.	52
4.1	Segment angular accuracy and precision.	55

4.2	Plot showing the segment angle variations from 2500 samples per reference angle.	56
4.3	Plots showing the bias and standard error of sampled segments. <i>Dashed</i> : The reference angle. <i>Dotted</i> : $3 \times$ angular standard error margins, encompassing almost all angle variations for the corresponding reference angle. <i>Solid (Black)</i> angle associated with the mean of the samples.	60
4.4	Antenna angular error propagation characteristics, Trial-1.	62
4.5	Antenna angular error propagation characteristics, Trial-2.	63
4.6	Antenna angular error propagation characteristics, Trial-3.	64
4.7	Antenna angular error propagation characteristics, Trial-4.	65
4.8	Antenna angular error propagation characteristics, Trial-5.	66
4.9	The first k -segments of an N -segment antenna	67
4.10	Error propagations depicted by covariance ellipse covering 3 magnitudes of \sqrt{MSE}	69
4.11	I ² C protocol for slave transmitter mode (Image credit: [39])	71
4.12	Sampling frequency versus segment numbers	72
E.1	PCB top layout of the vertical section of the segment	97
E.2	PCB bottom layout of the vertical section of the segment.	98
E.3	PCB top layout of the horizontal section of the segment.	98
E.4	PCB bottom layout of the vertical section of the segment.	98
I.1	Power+I ² C Dongle.	142
I.2	PCB layout of the I ² C + Power Dongle.	143
I.3	Programming Dongle.	143
I.4	PCB top layout0.8 the Programming Dongle.	144
I.5	PCB bottom lay0.8 of the Programming Dongle.	144
J.1	Assembly Stages - Parts.	146
J.2	Assembly Stages - Placing hairs.	147
J.3	Assembly Stages - Placing the electronic sub-assembly.	148

J.4	Assembly Stages - Coupling Cables.	149
J.5	Assembly Stages - Coupling Cables.	150
J.6	Assembly Stages - Second segment.	151
J.7	Assembly Stages - Second segment.	152
J.8	Assembly Stages - Integrating segments.	153
J.9	Assembly Stages - Integrating segments.	154
J.10	Assembly Stages - Integrating segments.	155
J.11	Assembly Stages - Integrating segments.	156
J.12	Assembly Stages - Integrating segments.	157
J.13	Assembly Stages - Fixing the magnet.	158
J.14	Assembly Stages - NiTi backbone.	159
J.15	Assembly Stages - NiTi backbone.	160
J.16	Assembly Stages - Completion	161

List of Tables

2.1	Sense organs of <i>Periplaneta</i> antenna flagellum. <i>Reproduced based on the table from Schafer et al. 1973</i>	15
2.2	Classification of Tactual Modes. <i>Reproduced from Loomis et al. 1986</i>	22
3.1	Design brainstorming summary to meet design criteria.	33
3.2	reserved I ² C addresses. Taken directly from www.i2c-bus.org	42
3.3	LED indicator meanings.	52
4.1	Segment Accuracies and precisions around 90°, 135°, 180° 225° and 270°. All units are in degrees.	58
4.2	Variance of segment standard errors s^2 per reference angle.	59
4.3	Antenna angular error propagation characteristics, Trial-1.	62
4.4	Antenna angular error propagation characteristics, Trial-2.	64
4.5	Antenna angular error propagation characteristics, Trial-3.	65
4.6	Antenna angular error propagation characteristics, Trial-4.	66
4.7	Antenna angular error propagation characteristics, Trial-5.	67
4.8	Sampling frequency data.	70

Chapter 1

Introduction

Tactile sensing is simply a process leading to the perception of an object property or touch event through physical contact between the sensor and the object [10, 29]. Mechanical, thermal, chemical and some other physical attributes of objects can be sensed by various tactile receptors [10] via a general event called “touch”. In animals, the corresponding induced feedback or the “sense of touch”, which of course can occur from one or multiple points in different forms simultaneously, is then interpreted so that properties such as surface roughness, shape, hardness, viscoelasticity, texture, force distribution, inertia and temperature [10, 30, 35] can be perceived. This function can be realized by tactile perception organs like the skin [10, 22] in humans, antennae in many arthropods [5, 19, 36, 41, 47, 50] or whiskers [34] in some mammals.

Tactile antennae are the focus of this work motivated partly due their prevalent utilization in nature but mainly because of the intertwined mechanics involved during the sensing action. This comes from the fact that the statics of each individual hair-like sensor on the antenna are mechanically coupled with the dynamical system describing the antenna’s overall flexible segmented structure due to the robot’s or animal’s motion (and basal actuation if present). As any contact force on the antenna is directly propagated through those hair-like contact sensors to the main antenna superstructure, we hypothesize that this coupling, for example in cockroaches, is utilized to keep the antenna in a shape favorable for wall following. We

further hypothesize that if the antenna shape is not in a favorable configuration, than the coupled mechanics will constantly force the antenna to return to the ideal configuration while wall following. We suspect that the distally pointing hair disposition may be the main reason for such behavior. The coupling between the local contact sensors and the global antenna configuration also exists at the perception level such that when both data are combined, the exact location of a contact can be easily discerned. We define this as one of the fundamental properties of the tactile antennae and will discuss this in detail.

We describe in this essay the design and testing steps of a novel tactile antenna which is conceptualized in the hopes of facilitating an experimental platform for addressing scientific hypotheses. In order to satisfy as many experimental requirements as possible, our design allows many of the common important antenna parameters to be changed easily. These properties include mass distribution, stiffness profile, length, hair stiffness and hair length which are established by bio-inspiration as well as by earlier related works in the literature. The design procedure of the antenna is presented in detail where in particular how an earlier design affected the next design is evaluated.

Lastly we briefly explore the mechanics of antennal sensing in general and lay the ground work for future investigations regarding the testing of some specific hypotheses for tactile antennae.

In addition we provide a definition for artificial tactile antennae and establish their fundamental characteristics after classifying the technology in a consistent framework that encompasses both the sensing and perception aspects of past, current and future antennal devices based on the haptic taxonomy.

1.1 Bioinspiration: Antennae and The American Cockroach

Antennae are arguably nature's multi-sensorial packaging form-factor of choice. With an evolution history over 400 million years [17] and capacity to encompass a very large number

of (on the order of tens-hundreds of thousands) diverse sensilla¹ categorized as mechanoreceptors, chemoreceptors, thermoreceptors and hygroreceptors² [7], the antennae are indispensable organs to all insects and other hexapods³. In fact with the exception of members of the subclass, Protura⁴, which have neither antennae nor eyes, all insects (or hexapods) possess a pair of antennae [44].

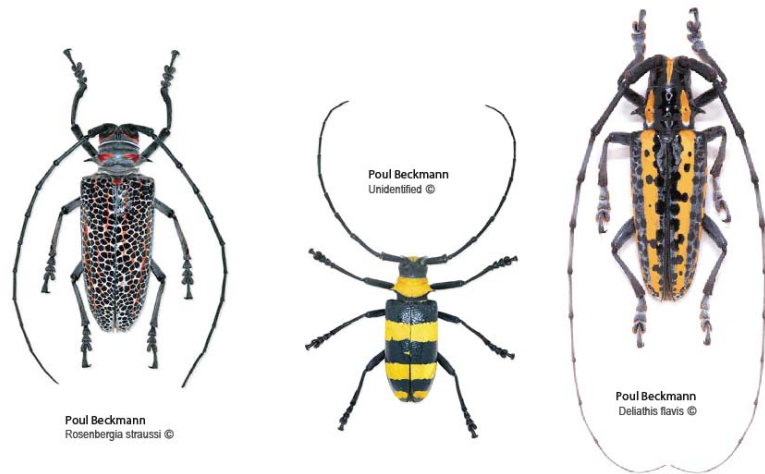


Figure 1.1: Antennae on insects (Paul Beckmann)(Image credit: [2]).

It is unclear whether or not those pair of flexible appendages protruding from the head play the most important role in the amazing success of the insects as a class, but the facts remain: some of the earliest insect species are still alive; the total insect biomass outweigh all other animals [51] and their sheer variety dominates all other life forms. After all, the upper limit for the Earth's entire biological species diversity is estimated from 3 million to 30 million to 50 million with more than 70 % belonging to the animal kingdom [32]. Of all the animal species, more than 95 % are invertebrates with vast majority being taken up by arthropods⁵ ranging from an estimated 2.5 million up to 5 million [15] to 30 million [14] species out of which practically all are insects. Also constituting about three quarter millions of the actually catalogued 1.5 million life forms [1], terrestrial insects are thus by far the most numerous classified living organisms yet. Indeed from a justifiable perspective (alien

¹A simple sensory receptor consisting of one cell or a few cells, especially a hair-like epithelial cell projecting through the cuticle of arthropods.

²Sensor that discriminates moisture levels

³Collembola (springtails) and Diplura

⁴Sometimes classified as a class on its own under the phylum of hexapods.

⁵Invertebrate having jointed limbs and a segmented body with an exoskeleton made of chitin

point of view) and quite insignificant error margin, all species are insects [32]. Consequently it follows that with a very crude approximation almost all species on the planet Earth have antennae.

The popularity of this primarily sensory organ [7] is not without reason. The American cockroaches (*Periplaneta americana*), for instance, make use of their antenna as tactile feelers [38] and thus able to use the surrounding objects such as walls as navigational guidance. Even if they are blinded, they execute this task so well that they can reach to speeds up to 80 cm/s (or about 25 body lengths/s) [25, 27], which would be analogous to a blind human running in a maze at around 100 mph just by using his arms to feel the walls [5, 25]. Such a performance is naturally a source inspiration for many robotic system developers, including the author of this essay.

1.2 Earlier Related Work

Despite the extensive utilization of antennae in nature, development and implementation of their mechatronic counterparts – although inspirational and encouraging – remains to be a slow progressing endeavor. In 2001, Barnes et al. [3] described a bio-inspired lobster robot antenna with three bending sensors embedded in a tapered structure (Figure 1.2). Each bending sensor would activate when a set threshold curvature is passed due to an

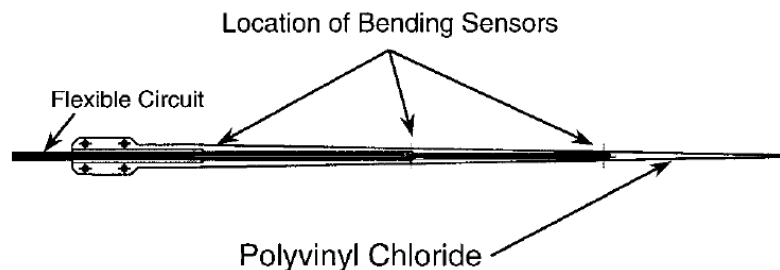


Figure 1.2: The artificial antenna of Barnes, et al. The tapered structure decreases stiffness towards the tip and each of the three bending sensors act as a switch depending upon whether or not a local curvature threshold is passed (Image credit: [3]).

external load so that the deflections caused by fluid flow and object contact at the tip of

the antenna can be distinguished from each other by the robot. The tapered structure considerably enhances the curvature distribution difference between the two cases which greatly increases performance of the discrimination task [3]. Soon after in 2003, Cowan et al. [8] presented an artificial antenna for facilitating the task of cockroach-like wall following for Sprawlette⁶, a hexapedal running robot (Figure 1.3).

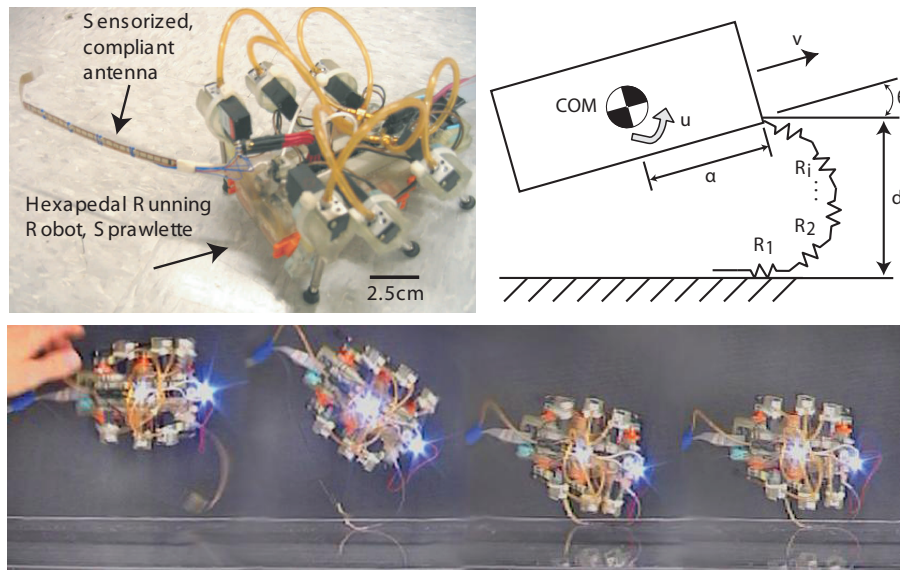


Figure 1.3: **top left** Artificial antenna of Cowan, et al. attached to Sprawlette. **top right** The varying resistances of the flex sensors allow the distance d and angle θ to be estimated. **bottom** Multiple exposures of the wall following Sprawlette on a treadmill (Image credit: [8]).

The antenna utilizes five slightly modified compliant flex sensors from Spectra Symbol⁷ that changes electrical resistance in proportion to strain, for the very large deflections that occur when the antenna touches the wall. Then based on the resistance changes of the individual sensors, the distance and angular orientation with respect to the wall can be inferred albeit with a fairly large error margin, assuming the global concavity of the antenna is preserved during operation [8]. This assumption is important since the flex sensor resistance would increase in both concave and convex curvatures suggesting multiple antenna configurations for a given sensor reading. This issue also provided important insight for the future antenna designs and will be addressed later.

⁶<http://www-cdr.stanford.edu/biomimetics/sprawlettes.html>

⁷<http://www.spectrasymbol.com/>

Beginning in 2004, further antenna prototypes were built, tested and employed in the “Locomotion In Mechanical & Biological Systems Laboratory” (LIMBS Lab)⁸ at Johns Hopkins University for some cockroach based wall following experiments [23, 24, 26, 27] which are worth mentioning as part of the author’s motivation.

Kutcher in 2004 as part of his MSE thesis describes a single rigid link antenna with five contact sensors located along the outside edge in order to implement a tactile mapping algorithm via a wall following mobile robot [23]. The antenna is attached to the robot’s chassis through a secondary fixed rigid link, which allows the antenna to detect the wall within an interval defined at some distance in front of the robot (Figure 1.4). This so-called

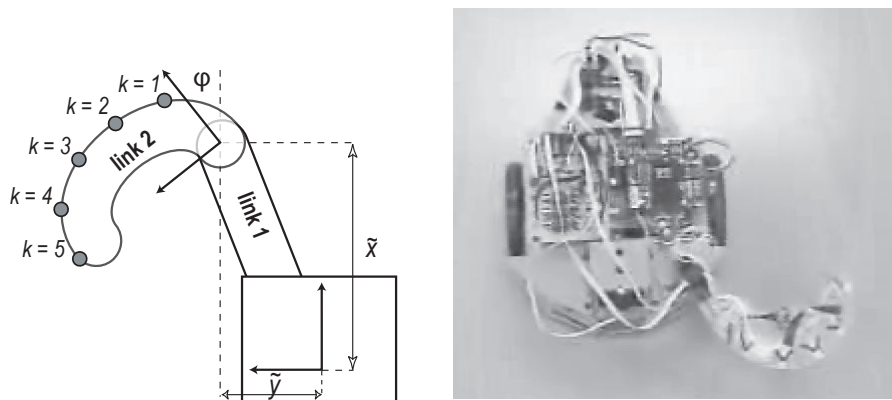


Figure 1.4: *left*. Antenna configuration designed and implemented by Brett Kutcher and Owen Loh: \tilde{x} , \tilde{y} , describe the position and orientation of the antenna coordinate system with respect to the robot coordinate system. Link 1 and link 2 are connected by a rotational joint located at the origin of the antenna coordinate system. This joint also contains a potentiometer and a torsional spring damper. $k = 1 \dots 5$ represent the five touch sensors. *right* Single link artificial antenna used for tactile mapping mounted on Garcia robot. (Image credit: [23]).

“preview” or “look-ahead” distance is analogous to the “visual range” in sighted systems and in principle allows the robot to know about the impending obstacle beforehand and steer away. In this particular design the free joint is coupled with a potentiometer, which permits the determination of the angle ϕ as a linear function of its measured resistance. In the case of multiple contacts, the one with the lowest enumeration k was fed into the controller [23]. The implementation is reported as successful with the acknowledgment of some critical antenna shortcomings. Indeed the issues presented for this early prototype

⁸<http://limbs.lcsr.jhu.edu/>

were very important in the design of the new antenna being discussed in this essay and will be referenced again later.

In 2005, Lamperski et al. [24] introduced an improvement to the design of the antenna with the purpose of implementing a new dynamic wall following controller to Garcia⁹, a differential drive wheeled robot. The fabricated tactile antenna is a two rigid link, three segment polycarbonate chain hinged on commercial potentiometers with a spring powered cam mechanism providing stiffness to each joint [24]. The device encapsulates one wide capacitive touch sensor per linkage such that any contact along a given segment will register a touch [24]. Thus the contact location can be inferred within a one segment length. Unlike the antenna used by Kutcher, this design allows other segments to be added to the chain which incorporated the first modularity feature for a bio-inspired tactile antenna (Image credit: [24]). During testing, the antenna caused several problems due to its rigidity and

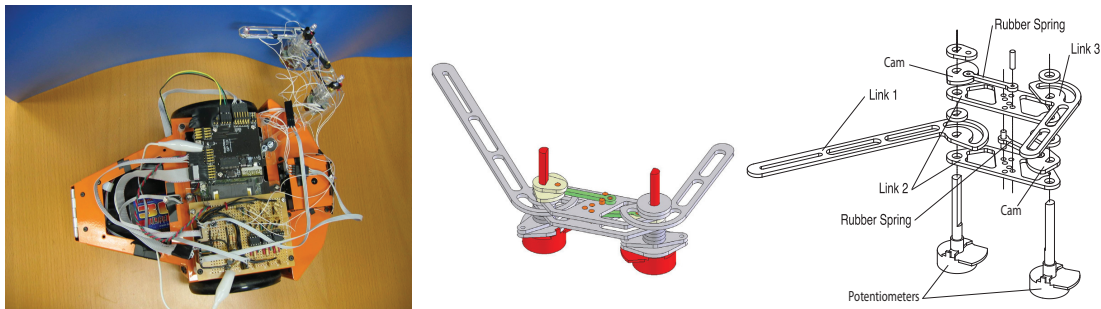


Figure 1.5: *left.* Two linked sensorized antenna mounted on Garcia. *middle* Assembled model. *right* The antenna is assembled by sliding the links onto the potentiometer shafts (some spacers and other minor parts are omitted from this figure for simplicity) [24]. The base of each potentiometer is fixed to the center link [24] (Image credit: [24]).

hence a more flexible solution was suggested [24]. Further investigations and results will be shown later in this essay regarding this suggestion. On the other hand Lamperski et al. also ran numerical simulations of a planar n-link kinematic chain structure representing the antenna coupled with the robot. In the simulation the parameters such as the number of links, spring and damping constants, link masses and equilibrium configuration are kept user settable for the purpose of forming hypotheses of which properties might be important in the design of a real antenna.

⁹ <http://www.acroname.com/robotics/parts/GO-GARCIA-CONFIG.html>

Sure enough, the work of Lamperski et al. greatly influenced our research. As the prospect of rapid hypothesis verification on a real antenna is one of our main goals, the adjustable parameters mentioned in the simulations actually formed the main design criteria of the new antenna.

Two years later Lee et al. [26] published as part of their results a successful implementation of a simple PD-control, an hypothesis partially shown to be the underlying control law for cockroach wall following behavior, on the Garcia robot. Lee et al. utilized a continuously flexible antenna which was designed and built by Owen Loh in 2005, similar in principle but more involved in the mechanical design aspect than the antenna presented by Barnes et al. in 2001 and Cowan et al. in 2003. Namely the antenna is comprised of an array of shortened flex sensors¹⁰, which provide local curvature information based on the resistance variations due to deflection, attached on a pliable substrate (Figure 1.6).

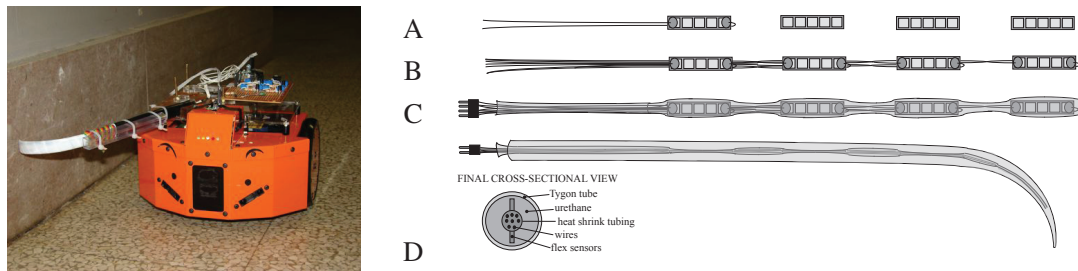


Figure 1.6: **left.** The pre-bent, continuously flexible Antenna designed by Loh and utilized by Lee et al. **right** The summary of the antenna’s assembly stages (Image credit: [26]).

Bio-inspired by the arthropod antenna physiology, this core disposition is embedded in a tapered, flexible superstructure composed of a Tygon¹¹ rubber tube shell, and a cast urethane mantle to accommodate decreasing stiffness [26], a property also featured by Barnes et al.. What was quite novel in this antenna was the first time deployment of a permanent pre-bent tip section. This pre-curvature guarantees the preservation of the global concavity of the antenna during wall following and thus exhibits one solution the issue mentioned in 2003 Cowan et al. paper due to the unidirectional nature of the flex sensors. A large section of the flagellum toward the base is stiffened by an external support structure and clamped

¹⁰Abrams Gentile 4” Flex Sensors

¹¹<http://www.tygon.com/>

at a fixed angle to the robot in order to facilitate a more consistent “preview distance”, also demonstrated by Kutcher [23].

Although research on creating artificial antennae is limited, from a mechanical engineering point of view, those previous works provide invaluable insight for determining all the considerations that should be factored into the design constraints. Yet just concentrating on fixing the issues that arose in earlier prototypes is not a healthy engineering design approach in accomplishing a research goal. It is therefore imperative to investigate the topic of “Antennal Tactile Sensing” in general before a final design criteria list can be formed.

Chapter 2

Antennal Tactile Sensing

2.1 Biological Antennae

2.1.1 At a Glance

As we mentioned earlier, antennae are mostly utilized by insects and therefore it is proper to explain the function and morphology of antennae based on insects. The origins of antennae on insects can be interpreted either as modified appendages which is homologous with mouth parts and thoracic legs or as sensory structures associated by the presegmental part of the body, analogous with tentacles on the heads of certain worms [17]. Antennae occur in many different forms but all are composed of three principal units from base to apex: scape, pedicel and flagellum (Figure 2.1).

The scape is inserted into a membranous socket of the head wall and pivoted on a single marginal point called the antennifier [7] acting like a ball joint and facilitates basal antenna rotations in all directions. The pedicel is typically a small joint containing the Johnston's organ, which is a specialized cell group designed to detect deformations [17], mechanical oscillations and stresses [44] in the cuticle¹. This constrained double joint (scape and pedicel) is moved by levator-depressor and flexor-extensor muscle pairs actuating the scape and pedicel respectively [7, 44](Figure 2.2).

¹carapace: hard outer covering or case of certain organisms such as arthropods and turtles

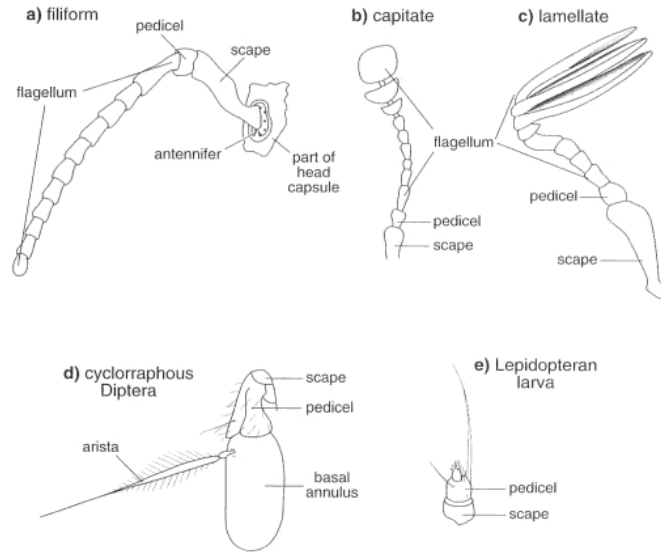


Figure 2.1: Different antenna forms in different insects (Image credit: [7]).

The flagellum is variable in length and shape and further divided into many similar subsegments called annulus or flagellomere [17]. These annuli forming the flagellum are connected to each other by soft membranes such that the entire superstructure is flexible [7]. In some hexapods² there is additional intrinsic musculature between each unit of flagellum providing actuation and hence regarded as segments, not annuli [7, 44] (Figure 2.2).

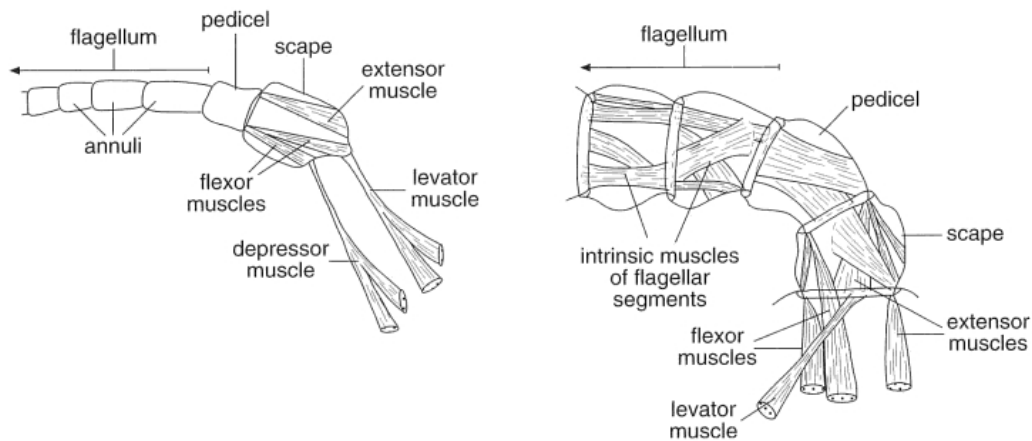


Figure 2.2: *left* Typical insect annulated antenna. Note that there are no muscles in the flagellum rendering it completely passive. *right* Segmented antenna of a non-insect hexapod. The flagellum can be actuated by means of intersegmental muscles.(Image credit: [7])

²Collembola (springtails) and Diplura (two-pronged bristletails)

Yet as the segmented antennae are not really anent to the focus of our research, they will not be further mentioned and the *segment* nomenclature will be used throughout this essay to refer to individual flagellum units. An important note for the annulated antennae is the fact that all the nerves traversing the flagellum are entirely sensory and not motor [17]. These nerves are connected to minute sensory structures (sensilla), which depending on their number, diversity and density dictate the overall shape and function of the antenna itself [7, 44]. Correspondingly, the mechanical properties of the flagellum in the global sense tends to favor the function, especially the mass and stiffness profiles. For instance applying a preset force to a locust flagellum will cause different amounts of bending for different directions [47]. This directionality is set in such a way that air drag cannot bend the flagellum easily backwards during flight. Non-uniform stiffness profiles are also utilized for example by the crayfish [3], *Cherax destructor* where their flagellum consist of 220-250 tapered segments [41]. This tapering differs among species but usually the function is to allow the distal tip of the antenna to deflect more easily than the proximal end. Besides, the cross-sectional shape of the flagellum is also a natural parameter that can introduce directionality to the stiffness of the antenna. If the cross-sectional area is an ellipse like that of the crayfish, then the deflections with the least mechanical resistance will occur around an axis that is parallel to the major semi-axis and visa versa.

One of the antennal roles that favors tapered very long antennae is the tactile feeler role [25] which is for example present in the cockroach. The extended length of the antenna not only allows a large number of mechanosensors [7] to be packed but also provides extreme compliance to the flagellum for this role. This also constitutes the most interesting antenna function from a robotics and mechanical engineering point of view as the complex mechanics of the flagellum directly affects the locomotion of the cockroach and thus will be further investigated in the next subsection.

2.1.2 Cockroach Antennae and Tactile Sensing

The cockroach, *Periplaneta americana* (The American Cockroach), is used widespread in behavioral and physiological studies. The natural outcome of this popularity is the well

documentation of this species in many aspects. Adding the fact that the overall structure and the growth characteristics of the *Periplaneta* antenna is similar to the other cockroach species [42], the antennal attributes of the *American Cockroach* is reviewed in this section as a representative.

Like other insects, the cockroach has the fundamental antenna structure composed of the scape and pedicel forming the double jointed base actuation mechanism and a distal, filiform³, passive, multi-segmented, haired flagellum.

The scape has two rotational degrees of freedom, allowing the flagellum to be swept over both vertical and horizontal [38] planes, whereas the pedicel has only one rotational degree of freedom providing extra flagellum flexibility in the vertical [37,38] direction (Figure 2.3).

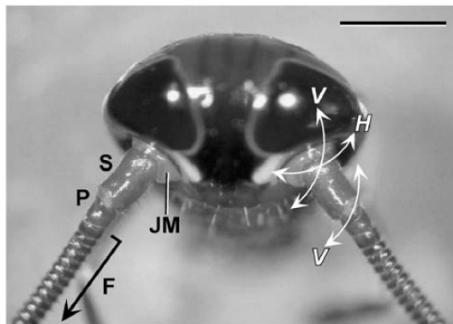


Figure 2.3: Surface view of antennae of *P. americana*. The scape actively moves both horizontally and vertically (see white arrows), while the pedicel move only vertically. Scale: 2 mm [37, 38](Image credit: [38]).

The approximately 50 mm long flagellum of an adult *P. americana* consist of 150-170 segments (Figure 2.4), innervated by various chemo-, hygro-, thermo-, and mechanoreceptors [45] (Table 2.1).

Here, out of these diverse sensors, the thick-walled mechanosensory hairs (S. Chaetica B), which are triggered by external contacts, are of our main interest not only due to their obvious contribution to the tactile perception but also due to their potential effects to the overall mechanical behavior of the flagellum during sensing. This particular type of hair-like

³Thread-like or hair-like. Composed of a series of cylindrical or flattened segments. Examples are cockroaches, crickets, grasshoppers, true bugs, bark lice [6]

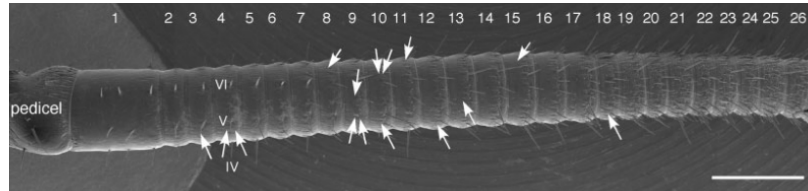
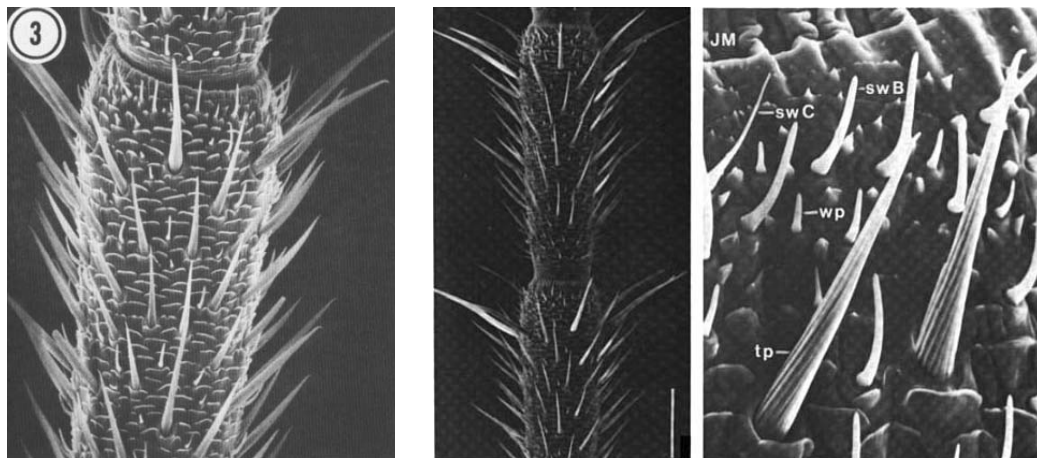


Figure 2.4: Scanning Electron Microscope view of the of a partial *P. americana* flagellum. The segmented structure of the flagellum, which for an adult *P. americana* is composed of 150-170 segments, is clearly visible. (Image credit: [36]).



(a) Flagellar segment of American Cockroach antenna, (x240 magnification) (Image credit: [42]).

(b) Low and high magnification scanning electron microscope view of an adult male middle flagellar segment of American Cockroach antenna (Image credit: [45]).

Figure 2.5: Flagellar segment of American Cockroach antenna. Thick-walled contact chemoreceptors (sensilla Chaetica B) and thin-walled olfactory sensilla (sensilla trichodea) cover the segment [42].

<i>Type of sense organ</i>	<i>Probable modality</i>	<i>Total no. units in adult antenna</i>	<i>Location and distribution on flagellum</i>
S. Chaetica B (Thick-walled chemoreceptors)	(a) Contact chemoreception (b) Tactile sense	(a) 2×10^4 (b) 6.5×10^3	Occur on all segments as orderly peripheral rings. Especially dense on flagellum.
S. Trichodea (Thin-walled chemoreceptors)	Olfaction	Male: 8.6×10^4 Female: 4.8×10^4	Occur primarily on antennal flagellum distal to meristal segments.
S. Basiconica (Thin-walled chemoreceptors)	Olfaction	1×10^2	Occur distal to first ring of S. Chaetica B on flagellar segments
Cold Receptor Sensillum	Thermoreception	1×10^2	Occur on ventral side of distal alternating segments in one-third of antenna, distal to first ring of S. Chaetica B
S. Campaniformia (Sensory domes)	Detection of stress in cuticle	2×10^2	Occur dorsally in flagellum with one sensillum/segment.
Marginal sensilla	Joint proprioception	2×10^2	Occur in threes on alternating segments of flagellum

Table 2.1: Sense organs of *Periplaneta* antenna flagellum. Reproduced based on the table from Schafer et al. 1973

contact sensor occurs on all segments (concentrated in the middle third of the flagellum [43]) and arranged around the entire circumference of the *Periplaneta* antenna (about 6500 per flagellum) [42] (Figure 2.5a, Figure 2.5b).

Mechanically, each sensillum itself is a long, tapering, highly grooved shaft between 35 μm to 250 μm in length mounted in a flexible circular socket with 10 μm to 25 μm in diameter. The shaft of the sensillum is always slanted distally and the tip of the shaft is curved outward [42](Figure 2.6). They are known to be the longest and most rigid hairs on the entire antenna [45].

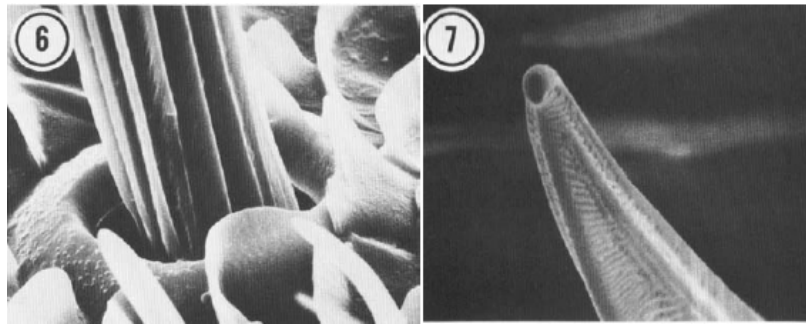


Figure 2.6: *left* Base of sensillum chaeticum B, (x2400 magnification). The insertion area of the base of the hair is wide, allowing basal shaft movements over a range of 35° to 250° . The fluted character of the contact sensor hair is also apparent. *right* The tapered structure of the distal tips of contact hairs (sensilla chaetica B), (x8000 magnification)(Image credit: [42]).

Another pertinent tactile sensorial element in the flagellum is the tiny (2 μm) pea shaped *marginal sensillum* (Figure 2.7).

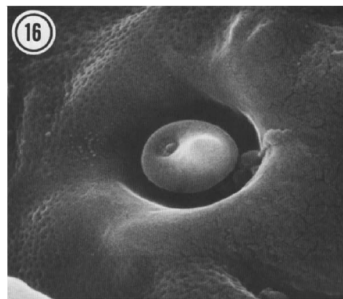


Figure 2.7: Scanning Electron Microscope view of the *Marginal Sensillum* of *P. americana*. It is believed to detect movements between consecutive antenna segments, (x10000 magnification)(Image credit: [42]).

Even though there is not a solid evidence regarding their exact function, these sensilla

are believed to detect movements of the antennal segments with respect to each other. The reasoning comes from the fact that marginal sensilla are located at the distal edges of every other flagellar segment [45], in other words very close to the flexible cuticle of joints between segments [42]. This suggestion is important since all the earlier and current artificial antennae adaptations so far require this related intersegmental curvature bending or angular orientation information to execute wall following.

In its entirety, the flagellum of the American cockroach has a tapered structure, shrinking in diameter towards the distal end, which can even be noticed under a magnifying glass (Figure 2.7). This suggest a decreasing stiffness like the crayfish and conforms to the early bioinspired artificial antennae mentioned earlier that use a tapered disposition to improve antenna behavior during wall following.



Figure 2.8: Macro view of the *P. americana* flagellum. The tapered structure is clearly visible (Image credit: [21]).

The biological antenna can be truly inspiring for the realization of their artificial counterparts as they are the living proofs for the effectiveness of the underlying design features for antennal tactile sensing. In this sense the research so far is convincing enough for us to conclude that cockroaches can sense both the configuration of their antenna and the position of a contact along their flagellum. Furthermore we know that the former is sensed through sensors in between the individual segments and the latter through hair-like distally pointed contact receptors. There are other mechanical and neural features [36, 50] of the antenna which contribute to tactile sensing but unfortunately, we can only employ a fraction of the intricate biological design concepts towards the development of the tactile antenna due to

several reasons which will be discussed in the next chapter. But first it is more appropriate to review the technology and methods devised or suggested for tactile sensing to assess the components and tools available for the artificial antenna development. Thus the following section, combined with concepts employed by nature and the experience gained from the early tactile antennae should provide all the constraints and criteria for a solid design.

2.2 Tactile Sensing Technology

The definition of tactile sensing does not change from biology to technology: measuring properties of an object through contact. In the robotics context, the sensed properties of the object are also needed to be interpreted to execute manipulative tasks, at which tactile sensing becomes tactile perception, just as it occurs in animals.

Artificial tactile sensing and perception in general were slow progressing and sometimes regarded as neglected [29] fields compared to optical sensing and computer vision, which have reached a level of maturity whereby now commercial hardware and software packages are widely available [28]. This may be the case since tactile sensing does not have localized sensory organ like the eye or ear that is solely based on a single sensing modality. On the other hand the tactile organs like *the skin* or — in our case — *the antenna*, are in essence substrates or platforms for various diffused single-modal receptors that are all triggered by touch but measure different object properties. Lee et al. in his review published ten years ago reports many other legitimate and conceivable reasons and further quantifies the tactile research activities based on their applications and types⁴ in a decade-by-decade basis.

Tactile sensing should be considered as a blanket term that has as many categories as the different properties that can be measured via physical contact. This includes all the different modes of touch, like single-continuous contacts to measure temperatures or point forces, single-repeated impacts to measure impulses, double contacts to measure point-to-point distances, or 2D array-like contacts to measure heat transfer rate, pressure etc. Except

⁴Such as sensor and transduction technology, tactile image processing, shape recognition (especially curvature), active and architectures and integration.

for the simple binary detection of the existence of touch, any tactile sensor has to utilize the mechanical contact to induce a detectable signal. The instrument of the sensor that achieves this mechanical to electrical translation are called tactile sensory transducers. It is the knowledge of the mathematical relationship from the transducer output to the desired physical quantity that turns a sensory transducer into a true sensor.

There are many transducer technologies currently available for various tactile applications. Common tactile transducers exploit the changes in properties like resistance, conductance, capacitance, piezoelectric, pyroelectric, magnetoelectric, mechanical, optical, or ultrasonic. Nicholls et al. [35] presents a comprehensive survey about the underlying methods of different transducer technologies. The important point about those devices is that most of them are focused on characterizing the direction and magnitude of forces that act on the sensitive surface. A typical device consists of a surface pad with a linear or rectangular array of scalar valued sensing points [28]. Today, these single-modal sensors can be manufactured in very small very scales, deposited on deformable surfaces and sold commercially ⁵. However, these force measuring sensors are not appropriate or necessary for the tactile antennae which will be addressed later. But in short we can infer that the technology mostly inspired from relatively smooth skin whereas the densely quasi-stiff haired cockroach like sensing is rarely developed.

2.3 Artificial Antennal Sensing and Perception

2.3.1 Classifying Antennae

If the tactile sensing technologies are to be considered as slow progressing, antennal artificial tactile sensing should be considered as almost non-existent. Indeed except the earlier related work described in the previous chapter, there are no published implementations regarding to this technology. This apparent immaturity combined with the currently emerging designs and the promising future applications call for a standard definition and appropriate classification of the artificial antennae under the major field of robotics.

⁵e.g. <http://www.pressureprofile.com/>

The need for classification comes from an antenna’s confusing multi-sensor-modality which is convoluted with its mechanical disposition. For now we can think of the case with purely sensorial deployment — as some biological antennae have direct manipulative or locomotive uses [13] — of an ideal antenna which does not manipulate its surroundings but rather gathers different kinds information about the environment it touches. In this broad sense the artificial antenna should be considered in engineering terms as a “multi-modal tactile sensor array”. However this definition is more appropriate for the skin rather than the antenna, since it lacks the emphasis of the underlying structural mechanics. Indeed different from the skin, the antenna encompasses the superstructure, which accommodates all the individual tactile sensors, and also additional sensors that measure properties that are relevant in perceiving the overall antenna shape. For the skin this emphasis is not necessary because as a very flexible 2D sensor array, it will inherit whatever special rigid body mechanics it envelopes.

In biology, at the sensory level, the antennal output from each individual tactile and proprioceptive⁶ sensors are independent. For instance humans can feel the orientation of their limbs even if there is no external tactile stimulation. This should be the case for cockroaches as the gravitational force or natural oscillations should trigger the intersegmental proprioceptive sensors even if the tactile hairs are not activated. This independence ends in the brain, where the information regarding the configuration of the antennal superstructure is coupled with the readings of the receptors at the *tactile perception* context [36]. That is why the classification of the antenna should entail not only the sensory features with the passive flagellum kinematics but also the tactile perception aspect.

Unfortunately, this taxonomical attempt is not trivial since as directly stated by Lee et al. [28,29] and Nicholls et al. [35], the area of tactile sensing itself is not matured yet. This apparently lead to some inconsistent or, more accurately, non-standardized usage of even the most basic terminology throughout the literatures of neuroscience, cognitive psychology (or cognitive science), philosophy of perception, electronics, haptics, mechanical engineering etc. For example it is reported that the Robotics Institute of America considers tactile

⁶The ability to sense the position, location, orientation and movement of the body and its parts

sensing and touch sensing in two separate categories in which tactile sensing is defined as “The continuous monitoring of forces in an array” and touch sensing as “sensing of force at one or just a few points” [35]. This would not be true for haptics, since it refers touch sensing not as a separate but as a subcategory of tactile sensing. On the other hand in biology, touch or tactile sensing hardly is constrained with just the measurement of force. In short, a self-contained framework that can accurately classify the modality of the antenna as a whole is necessary.

A good way of approaching this issue is to think of antennae as limbs like fingers or arms in humans but passive at the same time. The reason is that in the human domain, the coupling between the proprioceptive and exteroceptive⁷ sensors is literature-wise already established and studied under the area of haptics. In that sense, the multi-segmented antennae in insects can be said to resemble human fingers (motor wise paralyzed of course) where both proprioception and exteroception is utilized. As a relevant course project, a haptic device that externally actuates the human middle-finger in a master-slave, position-exchange teleoperation paradigm was built by the author to test the feasibility and performance of a purely tactile feedback remote control loop for mobile robots with antennae [12]. On the host side, a two segmented antenna was externally bent, which actuated the user’s finger at the client side without giving a initial clue about the antenna configuration. The relevant result for this section’s context was that anecdotally all test users were able to sense the configuration of the remote antenna without looking at their fingers or to the antenna. This suggest that even if the finger is treated as a passive appendage like an antenna, the proprioception remains intact. With this justification, we classify antennae using the tactile perception terminology of haptics.

In order to label the perceptive component of antennae, we use the classification framework presented by Loomis et al. [30], which not only explicitly redefines all the relevant terminology but also successfully organizes the concept of tactile perception into different groups called tactual modes Table 2.2.

⁷(also termed superficial sensation): receptors in skin and mucous membranes that facilitate tactile or touch along with pain and temperature sensations. [4]

		<i>Type of Information Available to Observer</i>	<i>Label of Tactual Mode</i>
No Control	1.	Cutaneous information	Tactile perception
	2.	Afferent kinesthesia	Passive kinesthetic perception
	3.	Cutaneous information plus afferent kinesthesia	Passive haptic perception
Control	4.	Afferent kinesthesia plus efference copy	Active kinesthetic perception
	5.	Cutaneous information plus afferent kinesthesia plus efference copy	Active haptic perception

Table 2.2: Classification of Tactual Modes. *Reproduced from Loomis et al. 1986*

To complement Table 2.2, the relevant haptic terminology will be also briefly defined according to Loomis et al.

Cutaneous Perception Exteroceptive sensations stimulated by all the tactile sensors convey the touched object properties.

Kinesthetic Perception Proprioceptive sensations such as the resistances to limb (segment) movement convey all the essential spatial information for a given task [30]. The contribution from cutaneous contribution — if there is any — is to indicate the existence of contact without any measured property.

Haptic Perception The information conveyed by both cutaneous sense and kinesthesia about distal objects and events [30].

Active Touch Subject controls the pickup of information by the way of efferent commands issued to the muscles used in touching [30].

Passive Touch Subject does not control the way the tactile information is picked up. The environment governs how and when the contact events occur.

As this framework groups perception based on the tactual modes, it will be appropriate to classify the biological antenna as a tactual limb and artificial antenna as tactual device. Now within this main class, for example artificial fingers can be categorized as devices facilitating *active haptic perception*, or manipulator arms as devices facilitating *active kinesthetic*

perception. As we have now reestablished the tactile perception framework in general, the product we have been referring so far as “tactile antenna” can be defined.

2.3.2 What is an artificial “tactile” antenna?

Considering all the arguments discussed so far, we define an artificial *tactile antenna* as a cantilever, slender-cored, multi-sensored, biologically inspired flexible tactual device facilitating passive haptic perception. Such a device has the following characteristics:

- Acquires information from the environment through physical contact.
- Acquires some level of information about its shape regardless of a presence of contact.
- Is flexible or pliable at least at one point.
- Accommodates the more than one sensor along its length.
- May or may not have basal actuation and sensing.

Antennae vs Whiskers

This definition distinguishes artificial antennae from the other tactual devices like artificial skin — classified as antennae only if the enveloped rigid body is a slender-cored, passive and flexible rigid body — or whiskers, in which the sensing is purely done at the mounting base.

Ueno et al. [48] in their paper describe such an implementation where the insensitive flexible beam is coupled with a torque sensor and a joint angular position. The artificial whisker can detect the position of a contact along the beam by reading the torque values at the base while repeatedly contacting the object in an oscillatory fashion. Kaneko et al. [20] also describe a whisker design where the contact location is sensed by continually exerting a force on the object and measuring rotational compliance at the base. There is proportionality between the contact distance along the beam assuming there is no lateral slip. The former design is depicted as an *dynamic antenna* and the latter is as an *active antenna*. It can

be speculated that the antenna categorization is chosen to emphasize the capability of contact position sensing as contact sensing is a functional requirement for both biological and artificial antenna, but since the device is not sensorized along its length, they perhaps should not be called antennae but rather whiskers.

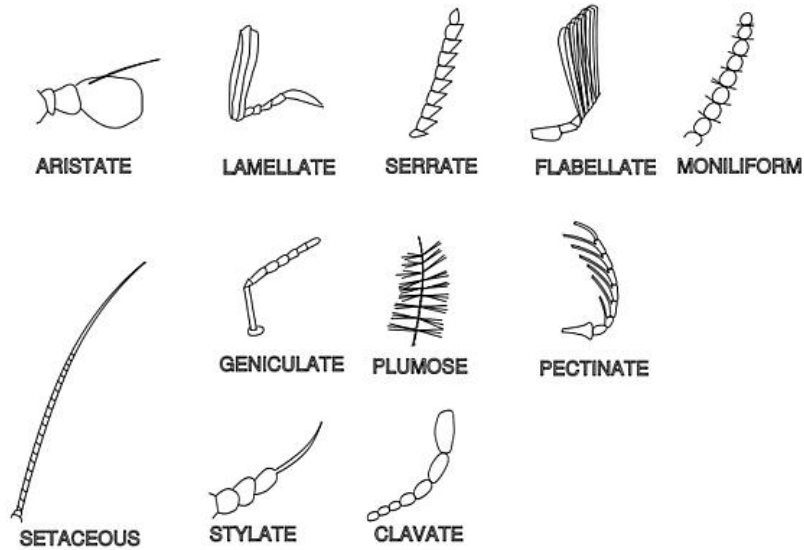


Figure 2.9: Different types of antennae in nature (Image credit: [46], Copyright©2007 L. Shyamal).

There may be other examples like whiskers vs antenna, where a distinction is perhaps not as easy to make. Even though it is impossible to think off all the cases that may soften the definition of tactile antennae, a potential case might be with the relativity associated with slenderness or pliability. In such scenarios one must look at the context and decide if it is classifiable as an antenna.

In Figure 2.10 we provide a conceptual template on which possible antennal features can be combined. We think of a tactile antenna as a flexible, slender, possibly branching, structure. This structure is populated by sensory receptors, joints, and possibly branches. The allows for fairly complex tactile antenna morphologies, as can be the case in nature (see Figure 2.9). A formal set of design criteria for tactile antennae will be provided in Chapter 3.

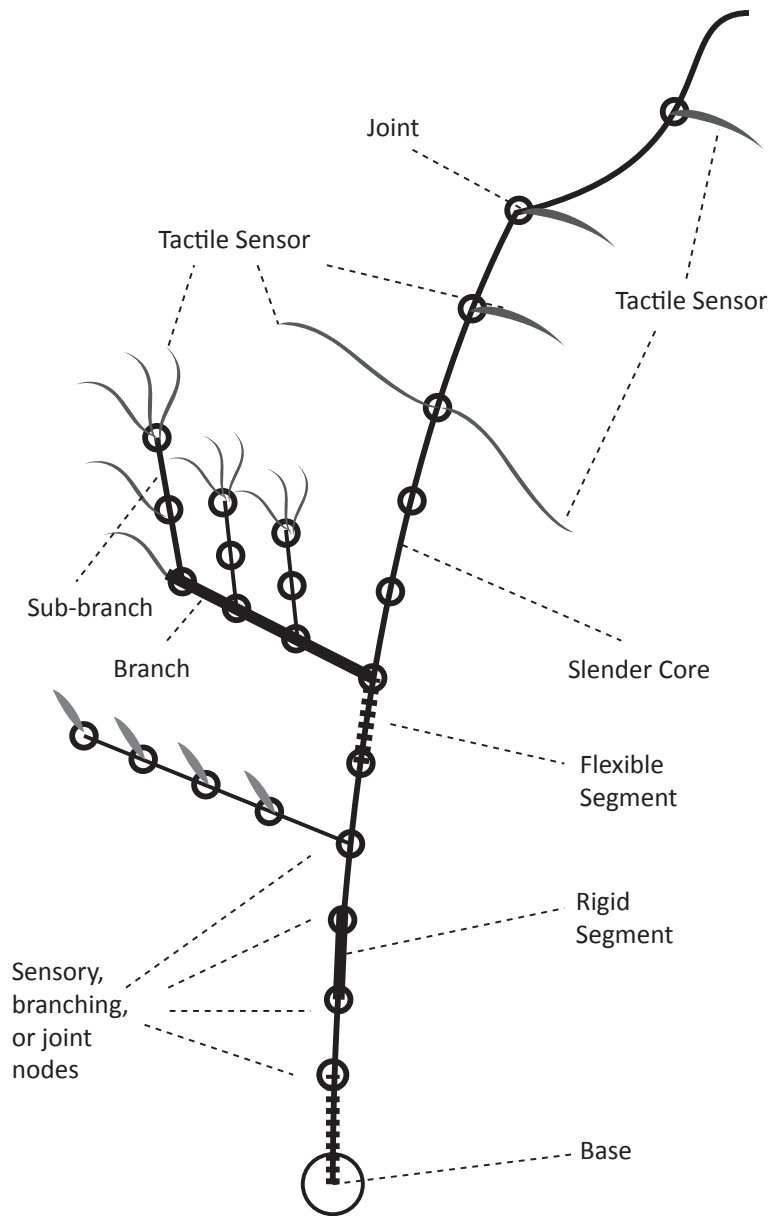


Figure 2.10: Features that do not violate the definition of being an antenna.

2.3.3 Sensing curvature

In order to sense curvature, we need a physical property, whose quantity would change monotonically and without hysteresis depending on the relative orientation of two segments. In the case of a continuously bending platform, the physical property should change proportional to deflection. There are a couple ways to achieve curvature sensing:

Use direct flex sensors as utilized by Barnes et al. [3] and Cowan et al. [3]. The flex sensors change their resistance proportional to bending which can be measured via the corresponding change in the applied voltage to the sensor.

Fiberoptic cables can be used in a few ways to detect bending. For example the fiber Bragg grating (FBG) method takes advantage of the phase shift of the reflected light in the cable. The change in light intensity change can also be measured due bending under some particular optical arrangements [9, 35]. There are also other novel methods for quantifying bending using fiber optic cables. One of such a method was presented by Gauthier et al. [16].

As bending of an elastic material will cause lateral tension and compression on the outer and inner surfaces respectively, a stretch sensor can be used to detect bending. A product is also available commercially⁸

2.3.4 Contact Sensing

As far as the electronics and circuitry of the contact sensors are concerned, we have two possible directions: the sensor either returns a binary response or an analog response. A binary sensor design would simply provide the information of whether or not an object is touching the sensor. An analog sensor would in addition provide details about the strength and perhaps the direction of the contact. Examples to the binary sensors are basically all detector, lever or tactile switches that are widely available commercially.

⁸<http://www.imagesco.com/sensors/stretch-sensor.html>

Chapter 3

Antenna Design

This chapter is organized based on a standard mechanics based design methodology.

3.1 General Statement of Goal

The goal of the work presented in this essay was to design, fabricate, test and deliver a prototype artificial arthropod antenna. The design improves upon earlier designs by conforming to the definition of a tactile antenna described in Chapter 2, specifically by integrating contact sensors along its length. The antenna will ultimately be attached to small (0.2 m to 0.5 m long), wheeled or legged mobile robots and will regularly make contact with objects.

3.2 Intended Market

Academic, commercial and military markets may exist for tactile antennae. Academic research in particular can utilize this design for testing hypotheses in their field. This includes research on bio-inspired robotics, tactile sensing and control, general biological antennae and antenna-mediated behavioral tasks. Tactile antennae can be used directly as navigation sensors for mobile robots facilitating tasks such as obstacle-avoidance, wall following or object

tracking. They can complement existing sensors by providing tactile information regarding an object. Potentially high resolution tactile mapping in dark environments can also be performed. Thus institutions or companies investigating ocean-floor, space or other geo-exploration as well as agencies interested in search and rescue, reconnaissance, fire-fighting, path-finding can benefit from the design. However the technology readiness level¹ of this product is not yet suitable for a commercial launch.

3.3 Design Constraints and Requirements

The following list contains the constraints imposed by the current state of the art, availability of components, physical demands, safety regulations, average host platform characteristics and of course the very definition of tactile antennae. The constraints and requirements stated in this list carve out the design space such that all innovative approaches or considerations towards the goal cannot violate the design criteria:

- The end design should be classifiable as a valid tactile antenna (See §2.3.2).
- The antenna measurements should be accurate enough to facilitate wall following on Garcia.
- The antenna should either carry its own energy source or work with a standard 3.3V to 5V I/O port output. For Garcia, the electrical demand of the antenna should not exceed 7.2 Volt at 1A.
- The antenna has to be mountable to the host platform. As there is no standard for achieving this constraint, a per-host base mounting piece should be provided.
- The antenna should represent a minimal dynamic load relative to the host robot's payload capacity.
- The antenna should be able to electronically interface with the host platform. Garcia has 2 free I²C connections and an extra serial port for communication.

¹Technology Readiness Level (TRL) is a measure to assess the maturity of evolving technologies prior to incorporating that technology into a system or subsystem. See Appendix K

- The antenna should be durable enough to withstand:
 - vibrations caused by the robot during operation
 - withstand repeated impacts at up to 0.5 m/s with the hard surroundings
 - withstand wear caused by the prolonged frictions during wall following
- The components of the antenna should be either purchasable from a valid third-party vendor or easily producible with the tools and services available to the Whiting School of Engineering
- The cost associated with the design should not exceed the budget limits reserved for the project (\$10,000)
- The antenna design and the deliverable should conform with the university safety and legal regulations.

3.4 Engineering Design Criteria

This section specifies a set of standards or categories that the antenna design should both conform and improve upon. It also provides specific benchmark points against which the antenna design can be gauged:

- Antennal structure
- Memory of flexible structure
- Bending and/or Strain Measurement
- Contact Detection and Location
- Base actuation
- Sensor interfacing

The criteria list above only encompasses the antenna superstructure and the overall functionality in general. Yet we know that the antenna itself is also composed of many different

tactile sensors. Harmon [18], after a comprehensive survey conducted through questionnaires with industrial manufacturers, research consultants, industrial, private and government researchers, determined the criteria for a good tactile sensor. In fact this survey work is reported to be a widely cited source for justifying the designs of many tactile sensors [35]. Hence we decided to incorporate the Harmon design criteria as a supplementary list to be able to classify our design as a good or bad tactual device. Nicholls et al. [35] summarized the Harmon design criteria in a list format which is quoted below verbatim:

1. The sensor surface should be both compliant and durable.
2. Spatial resolution should be 1 mm–2 mm.
3. A range of 50–200 tactile elements (in a 2-D array form) is acceptable.
4. The sensor should be able to detect as small as 5 g. (0.049 N), ideally 1 g (0.0098 N).
5. A dynamic range of 1000:1 is satisfactory.
6. The sensor must be stable, repeatable and without hysteresis.
7. The response must be monotonic, though not necessarily linear.
8. The temporal resolution for the sensor should be at least 100 Hz.

Again, the numbers presented here are just values for benchmarking purposes. This is because by definition, a criterion should only entail the standard or category at which the design will be judged on. Also, note that this list was designed in relation to 2D tactile arrays but can be adopted to 1D tactile antennae Thus beside those numbers, which are just suggested values based on Harmon’s survey, we should look the underlying design criteria:

- Compliance and durability
- Spatial resolution
- Sensor spatial density
- Contact detection threshold
- Output resolution

- Stability, repeatability and hysteresis
- Monotonicity

Considering those design criteria and having the early design works in mind, we started to conceptualize the final design features.

3.5 Evolution of Design

3.5.1 Brainstorming

A brainstorming session with several members of the LIMBS Lab was conducted before the development of the new antenna in order to consider all the potential methods. Various different ideas were collected to achieve most of the standards given by the design criteria at least in some level of success. The compilation summary of the ideas are given in 3.1. The brainstorming session resulted in the settlement of the following design features:

- Structure: A multi-segmented antenna will be built with identical units that have some flexibility between the segments.
- Structural memory: A super-elastic shape-memory-alloy backbone will restore the natural angle of the antenna (although shape-memory properties will not be used).
- Bending: Strain gauges will provide both flexibility between joints and give angle measurements (ultimately modified to be Hall-effect sensors).
- Contact Location: Small switches will be the contact detecting components.
- Base actuation: Considered to be a low priority feature.
- Interface: An I²C bus will be utilized to integrate all segments.

In the next subsection the different prototypes and proofs of concepts, which eventually lead to the final conceptualization of the current design, will be presented.

<i>Structure/ Durability</i>	<i>Structural Memory</i>	<i>Bending / Strain</i>	<i>Contact Location</i>	<i>Base Actuation</i>	<i>Computing / Interfacing</i>
Segmented Antenna.	Use of shape memory alloys	Fluid pressure changes	Use of strain gauges	Artificial muscles	Two line data bus
Sof tissue connections (change in size)	Spinal backbone	Use of strain gauges	Fiberoptics	DC, 2-axis Servo motors	Microprocessors (PICs in each segment)
Identical units	Bimetal	Fluid chambers	Leaf-like switches	Stuart platform	Basal computing
Identical size connections (but change in material)	Urethane	Piezo-electric	Capacitive (PPS)	Ball and socket	
Long spring mantle	Any elastic material	Contact force measurement	Pin through hole	Hinge joints	
Slinky		Fiberoptics	Leaf-like strain gauges		
Flexibility between segments		Individual LED and sensor for each link	Backwards computation based on strain geometry		
Wire backbone			Small switches		
Ribbon cable backbone			Vibration		
			Temperature		
			Light sensor		
			Air hockey (sense back pressure)		

Table 3.1: Design brainstorming summary to meet design criteria.

3.5.2 Evolution

The starting point of the evolution period was actually the outcome of this brainstorming session. The first proof of concept that had to be verified was the I²C bus communication. Thus a mock antenna with three segments featuring main electrical components was build on a single prototyping board, which incorporated a flex sensor, various different small switches and an ISP programming port (Figure 3.1). We selected three different microcontrollers (P89LPC925, P89LPC935 and P89LPC938) from Phillips Semiconductors. All of them had I²C support but their ADC characteristics were different. Among those, we chose P89LPC938 for its 10bit ADC capacity.

This proof of concept platform actually constituted the LIMBS Lab's first of the third generation antennae. The first and second generation antennae were previously presented by Brett Kutcher, Lamperski et al. and Lee et al.

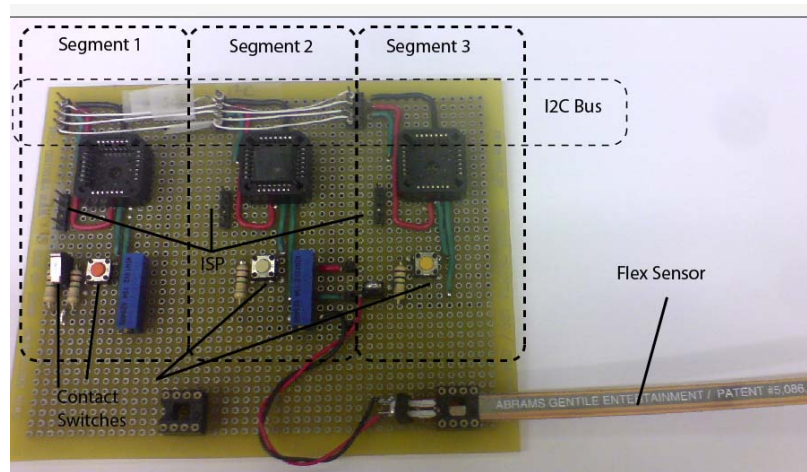


Figure 3.1: The earliest proof of concept platform for the new antenna.

As the next logical step, we wanted to implemented the same design around a flex sensor. So a much smaller surface mount (TSSOP) version package was ordered for P89LPC938. As we did not want to invest in custom PCB's at the time, we ordered an off-the-shelf break-away circuit board, on which we could solder the chip. The proof of concept we tried (Figure 3.2) to test was the interconnection of 3 the individual segments on a mostly flexible surface, but the interconnection test quickly evolved into the integration of modularity to

antennae.

The idea behind modularity is that each segment can be powered up stand alone and can provide angle information without requiring other. They can be taken out from the antenna chain and put on another place on the antenna. Another design goal for this next step was to reduce the length of the rigid section of the segment as much as possible. This would allow the length of the antenna to be assumed entirely flexible as the flex sensor to make dynamical analyses simpler.



Figure 3.2: The next step in evolution. Modularity and embedded computing on an antenna superstructure was tested first time.

A more involved design approach was taken for the fabrication of the next prototype (Figure 3.3), which incorporated a design of a double-sided printed circuit board. The top side contained the microcontroller, RS-232 service port and a sensitivity potentiometer for the flex sensor. This design incorporated the usage of the flat flex coupling for the first time, but the modularity was sacrificed. That is, the coupling cable had to be soldered to the holes on both segments in order to maintain a connection with the subsequent segment. The main salient feature of this prototype was the embedded touch sensors on the back side of the PCB, which could be attached with hairs as well as depicted in the CAD model given in (Figure 3.4a)

This design highlighted an issue with regards to the touch sensors. Since the contact sensors could only be placed on the PCB's, the flexible section of the antenna would not be able to detect contacts. The relatively long nature of the flex sensor also made the detection of the bending location harder. This is intuitive since a long flexible material like a flex sensor can bend at different locations and still output the same voltage (Figure 3.4b). At the end,

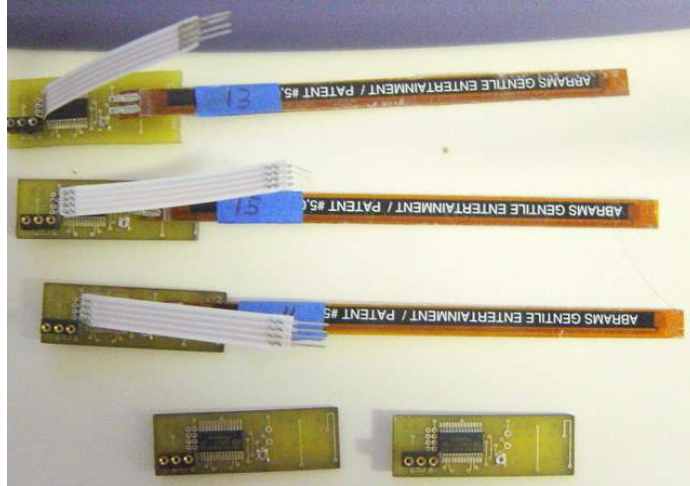
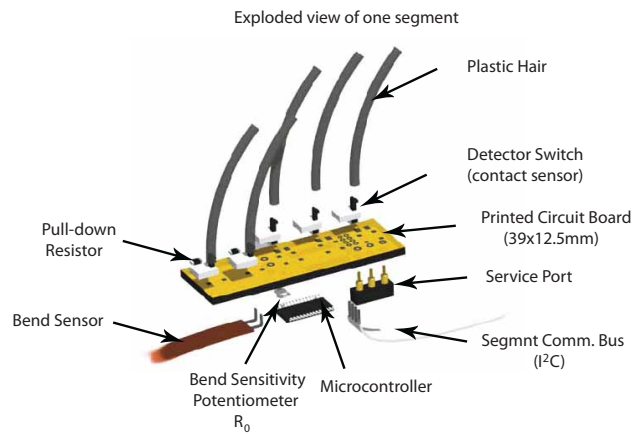


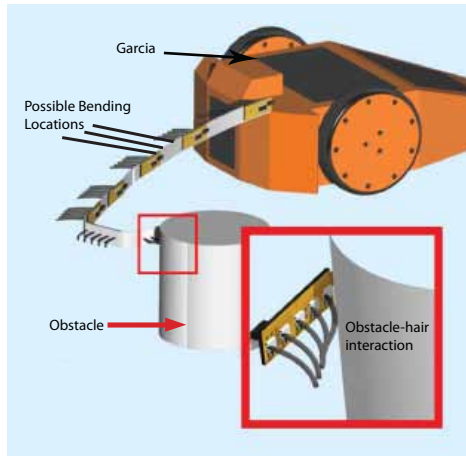
Figure 3.3: The third iteration in antenna design. This is the first antenna design with a custom PCB and touch sensor incorporation.

those problems lead us to consider a major revision of the design, in which the *solid-flexible-solid-flexible* biperiodic structure paradigm was abandoned. Instead, we adopted a simpler rigid serial link structure, which is not only the morphology of insect antennae but also is easier to analyze from a robotics point of view.

The next antenna prototype thus took a completely different approach for detecting angles. The simple series of rigid link structure limited the possible places where bending can occur to a single point per link. This new configuration lead us into more thinking to evaluate if there are more accurate ways of measuring rotations. At the end, the Hall-effect sensor solution was reached and implemented. This final iteration before the current antenna also featured modularity, a replaceable NiTi backbone for varying stiffness and contact hairs on touch switches at the same time (Figure 3.5). The segmental superstructure which carries the bearing and the electrical connectors was made of acrylic and the rest was accommodated by two PCB boards that are perpendicular to each other. The vertical board holds the five contact sensors and the horizontal one holds the rest of the electronics. The orthogonal orientation of two PCB's allowed the hall effect sensor to be in the correct orientation (horizontal) while also facilitating a good posture for the touch sensors to make contact with a wall. Hence, this antenna also takes advantage off the orthogonally oriented PCB's in the electronics sub-assembly. The microcontroller used for embedded computing



(a) The exploded view of the first antenna with touch sensors.



(b) The segments are integrated in an antenna form.

Figure 3.4: Figure depicts how this antenna version cannot detect contacts at the flexible section. Also it shows that a single flex sensor can bend in different locations.

was still the legacy P89LPC938 from the earlier designs but the packaging type changed from a rectangular TSSOP into a 6 mm square HVQFN. This choice of form factor carried to the current design as well.

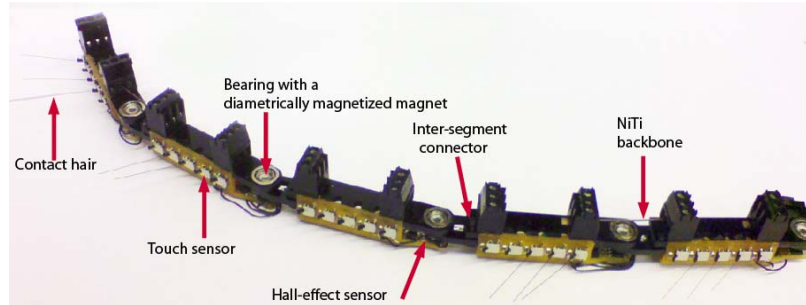


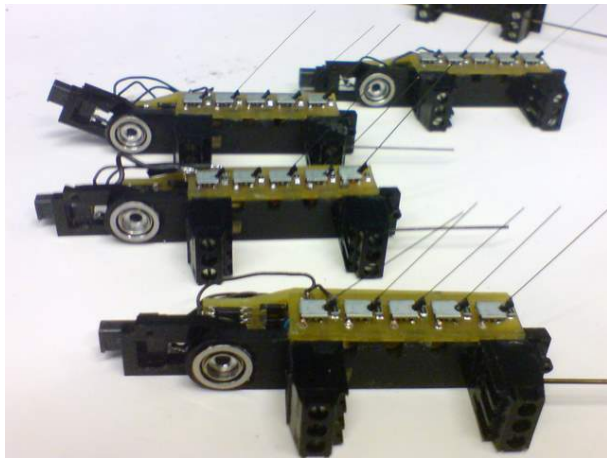
Figure 3.5: The fourth iteration of the tactile antenna. This version incorporated haired touch sensors, flexibility via NiTi, Angle sensing via Hall-effect sensors and modularity.

The modularity was achieved through electrical *snap-on* connectors (Figure 3.6b), which made connecting and disconnecting of the individual segments easy. On the other hand it also introduced a sagging problem, where the tip of the antenna would get closer to the ground after being attached as a cantilever. The reason for the sagging was that the electrical connectors were not strong enough to hold the added segments after a certain threshold. This is due to the increasing moment arm and weight of the each added segment (Figure 3.6a). The sagging could be fixed to a certain degree using the NiTi backbone, affixed to the segments in tension. This problem influenced the design of the current antenna greatly.

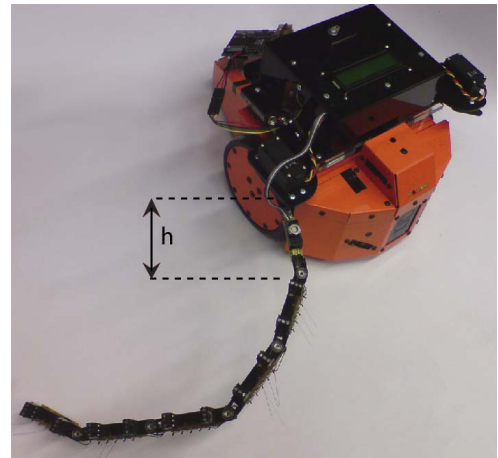
3.6 Final Design

3.6.1 Overview

Our final design follows the rigid body chain approach utilized by Kutcher [23], Lamperski et al. [24] and the previous antenna iteration. Each link has an identical length of 40 mm and can rotate about the subsequent joint from -90° to 90° (Figure 3.7a — 3.7b). The angle between adjacent segments is measured by a Hall-effect rotary position sensor chip. The Hall-effect chip sends the angle values through a built-in 12-bit digital to analog converter,

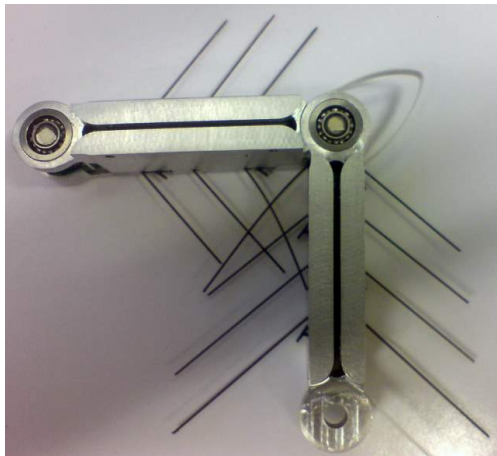


(a) Modularity of the segments allow them to be connected in one action.

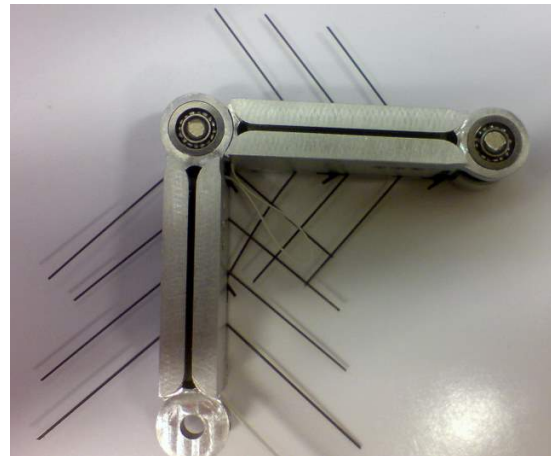


(b) This antenna version has a sagging problem in which the free end of the antenna is pulled down. The tip point in this picture actually touches the ground.

Figure 3.6: The fourth iteration of the tactile antenna.



(a) Angular motion limit at -90°



(b) Angular motion limit at 90°

Figure 3.7: Angular motion range of a segment.

which is then sampled again by the segment’s main microcontroller through a built-in 10-bit analog to digital converter. The firmware currently in place encodes this information into a 2 byte data structure where the least significant 4-bit of the second byte is reserved for touch sensors. This 2 byte data is sent via a standard I²C protocol to the host computer whenever such request is made. I²C is a two-line bus consisting of clock and data. There is a single I²C bus that connects all segments and the host robot computer. The master of the devices is the the robot host which issues a “read segment” command to a specific segment rather than the whole antenna. The addressed particular segment then transmits the 2 byte angle and touch information. Each segment has two touch sensors on both sides, which are activated by contact. For detailed CAD drawings, please refer to Appendix B. Next section covers these and other design features of the antenna in more detail. The binary approach was considered simply because it was less complicated to design, test and accommodate; In particular no additional analog to digital converters would be necessary, and simpler structural designs would be possible. The binary approach basically suggested a mechanical switch that would open or close an electrical circuit in case of an external contact. The information should be then passed to one of the inputs of the microcontroller to be interpreted.

3.7 Design Features

3.7.1 Embedded computing

Each segment contains an NXP Semiconductors P89LPC938 8-bit microcontroller with an accelerated two-clock 80C51 core and a 8kB byte-erasable Flash memory. A 20mA current at 3.3V can be supplied through the I/O pins. The microcontroller possesses a 10-bit analog to digital converter Except multiplication and division, all instructions take from 111ns to 222ns to execute.

3.7.2 I²C communication backbone

One problem associated with the flexible antennae comprising of many flex sensors is the amount of cabling required (Figure 3.8). The problem was predominantly exhibited in the flexible urethane antennae designed and built by Owen Loh as they accommodated many bend sensors. The solution was proposed in the brainstorming session mentioned in the *Evolution* section, namely, the utilization of a two-line bus like I²C. In the case of I²C, these lines are clock and data. The clock synchronizes the devices on the bus, whereas the data line carries the actual data. There is a lot of information available on I²C but the details of the bus itself is outside of the scope of this essay. What is important is that using a bus architecture not only eliminates the cable problem but also allows other devices to be added more easily. However the I²C cannot handle an infinite number of devices so it is helpful to briefly mention the addressing system and the associated limits of an I²C bus.



Figure 3.8: Using a bus architecture prevents the accumulation of wires as new sensors are added. This is the base connection of an antenna with a series of flex sensors.

Each I²C device has 2 consecutive 8-bit addresses e.g (0×03 and 0×04). The most significant 7-bits define the general address and the 8th bit defines the write or the read task. Odd numbered addresses are assigned for *writing* and even numbered addresses are assigned for *reading*. So for 8-bit addressing, up to 128 devices can be on a single I²C bus. However some addresses² are reserved (Table 3.2). Discarding those yields a total number of 111 segments and a host computer to be connected on the same bus.

²www.i2c-bus.org

<i>I²C address</i>	<i>Reserved for</i>
0 × 00	General Call
0 × 01	START Byte
0 × 02	C-Bus (obsolete)
0 × 03	C-Bus (obsolete)
0 × 04	Different bus formats
0 × 05	Different bus formats
0 × 06	Future purposes
0 × 07	Future purposes
0 × 08-0 × 0F	High-speed Master Code
0 × F0-0 × F7	10-bit Slave Addressing
0 × F8-0 × FF	For future purposes

Table 3.2: reserved I²C addresses. Taken directly from www.i2c-bus.org.

3.7.3 Variable parameters

As we mentioned earlier, Lamperski et al. [24] described a simulation program for an antenna in which several parameters could be adjusted. Those parameters were:

- Number of links
- Spring and damping constants
- Link masses
- Equilibrium configuration

Lamperski et al. states that those parameters were adjustable to facilitate testing of antenna hypotheses in the simulation environment. Our design aims to incorporate almost all of those parameters to allow antenna hypotheses to be tested on a real system.

We already mentioned that the number of links can be adjusted by virtue of the I²C bus. The spring, i.e. the stiffness between each segment, can also be adjusted by inserting wires or other materials that are up to 0.8mm wide into the top channel of the antenna. This channel traverses the entire length of the segment — thus the antenna — so material lengths that are longer than one segment do not pose a problem. In fact a uniform stiffness can be easily imposed to the antenna by inserting one long wire throughout the entire antenna. The inserted wires can be affixed to the segment via two 0-80 set screws provided on the

side. Please refer to Appendix J.1 for more details.

Link masses can also be changed by utilizing the bottom two mounting holes at each segment. Longer socket cap screws can be purchased and sheets of material can be squeezed between the cap and the bottom piece of the segment.

3.7.4 Non-Sagging structure

The previous prototype that incorporated many of the major features of the new antenna had two significant problems: structural sagging and weakness of coupling wires. The sagging problem arose directly from the high modularity of the design. The snap-on electrical connectors simply could not hold that the added weight of the new segments as the moment arm got larger as well. This design addresses the issue by making the hinge as tall as the segment itself, and by minimizing the joint tolerances. Basically two connected segments mesh with each other in such a way that there is not much play in the sagging direction. So the segment that is sagging would hit the surface of the other segment before the sagging become apparent. Please refer to Appendix B for more details.

3.7.5 Circuit protection

The need for protecting the circuitry came also directly from the previous prototype of this generation of antennae. As we were testing the previous prototype, occasional human contact would cause the segments to reset. This could have been due to the static charge build-up or just because touching would make the loose wires to touch each other. To overcome this, we made this design to fully engulf the circuitry.

We developed a two-piece thin-walled aluminum shell body design that could be screwed together. Please refer to Appendix B for detailed CAD models and Appendix C for the relevant engineering drawings.



Figure 3.9: The top piece of the designed aluminum shell.

3.7.6 Frictionless angle sensing

An important salient feature of the antenna is the capability of measuring the inter-segmental angles without introducing friction. This is facilitated by a Melexis³ Hall-effect rotary position sensor chip, which measures the change in the magnetic flux due to a rotation of a diametrically magnetized magnet (Figure 3.10). The chip has a 12bit angular resolution, which corresponds to approximately 0.09° . In our design however, the analog output that comes out of the 12bit DAC pin is supplied into a 10bit ADC pin in the microcontroller, reducing accuracy to approximately 0.35° . Furthermore, the measured 10bit quantity is rounded up such that the range corresponds from 0° to 360° . This value is then encoded into a 2-byte data structure and sent through the I²C bus.

What is appealing in the Hall-effect method is the fact that it does not introduce friction during the measurement. The antennae designed both by Brett Kutcher [23] and Andy Lampersky [24] had potentiometers to compute the angle, which have non-trivial internal contact interactions. As accurately characterizing the friction introduced to the joints by potentiometers is challenging, a contactless solution is more favorable. Also in addition, the

³<http://www.melexis.com/>

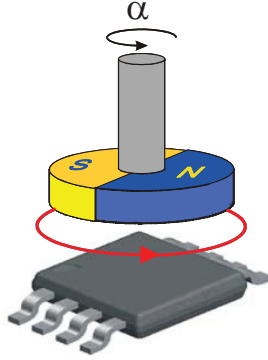


Figure 3.10: The Hall-effect sensor can measure the angular orientation of a rotating diametrically magnetized magnet (Image credit: [33]).

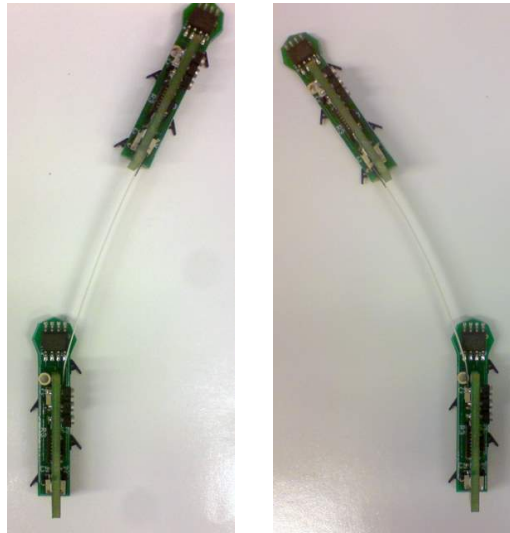
smaller the size of the potentiometers become, the harder it would become to manufacture a coupling between the joint and the potentiometer. This would in turn raise concerns about the robustness of the joint. A final obvious difference between the Hall-effect and potentiometer sensors is their form factor. Since potentiometers are mechanics based sensors, it is only natural for them to be bulkier.

To complement the advantage gained by the contactless sensing, the joints themselves are connected together via small ball-bearings. This further minimizes the friction between the joints and allows us to assume that the stiffness properties are dominated by the shape-memory alloy backbone of the antenna.

3.7.7 Symmetric structure

The antenna segment is designed to be symmetric about the sagittal plane in terms of function. This allows the same segment to be mounted on both right and left sides of the robot. In particular, it allows the coupling cable, which carries the power, ground, clock and signal lines, to be connected on both sides of the segment (Figure 3.11a- 3.11b). This is important since if the coupling cable is on the wall-side, then it can interfere with the touch sensing function of that particular segment (Figure 3.12).

Sometimes though changing the side of the coupling cable is not always sufficient. This may be the case if the antenna is expected to make contact on both sides of the antenna.



(a) Coupling cable mounted on the right side. (b) Coupling cable mounted on the left side.

Figure 3.11: Symmetric nature of the segment design.

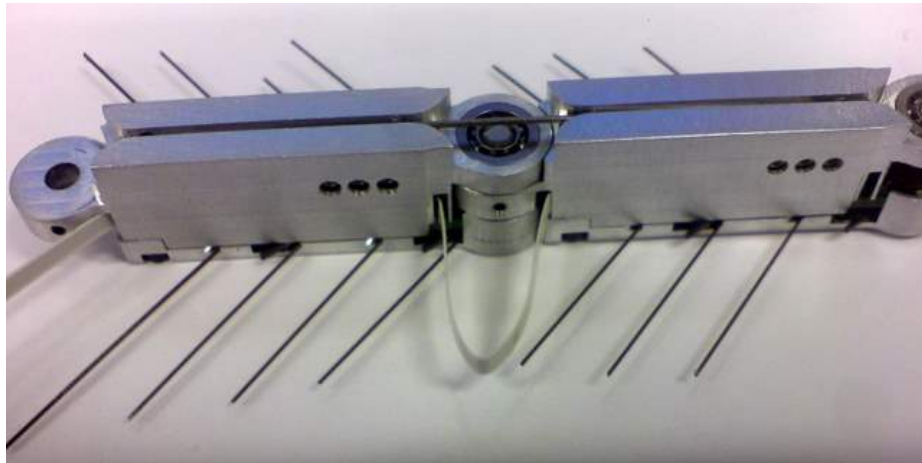


Figure 3.12: If the coupling cable is on the side where the antenna is making contact with an obstacle, then the coupling cable can interfere with contact sensing.

A possible solution is to bend the coupling cable in four locations such that it does extend in the direction of hairs but upward. This particular method has been employed in our experiments (Figure 3.13).

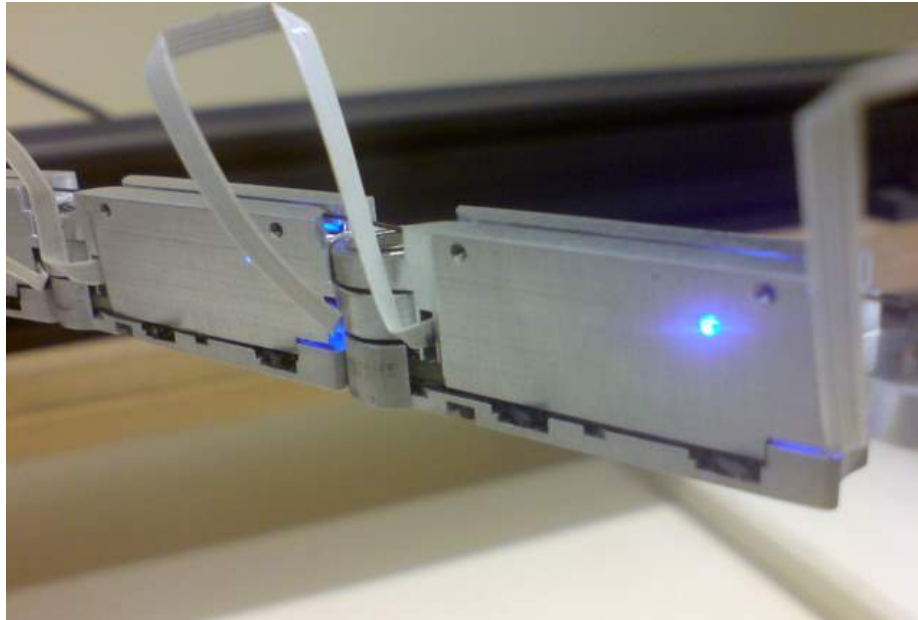


Figure 3.13: Coupling cable can be bend such that it does not interfere with the contact sensors.

3.7.8 In system programming

Firmware updates are integral for the purpose of this design since they constitute the most direct way to incorporate new calibration methods or communication protocol improvements to the segments. The microcontroller, NXP⁴ P89LPC938, used in this design allows the firmware to be updated. This function can be performed even after the chip is taken out from the evaluation board and soldered to the actual printed circuit board [40]. We took advantage of this feature by adding a RS-232 serial port to the segment which consists of three pins (Figure 3.14):

- RST: Microcontroller reset pin.
- RXD: Receive pin from the programmer to the segment.

⁴NXP semiconductors <http://www.nxp.com/>

- TXD: Transmit pin from the segment to the programmer.

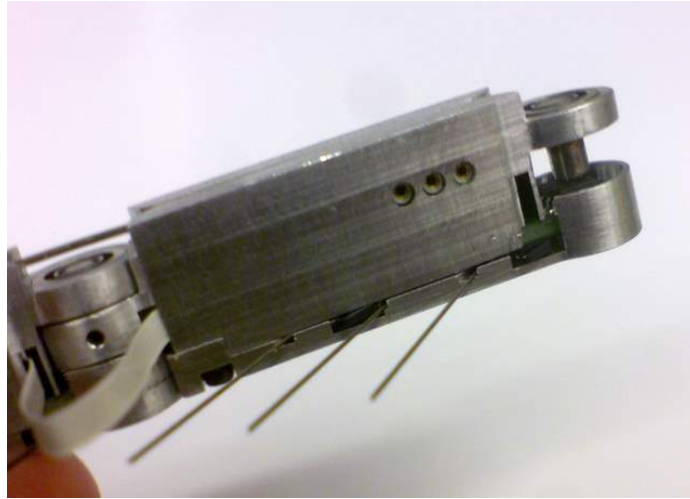


Figure 3.14: The three pins on the side of the segments. The pins are from left to right: TXD, RXD and RST. See Appendix D for the segment circuit diagram.

The sequence of images in Figure 3.15a – Figure 3.16b illustrate the hardware steps of how individual segments in an antenna can be *flashed* with a new firmware.

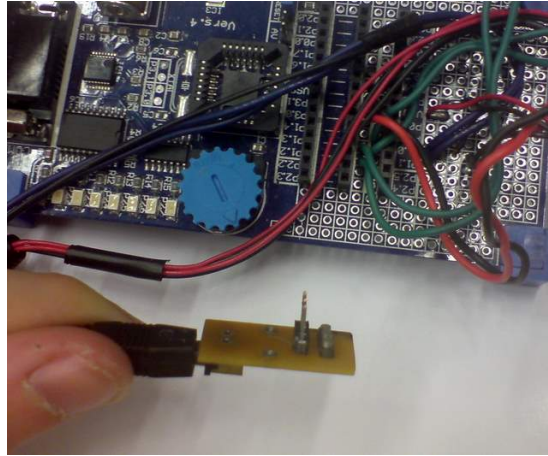
We use a Keil⁵ MCB950 evaluation board that facilitates the signal sequence that would put the chip into the programming mode. A software called Keil μ vision is used as an integrated development environment (IDE) in order to compile and upload the firmware. See the *Firmware Update* section of the Appendix J.2 for a detailed tutorial on the specific settings and usage of this software. In addition, you can check Appendix I for the CAD models, circuit diagrams and PCB layout for the dongles mentioned for interfacing.

3.7.9 Contact sensing

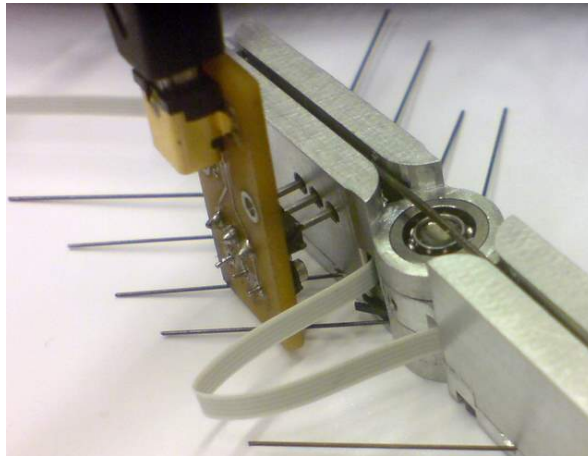
Contact location measurement is one of the salient features of this antenna. It uses the knowledge of segment lengths and the physical locations of the contact sensors on the segment. Then combining the output from the angle sensors and the contact switches, the location of the triggered switch can be discerned.

There are four touch sensors on a given segment (Figure 3.17). These small switches are

⁵<http://www.keil.com/mcb950/>

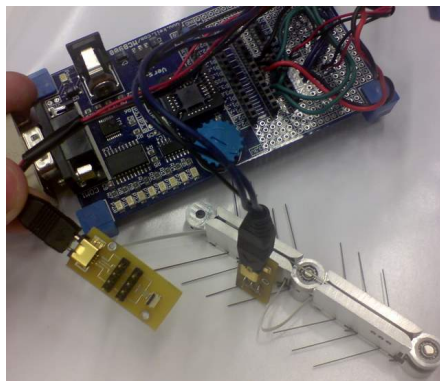


(a) The Keil MCB950 Evaluation board and the custom RS-232 serial dongle for communication.

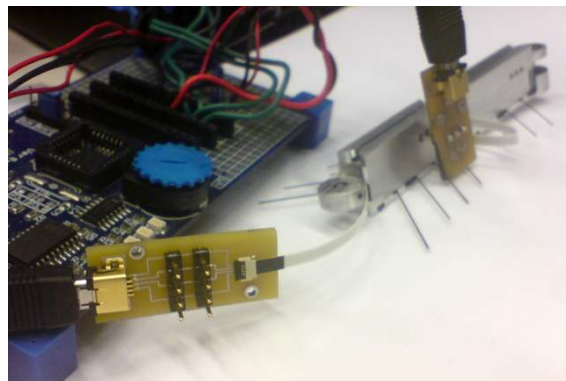


(b) The serial dongle is connected to the segment in this way.

Figure 3.15: In System Programming of the segments.



(a) The custom power+I²C bus dongle necessary for powering up the segment chain.



(b) The power+I²C dongle is connected to the segment.

Figure 3.16: In System Programming of the segments.

called detector switches and used in cell phones to distinguish if for instance the lid is turned on or not. The selected switch for contact sensing is actuated by a short distally pointing lever arm which provides a convenient base for the hairs. In fact the switches can act by themselves as very short spines without the need for additional hairs. Each subsequent touch sensor is a mirror of the previous touch sensor in order to achieve a collective hair-wise distal orientation.

In the electrical level, each contact switch blocks a 3.3 V V_{dd} path to a specific I/O pin on the microcontroller. Pressing the lever on the contact switch closes the circuit, and allows the current to bring the corresponding IO pin to high. A pull-down resistor of 475 k Ω is used to prevent current floating at the I/O pins.

In the software level, all relevant I/O pins are read at the same time by using a keyboard interrupt routine defined for the microcontroller. No contact and contact correspond to a 0 and 1 in binary form which are then concatenated together to form a 4-bit value. This 4-bit constitutes the least 4 significant bits of the 2 byte I²C package that would be send to the host robot computer. Refer to the firmware code in Appendix F for more details.

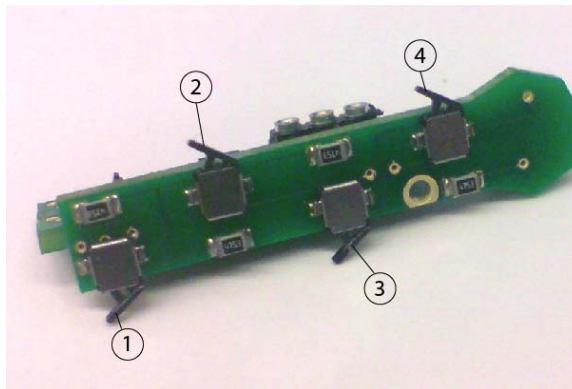


Figure 3.17: There are four detector switches on each segment, where all lever actuators of the switches are pointing towards the distal end of the antenna.

Another feature of the contact sensing is the decoupling of the touch sensors and the hairs. Simply when a hair is bent towards the distal end of the antenna, then the contact sensor would be engaged and contact would be registered. If the hair bends towards the proximal end of the antenna, then the coupling will prevent any damage to the contact sensor lever

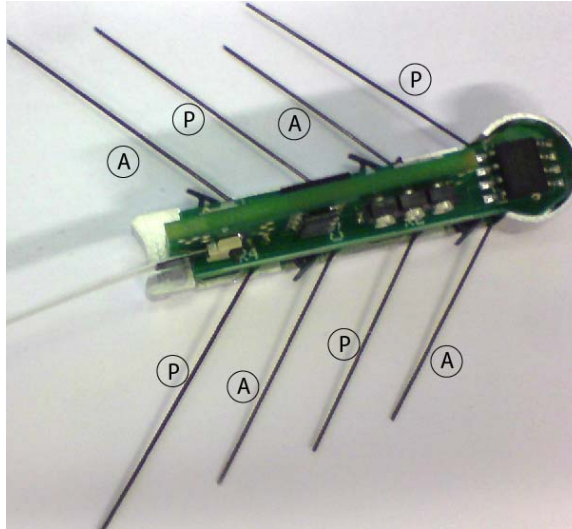


Figure 3.18: The hairs labeled with *P* are passive, meaning that their contact will not register as a detected touch. However their mechanical properties will still impact on the overall antenna structure . Conversely, the hairs labeled with *A* are active, meaning that if they move in the direction of the switch, a contact will be registered.

that would occur if the hair was directly attached to the contact sensor.

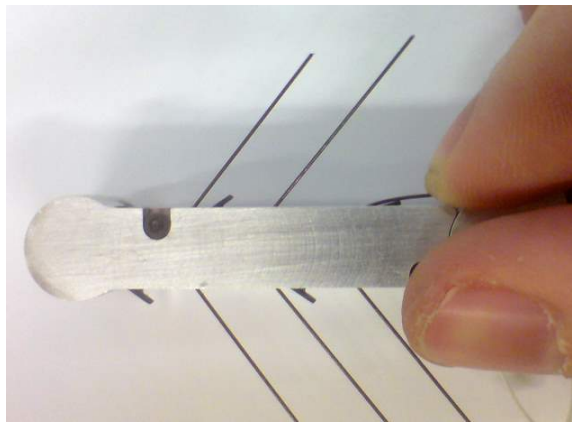


Figure 3.19: The detector switch is triggered by the bending of the hair.

3.7.10 The indicator LED

There is a single blue LED integrated with each segment that provides simple but vital information about the status of a segment (Figure 3.20). Below is a table that summarizes the currently programmed LED modes for a segment (Table 3.3). Our particular LED was selected to exactly conform the microcontroller output characteristics which is 20mA



Figure 3.20: Two segments with continuously lighting LED's. This indicates that at some point the angle sensor did not provide a valid angle measurement. If an LED is lighting after an experiment, then this suggests that data is partially bad.

<i>LED status</i>	Mode	<i>Meaning</i>
A long one time blink	Startup	Successful power cycle
Rapid uneven blinks	Anytime	ISP programming executed
A continuous light	Sampling	Angle sensor problem
A single fast blink	Segment validation	Segment validated by host
A continuous light	Segment Ordering	Segment order unknown, Expecting user input.
Periodic blinks	Sampling	LED mode on Segment is sampling
No light	Sampling	LED mode off Segment is sampling

Table 3.3: LED indicator meanings.

current at 3.3V. Refer to Appendix D for the circuit diagram.

Chapter 4

Antenna Performance

In this chapter the performance of the individual segments and the antenna in general will be gauged. By performance we mean first how well the angle can be measured by each segment. This primary performance metric is then broadened to show how the errors propagate along the segmental chain depending on the antenna configuration. In addition, we present performance metrics regarding communication and sampling frequency on the I²C communication bus.

4.1 Angle measurement performance

We conducted the following experiment in order to characterize the average angle measurement accuracy and precision for the antenna segments. These two quantities are crucial for describing sensor performance, since they are direct measures of the systematic and random errors. The measured quantity for all sensors are thus modeled by (4.1):

$$X = x_0 + \beta + \epsilon \tag{4.1}$$

where β is the systematic error (also called bias) and ϵ the random error. We define the scatter of the random error quantified by its variance as our segment's measure for precision. Likewise the accuracy of the segment's angle measurement is defined by the bias.

The details of our experiment are provided in the next section:

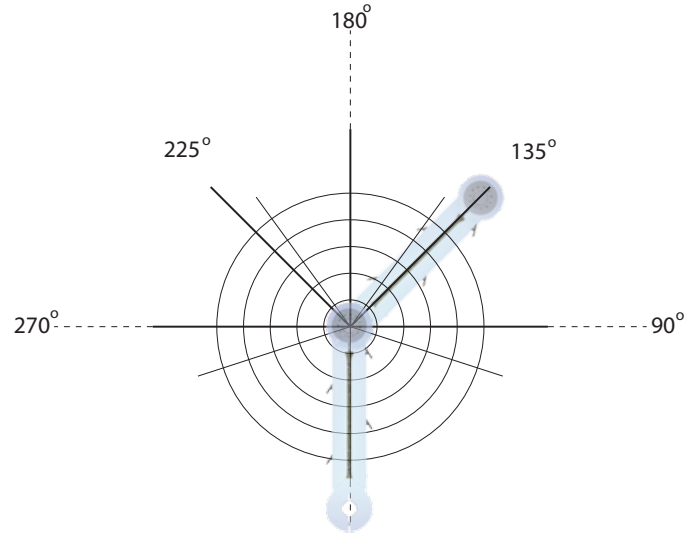


Figure 4.1: Measuring segment angular accuracy and precision.

4.1.1 Setup & Procedure

- An antenna arrangement of $n_s = 5$ random segments was used.
- For all 5 trials ($i = 1, 2, 3, 4, 5$) the antenna rests on a flat surface.
- Each segment is calibrated for 180 degrees with respect to the subsequent segment using the method described in the previous chapter.
- For each trial the joint angle measurement is sampled from a single segment, where the angle with the previous segment is manually brought to five known reference values : $\phi_1 = 90^\circ$, $\phi_2 = 135^\circ$, $\phi_3 = 180^\circ$, $\phi_4 = 225^\circ$, $\phi_5 = 270^\circ$ (Figure 4.1).
- At each trial the angular orientation was reset to the reference angle five times in order to average human placement error or bias.
- For each trial $n = 500$ (100 per re-adjustment) angle measurements ϕ_{ij} were sampled per reference angle ϕ_i . The raw data plots for two of them are presented here in Figure 4.2a (90°) and Figure 4.2b (135°).
- All samples from the individual segments were combined and organized in five groups

based on their reference angle (ϕ_i). Small systematic errors associated with each individual segment are thus averaged.

- We determined the measure of accuracy per segment at each reference angle by computing how much the mean of the measurements $\bar{\phi}_i$ varied with the reference angle (ϕ_i). In other words we computed the bias β_i .
- We determined the measure of precision by computing the sample variance σ^2 and standard error of the measurements σ .

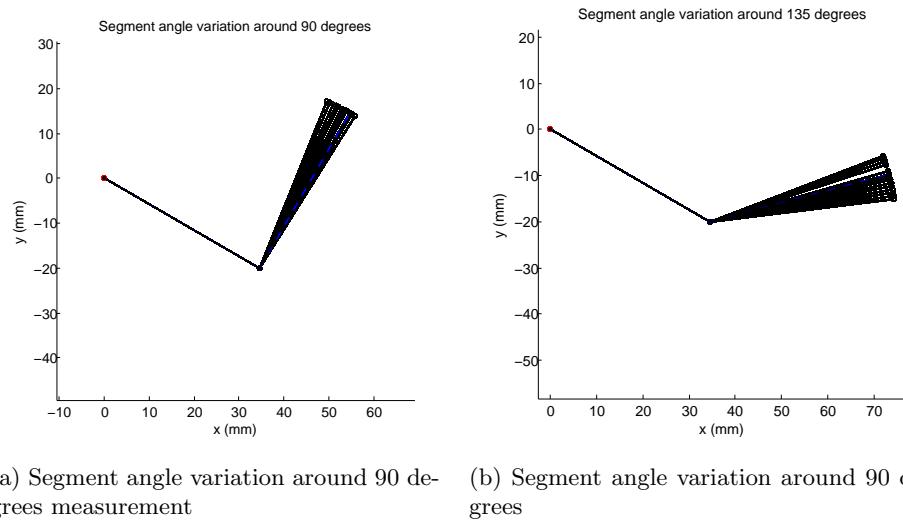


Figure 4.2: Plot showing the segment angle variations from 2500 samples per reference angle.

4.1.2 Analysis & Discussion

Ultimately, our goal is to estimate the angle, ϕ_i of each of the joints, $i = 1, \dots, N$. However, due to small errors in fabrication and magnet alignment, each sensor will have a bias, β_i , and due to small variations in measurement, there will be some amount of random error at each sampling. So, neglecting quantization errors, we model our sensor as providing a measurement, treated as a Gaussian random variable with mean $\phi_i + \beta_i$:

$$Y_i \sim \mathcal{N}(\phi_i + \beta_i, \sigma^2) \quad (4.2)$$

For our experiments, we selected $n_s = 5$ of these segments at random. We assumed that the variance was the same for each sensor. Also, while ultimately each of the biases could be individually estimated and corrected for, we chose to estimate the total mean-squared error (MSE). For the purposes of the essay this employed approach will compute the expected PDFs of the tip of the antenna. This is essentially like assuming that an antenna was constructed from a random sampling of segments, so that the biases can be treated like part of the random sampling error, thus providing a prediction of performance for a coarsely calibrated antenna.

As the internal angle sensor sampling frequency is much higher than the I²C transfer frequency, we can assume that all sampled angle values ϕ_{ij} are independent measurements. Thus the sampled mean $\bar{\phi}_i = \hat{\phi}_i$ of each segment (4.3) is an estimator for the reference angle ϕ_i . So consequently $E[\hat{\phi}_i] = \phi_i$ would correspond to a perfect accuracy, i.e. $\beta_i = 0$. In this sense any deviations from this equality is the bias of the estimator and will be noted as the accuracy error of the segment around the associated reference angle ϕ_i . We computed this accuracy error for five known angles in order to profile the change of accuracy from 90° to 270° (Table 4.1a – Table 4.1e). Since our calibration was done by fixing the relative angle between two joints at 180°, we expect the accuracy to be highest at that angle. Summarizing:

$$\hat{\phi}_i = \frac{1}{n} \sum_{j=1}^n \phi_{ij} \quad (4.3)$$

$$\text{Accuracy} = \text{bias}[\hat{\phi}_i] = E[\hat{\phi}_i] - \phi_i = \beta_i \quad (4.4)$$

A final accuracy metric is performed by taking account all five segments and computing the mean $\bar{\phi}$ and bias (Table 4.1a – 4.1e) over all segments and all angles. As this metric represents an overall bias for a given reference angle, it can be considered as a systematic error likely due to magnet misalignment with the sensor. If desired, these errors can be compensated for on a segment-by-segment basis at the software level.

Precision of each sampled segment is a measure of how dispersed the individual angle measurements are from the mean value. Thus by definition the standard deviation (4.5) σ_i

Segment	Mean $\bar{\phi}_1$	Bias β_1	Std. Error σ_1	Mean $\bar{\phi}_2$	Bias β_2	Std. Error σ_2
1	90.00	0.00	1.26	130.67	-4.33	0.76
2	85.33	-4.67	2.18	138.49	3.49	2.87
3	86.12	-3.88	0.61	132.80	-2.20	0.98
4	89.26	-0.74	0.86	140.70	5.70	1.84
5	87.64	-2.36	0.79	135.34	0.34	1.44
Average	87.67	-2.33	1.28	135.60	0.60	1.75

(a) Segment performance for 90°

(b) Segment performance for 135°

Segment	Mean $\bar{\phi}_3$	Bias β_3	Std. Error σ_3	Mean $\bar{\phi}_4$	Bias β_4	Std. Error σ_4
1	181.12	1.12	0.75	224.79	-0.21	1.49
2	179.07	-0.93	0.89	230.42	5.42	1.50
3	179.87	-0.13	0.33	225.09	0.09	1.30
4	178.86	-1.14	0.72	232.51	7.51	1.81
5	180.15	0.15	0.72	226.63	1.63	0.74
Average	179.81	-0.19	0.71	227.89	2.89	1.41

(c) Segment performance for 180°

(d) Segment performance for 225°

Segment	Mean $\bar{\phi}_5$	Bias β_5	Std. Error σ_5
1	276.10	6.10	0.73
2	272.18	2.18	1.82
3	272.99	2.99	1.22
4	275.00	5.00	0
5	272.99	2.99	1.22
Average	273.85	3.85	1.17

(e) Segment performance for 270°

Table 4.1: Segment Accuracies and precisions around 90°, 135°, 180°, 225° and 270°. All units are in degrees.

of the measurements provides a measure of precision of an individual segment at a given reference angle. We can also determine the variations s^2 of the standard deviations σ_i to quantify how the precision changes from 90° to 270° (4.6). The results are presented in Table 4.2.

90°	135°	180°	225°	270°
0.61	0.81	0.20	0.38	0.66

Table 4.2: Variance of segment standard errors s^2 per reference angle.

Finally we can define a general average precision of all the *sampled* segments for a given reference angle. For that we concatenate all angle measurements corresponding to the same reference angle and compute the standard error (Table 4.1a – Table 4.1e). With the knowledge of the variances of the standard errors computed earlier, the total sample standard errors also give us a good idea about the overall precision.

$$\sigma_i = \sqrt{\frac{1}{n} \sum_{j=1}^n (\phi_{ij} - \bar{\phi}_i)^2} \quad (4.5)$$

$$s^2 = \frac{1}{n_s - 1} \sum_{i=1}^{n_s} (\sigma_i - \bar{\sigma}_i)^2 \quad (4.6)$$

As a measure of the average measurement error for all segments and all angles, we can determine the *mean squared error* (4.7). For the bias and variance components of MSE, we choose the mean of the biases and the maximum of the standard errors of all angles and segments respectively. Then,

$$\begin{aligned} \text{MSE} &= \beta^2 + \sigma^2 \\ &= \frac{1}{n_s} \sum_{i=1}^{n_s} (\text{bias}[\hat{\Phi}_i])^2 + \max(\sigma^2) \\ \bar{\beta} &= \frac{-2.33 + 0.6 + 0.19 + 2.89 + 3.85}{5} = 1.04^\circ \end{aligned} \quad (4.7)$$

$$\text{MSE} = 1.04^2 + 1.75^2 = 4.14^\circ$$

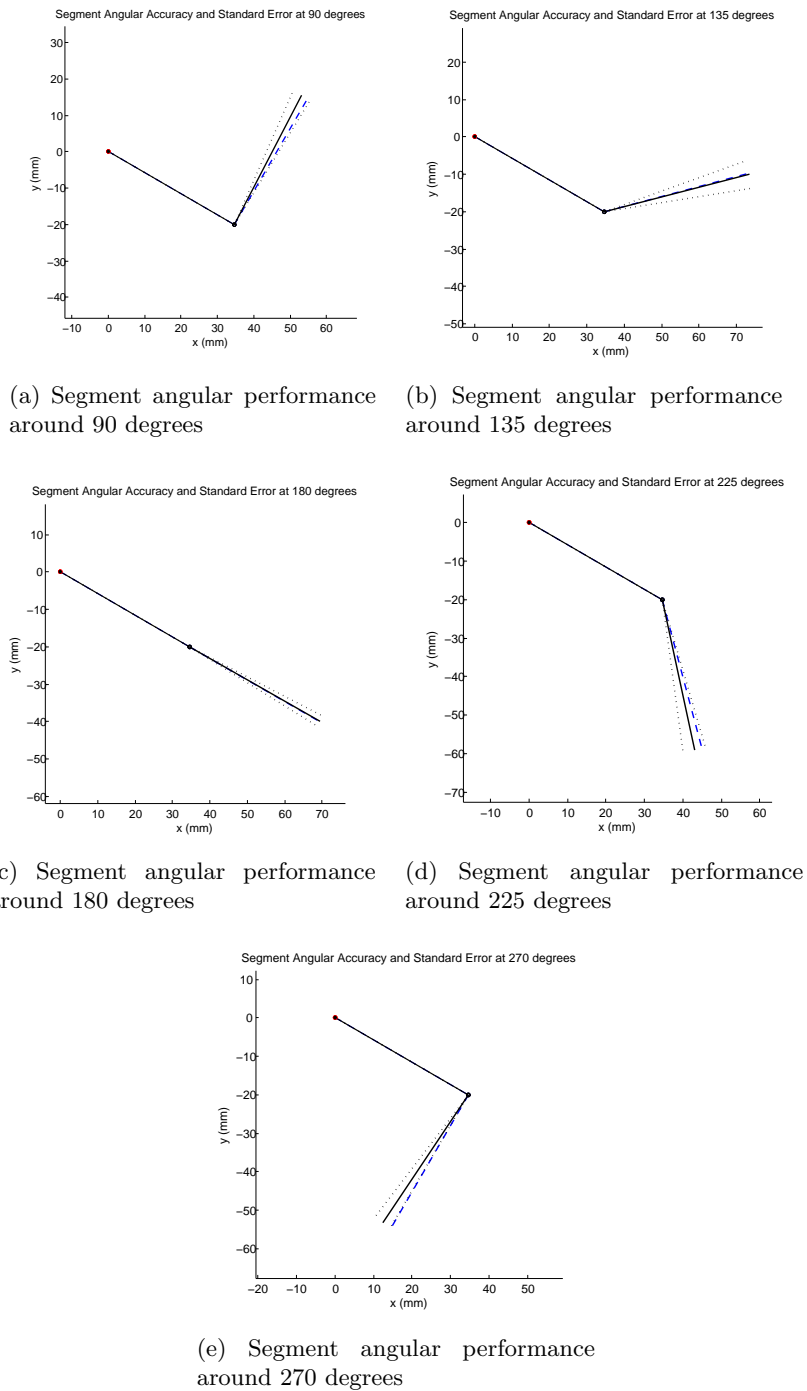


Figure 4.3: Plots showing the bias and standard error of sampled segments. *Dashed*: The reference angle. *Dotted*: $3 \times$ angular standard error margins, encompassing almost all angle variations for the corresponding reference angle. *Solid (Black)* angle associated with the mean of the samples.

gives us a reasonable error quantity for a given measured angle by each segment.

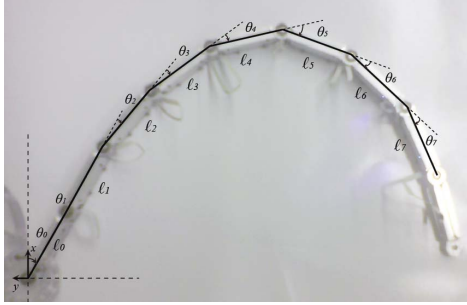
4.2 Angular Error Propagation

The following set of experimental trials were conducted with the intent of characterizing the propagation of angle measurement errors from the first to last segment.

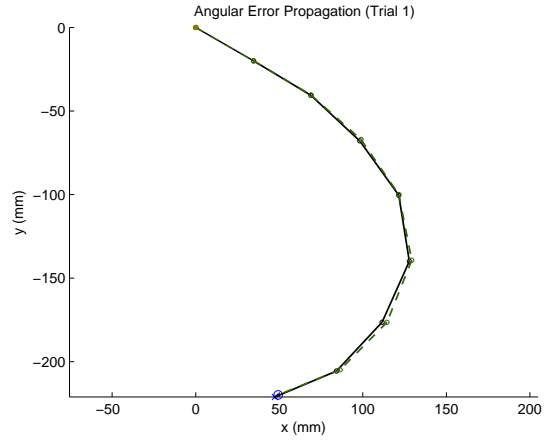
4.2.1 Setup & Procedure

- An antenna arrangement of 7 segments was used.
- For all trials the antenna rested on a flat surface.
- For each trial a random shape was imposed to the antenna.
- A photo of the antenna was taken with a digital camera from top for establishing a reference for ground truth angle measurements.
- For all trials the antenna base angle was fixed at -30° from the x-axis.
- 100 angles measurements were sampled and their mean was used for each joint.
- For each trial, the antenna image was traced via Adobe IllustratorTM. Angles $\theta_0, \theta_1, \dots, \theta_7$ in degrees and segment lengths l_0, l_1, \dots, l_7 are measured in points.
- The variance of the segment lengths were used to indicate the optical distortions and digital tracing errors.
- The angles extracted from the image were compared with the mean of the angle measurement samples.
- For each trial, a figure showing the manual image tracing and antenna shape deviation was presented.

4.2.2 Trial 1



(a) Trial 1 - Photo vector tracing for true angle measurement



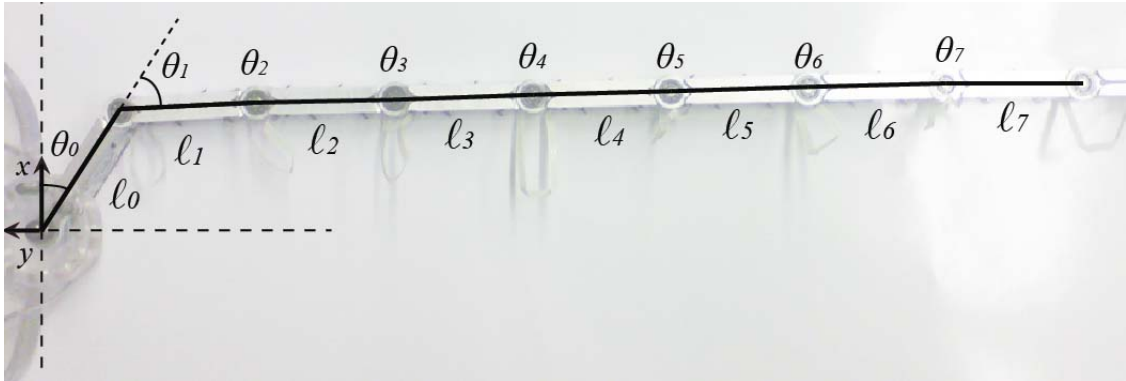
(b) *Dashed*: Based on angles from image tracing. *Solid*: Based on antenna sensor output

Figure 4.4: Antenna angular error propagation characteristics, Trial-1.

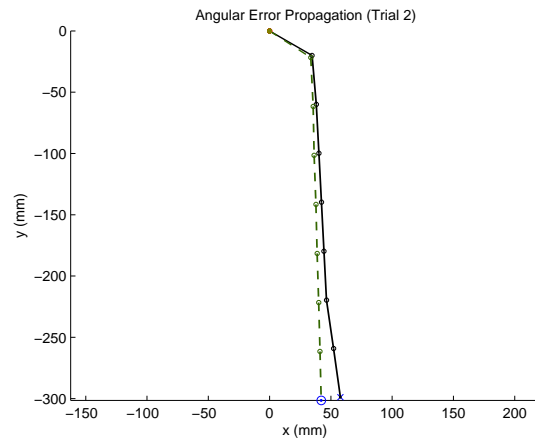
True Angles θ_i	Means of Measured Angles $\tilde{\theta}_i$	Angular Error ϵ_i
-29.94°	-30.00°	-0.06°
-0.84°	-1.00°	-0.16°
-10.92°	-12.00°	-1.08°
-13.78°	-11.37°	2.41°
-23.38°	-26.47°	-3.09°
-32.82°	-33.21°	-0.39°
-22.98°	-19.00°	3.98°
-23.27°	-24.13°	-0.86°

Table 4.3: Antenna angular error propagation characteristics, Trial-1.

4.2.3 Trial 2



(a) Trial 2



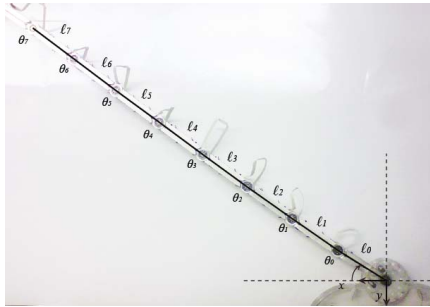
(b) *Dashed*: Based on angles from image tracing. *Solid*: Based on antenna sensor output

Figure 4.5: Antenna angular error propagation characteristics, Trial-2.

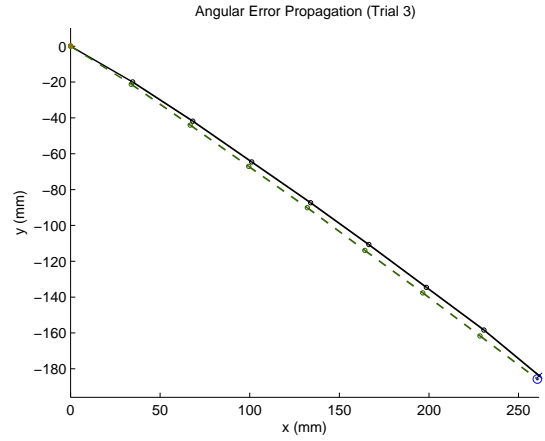
True Angles θ_i	Means of Measured Angles $\tilde{\theta}_i$	Angular Error ϵ_i
-32.80°	-30.00°	2.80°
-54.49°	-55.00°	-0.51°
-1.54°	-2.00°	-0.46°
0.90°	0.00°	-0.90°
-0.59°	0.00°	0.59°
0.31°	-0.06°	-0.37°
-0.31°	5.31°	5.62°
0.00°	-0.22°	-0.22°

Table 4.4: Antenna angular error propagation characteristics, Trial-2.

4.2.4 Trial 3



(a) Trial 3 - Photo vector tracing for true angle measurement



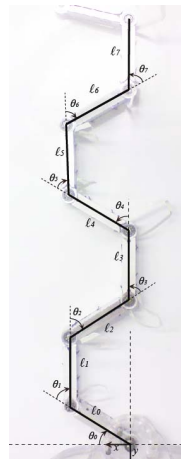
(b) *Dashed*: Based on angles from image tracing. *Solid*: Based on antenna sensor output

Figure 4.6: Antenna angular error propagation characteristics, Trial-3.

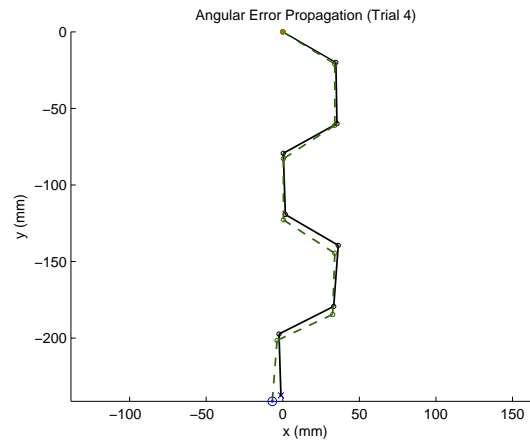
True Angles θ_i	Means of Measured Angles $\tilde{\theta}_i$	Angular Error ϵ_i
-32.04°	-30.00°	2.04°
-2.72°	-3.00°	-0.28°
-0.43°	-1.71°	-1.28°
0.00°	0.00°	0.00°
-1.38°	-1.00°	0.38°
0.36°	-0.85°	-1.21°
-0.76°	0.00°	0.76°
0.00°	-3.17°	-3.17°

Table 4.5: Antenna angular error propagation characteristics, Trial-3.

4.2.5 Trial 4



(a) Trial 4



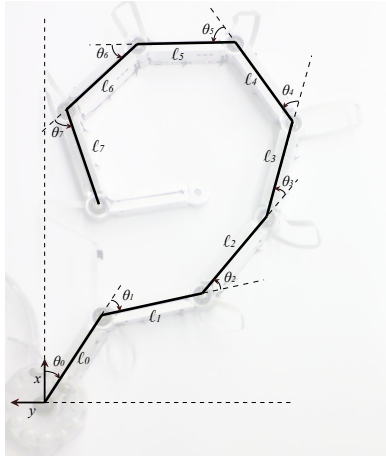
(b) *Dashed*: Based on angles from image tracing. *Solid*: Based on antenna sensor output

Figure 4.7: Antenna angular error propagation characteristics, Trial-4.

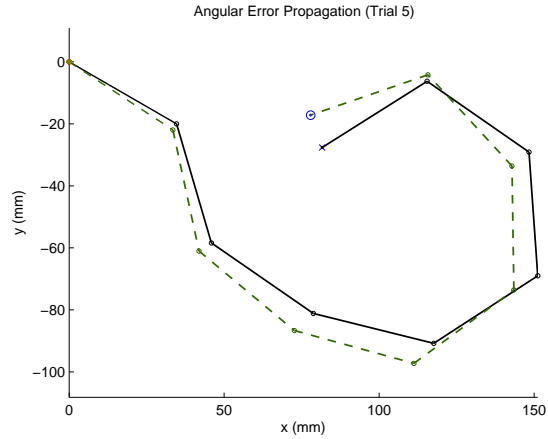
True Angles θ_i	Means of Measured Angles $\tilde{\theta}_i$	Angular Error ϵ_i
-31.85°	-30.00°	1.85°
-58.15°	-59.00°	-0.85°
-57.15°	-62.09°	-5.02°
57.07°	63.00°	5.93°
57.07°	57.85°	0.78°
-59.12°	-64.00°	-4.88°
-62.99°	-59.00°	3.99°
60.56°	64.96°	4.40°

Table 4.6: Antenna angular error propagation characteristics, Trial-4.

4.2.6 Trial 5



(a) Trial 5 - Photo vector tracing for true angle measurement



(b) *Dashed*: Based on angles from image tracing. *Solid*: Based on antenna sensor output

Figure 4.8: Antenna angular error propagation characteristics, Trial-5.

4.2.7 Analysis

The contact sensing accuracy of the antenna also depends on its global configuration, which we have shown experimentally. This can also be shown mathematically. Assume that the antenna with N segments can only sense contacts at the joints and the segment lengths l are identical. Then the position coordinates x, y of each possible contact location can be

True Angles θ_i	Means of Measured Angles $\tilde{\theta}_i$	Angular Error ϵ_i
-33.2°	-30.00°	3.20°
-44.6°	-43.68°	0.92°
38.0°	39.00°	1.00°
24.4°	20.72°	-3.68°
51.7°	47.00°	-4.7°
54.6°	61.00°	6.4°
41.8°	51.20°	9.4°
66.3°	67.00°	0.7°

Table 4.7: Antenna angular error propagation characteristics, Trial-5.

expressed using forward kinematics (Figure 4.9) with respect to the base joint (x_0, y_0) as

$$\begin{aligned}
 \begin{bmatrix} x_k \\ y_k \end{bmatrix} &= l \begin{bmatrix} \cos \phi_1 + \cos(\phi_1 + \phi_2) \cos(\phi_1 + \phi_2 + \phi_3) + \dots + \cos(\phi_1 + \phi_2 + \dots + \phi_k) \\ \sin \phi_1 + \sin(\phi_1 + \phi_2) \sin(\phi_1 + \phi_2 + \phi_3) + \dots + \sin(\phi_1 + \phi_2 + \dots + \phi_k) \end{bmatrix} \\
 &= \sum_{i=1}^k l \begin{bmatrix} \cos \sum_{j=1}^i \phi_j \\ \sin \sum_{j=1}^i \phi_j \end{bmatrix}
 \end{aligned} \tag{4.8}$$

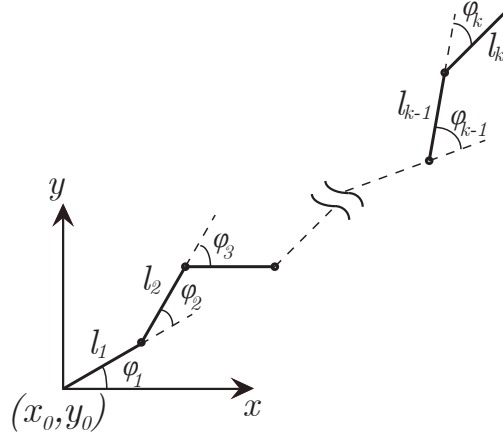


Figure 4.9: The first k -segments of an N -segment antenna

The Jacobian of this planar forward kinematics (4.10) can be interpreted as a mapping from the joint velocity space to the k^{th} segment configuration space. So the average small angular mean squared error (MSE) of the segments, which incorporates both the bias and

the variance, can be used to create a “landing area” bound for the tip of the final segment. We transform the angular MSE in the joint space to an ellipse in the work space that depicts a probable area for the tip of the final segment. As we treat the MSE like a variance measure without bias, \sqrt{MSE} becomes a de facto standard error:

$$J = \begin{bmatrix} \frac{\partial x}{\partial \phi_1} & \cdots & \frac{\partial x}{\partial \phi_k} \\ \frac{\partial y}{\partial \phi_1} & \cdots & \frac{\partial y}{\partial \phi_k} \end{bmatrix} \quad (4.9)$$

$$J = \begin{bmatrix} \sum_{i=1}^k -\sin \sum_{j=1}^i \phi_j & \sum_{i=2}^k -\sin \sum_{j=1}^i \phi_j & \cdots & \sum_{i=k}^k -\sin \sum_{j=1}^i \phi_j \\ \sum_{i=1}^k -\cos \sum_{j=1}^i \phi_j & \sum_{i=2}^k -\cos \sum_{j=1}^i \phi_j & \cdots & \sum_{i=k}^k -\cos \sum_{j=1}^i \phi_j \end{bmatrix} \quad (4.10)$$

Note that this tip location estimation by no means indicate that the probability of the tip landing is the same for all points in the ellipse. A more rigorous work has been done by Wang et al. [49] for creating a probability distribution which shows the error propagation in a much precise manner. The analysis of the error propagation using the described method in Wang et al. is a future goal.

4.3 Communication Performance

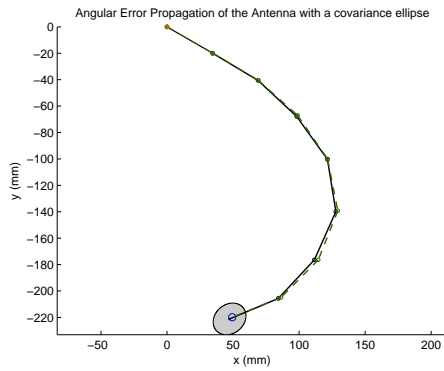
This section presents the I²C bandwidth usage of the antenna. Specifically, we determined the theoretical limit for the I²C and compared it with our experimental data. The list below describes the procedure of our experiment.

4.3.1 Procedure

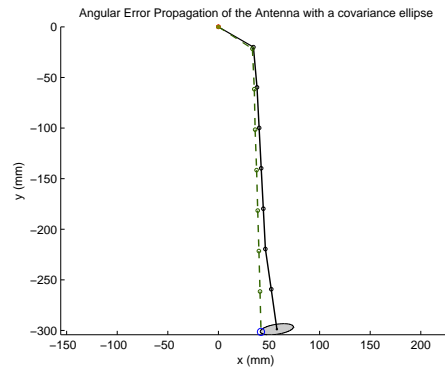
- A 7-segment antenna is connected to a 600 MHz Gumstix¹ Verdex Pro embedded computer package² running on a 2.6.27 Linux kernel.
- At each trial we reduced the number of segments by one. Therefore a total of 7 trials

¹<http://www.gumstix.com/>

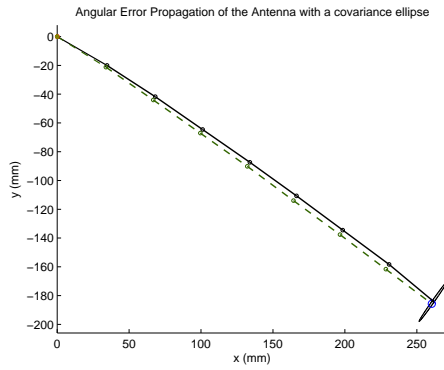
²<http://www.acroname.com/robotics/parts/R321-VERDEX-PRO-PKG.html>



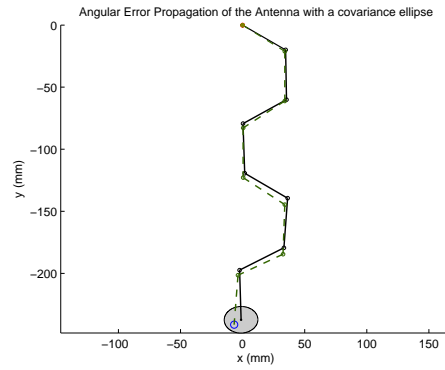
(a) Trial-1 *Dashed*: Based on angles from image tracing. *Solid*: Based on antenna sensor output



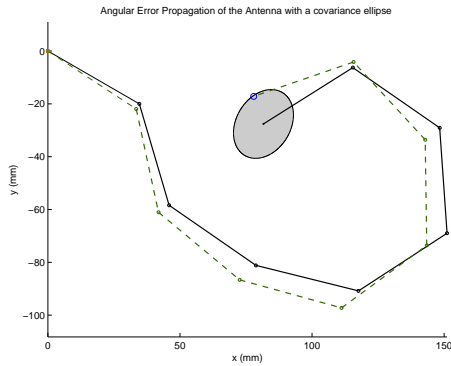
(b) Trial-2 *Dashed*: Based on angles from image tracing. *Solid*: Based on antenna sensor output



(c) Trial-3 *Dashed*: Based on angles from image tracing. *Solid*: Based on antenna sensor output



(d) Trial-4 *Dashed*: Based on angles from image tracing. *Solid*: Based on antenna sensor output



(e) Trial-5 *Dashed*: Based on angles from image tracing. *Solid*: Based on antenna sensor output

Figure 4.10: Error propagations depicted by covariance ellipse covering 3 magnitudes of \sqrt{MSE} .

were conducted.

- At each trial we collected 10 sets of data.
- Each set of data consists of $N = 1000$ angle measurements.
- During this sampling process, the time was kept using the standard Unix *gettimeofday()*³ function. We recorded the time right before and right after of the sampling process. The difference of the two timestamps are computed in microseconds and divided by the number of samples (1000).
- The sampling frequency was computed for comparing the performance variance of different length antennae.
- The communication between the host computer and the antenna segments slow down considerably. Thus those cases are discarded. Out of the 70 samplings, such errors occurred only 3 times.

The data regarding for each number of segments is presented in the following table. The mean frequencies are also provided in the last row (Table 4.1a).

Number of Segments	7	6	5	4	3	2	1
	155.394	181.084	216.062	268.177	353.152	515.842	964.949
	155.353	180.972	216.021	268.122	353.050	516.305	964.457
	155.335	181.133	215.962	268.038	353.154	516.109	968.090
	155.391	181.057	215.998	268.091	353.324	515.729	964.793
	155.350	181.113	215.961	268.128	352.879	515.985	964.713
	155.436	181.070	215.956	268.074	353.492	515.827	964.609
	155.876	181.039	216.065	268.181	353.150	515.932	965.093
	155.088	181.070	215.998	268.14	353.278	515.919	964.507
	155.400	181.097	216.015	268.069	353.132	516.165	963.713
	155.426	181.089	216.005	268.405	353.246	516.111	964.213
Mean Frequencies	155.405	181.072	216.004	268.143	353.186	515.992	964.914

Table 4.8: Sampling frequency data.

³<http://linux.die.net/man/3/gettimeofday>

4.3.2 Analysis

We know that the I²C bus capacity is independent of the number of segments. Thus adding one segment to the antenna should cause a proportional amount of more data to be sent and received from the bus. For example if one segment sends and receives 1 byte of data from the bus, then the total data sent and received from two segments would be 2 bytes. So the sample frequency value should follow a sequence of $f = x\frac{1}{n}$ where $n > 0$ is the number of segments (Figure 4.12).

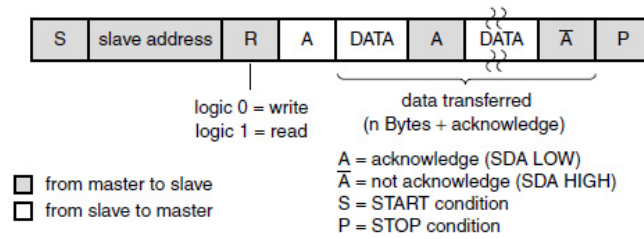


Figure 4.11: I²C protocol for slave transmitter mode (Image credit: [39]).

The frequency can also be computed theoretically from the I²C protocol specifications. As we specified in the design section, the segments are treated as slave devices where the master is the host computer. When a *read* command is issued by our program to one of the segments, then the corresponding data exchange is given in the user manual [39] of our microcontroller’s family (Figure 4.12). From the figure we see that there is always an address byte and an acknowledgement bit that is sent before the actual data. We also see that after each byte of data transmission, there is another bit of acknowledgement. Our segment sends two bytes each time it is addressed. So we get:

$$\begin{aligned}
 \text{Total bits per sample} &= \text{address byte} \times 8 \frac{\text{bits}}{\text{byte}} + \text{ack. bit} + 2\text{bytes} \times 8 \frac{\text{bits}}{\text{byte}} + \text{ack. bit} \\
 &= 26\text{bits}
 \end{aligned}
 \tag{4.11}$$

We also set the I²C bus transfer rate of the microcontroller to 100kbps [39]. Consecutively this yield to theoretical frequency of $\frac{100000}{26} = 3846Hz$ for our I²C setting. Hence it seems

that the speed can be improved by almost fourfold. The experimental values and the upper bound for the I²C transfer rate is depicted below (Figure 4.12).

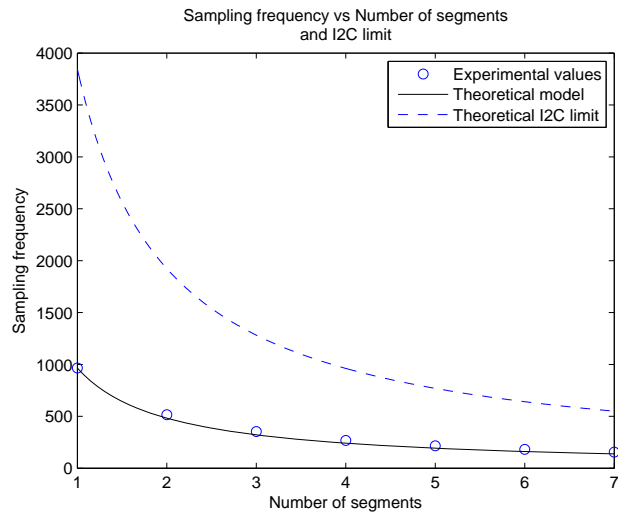


Figure 4.12: As expected, as the number of segments are doubled, the speed halves.

This performance testing indicates that our design can sample angles at around 100 Hz which is considered good by the temporal resolution criterion of Harmon we mentioned in the previous chapter.

Chapter 5

Conclusions and Future Work

In this essay we described a novel tactile antenna design for the purpose of exploring the mechanics of antennal tactile sensing. We also laid the groundwork of a general antennal sensing framework and an overall definition for similar devices in order to make future classifications of such developments easier.

Further work for this project will continue in two parallel tracks: one for scientific research and one for engineering development. The first track will entail the extensive utilization of the tactile antenna to test various hypotheses regarding biology. As addressed earlier in this essay, our first milestone be the testing of the effects of the distally pointing spines. We observe from cockroaches that their antennae flip backwards during wall following if the flagellum tip is pointed forward. We hypothesize that the distally pointing hairs (sensilla Chaetica B), which are distributed along the entire flagellum, significantly enhance this phenomenon. Our reasoning behind this hypothesis is that when the flagellum is pointed toward the cockroach's running direction, then the tips of the distally pointing hairs would sweep the rough surface of the wall like an "anchor". This eventually would cause the spines to get stuck in the irregularities of the wall and ultimately force the antenna to buckle and bend backwards as the cockroach continues to move forward. The structure of our new antenna constitutes a suitable platform to test this hypothesis.

The development part of the project aims to further advance the antenna. In particular

we would like to have the antenna flex not only on the horizontal plane, but also along the sagittal plane for characterizing 3D aspects of the environment. Another improvement we are seeking is to minimize the mechanical effects of the electrical couplings between the joints such that they do not introduce additional stiffness.

We also would like to investigate the other possible implementations of the antenna as a tactile sensor. One feasible implementation would be to continue on Kutcher's work regarding tactile mapping. Another topic of utilization is in simultaneous localization and mapping (SLAM) [11]. In this context a host robot mounted with our antennae would collect repeated spatial tactile information about an unknown environment, and later locate itself based on the tactile information it gathered up until that point. Efforts of integrating the antenna to legged platforms constitute a work in progress, which would allow us to investigate antenna based robot control under more complex locomotion schemes.

Besides its scientific value, our new antenna presents new opportunities for applied robotics, especially considering the potential applications where traditional navigational instruments are insufficient or undesirable. For example active sensors like sonar and vision exhibit sensitivity to surface reflectivity and lighting conditions [24]. In particular sonar performance degrades in the presence of highly polished surfaces such as glass walls and at very close proximities; vision fails without adequate light [24] and similarly infrared sensors – like sonars – have a minimum range below which they become unreliable. Our tests showed that bio-inspired tactile antennae offer an alternative, near-future, robust solution where reliable robotic navigation is crucial but the limitations mentioned above may pose problems. Such areas of applications include emergency search and rescue, military operations in urban terrain, seafloor navigation and space exploration.

Bibliography

- [1] J. Adis. Thirty million arthropod species-too many or too few? *Journal of Tropical Ecology*, 6(1):115–118, 1990.
- [2] G. Aloï. A new entomology display cabinet? *Antennae*, 2(3):4–9, Autumn 2007.
- [3] T. G. Barnes, T. Q. Truong, G. G. Adams, and N. E. McGruer. Large deflection analysis of a biomimetic lobster robot antenna due to contact and flow. *Journal of Applied Mechanics*, 68:948, 2001.
- [4] G. K. Bigley. Sensation. In H. K. Walker, W. D. Hall, and J. W. Hurst, editors, *Clinical Methods: The History, Physical, and Laboratory Examinations*. Butterworth Publishers, 3 edition, July 1990.
- [5] J. M. Camhi and E. N. Johnson. High-frequency steering maneuvers mediated by tactile cues: antennal wall-following in the cockroach. *J Exp Biol*, 202(5):631–643, 1999.
- [6] J. L. Castner. General entomology and arthropod biology. In J. H. Byrd and J. L. Castner, editors, *Forensic Entomology: The Utility of Arthropods in Legal Investigations*. CRC, 1 edition, September 2000.
- [7] R. F. Chapman. *The Insects: Structure and Function*. Cambridge University Press, The Edinburgh Building, Cambridge CB2 2RU, UK, 4 edition, November 1998.
- [8] N. J. Cowan, E. J. Ma, M. Cutkosky, and R. J. Full. A biologically inspired passive antenna for steering control of a running robot. In *Proceedings of the 11th international*

- symposium on robotics research (ISRR 2003)*, 2003.
- [9] J. J. Crosnier. Grasping systems with tactile sense using optical fibers. *Robot Sensors*, 2:209–217, 1986.
- [10] J. Dargahi and S. Najarian. Human tactile perception as a standard for artificial tactile sensing—a review. *The International Journal of Medical Robotics and Computer Assisted Surgery*, 1(2):23–35, 2004.
- [11] A. De, J. Lee, N. Keller, and N. J. Cowan. Toward SLAM on graphs. In *Proceedings of the Workshop on the Algorithmic Foundations of Robotics (WAFR)*, 2008.
- [12] A. Demir and J. Riley. Human tactile perception as a standard for artificial tactile sensing. Johns Hopkins University, 530.651 Final Project Paper, July.
- [13] V. Dürr, Y. König, and R. Kittmann. The antennal motor system of the stick insect *carausius morosus*: anatomy and antennal movement pattern during walking. *Journal of Comparative Physiology A: Neuroethology, Sensory, Neural, and Behavioral Physiology*, 187(2):131–144, 2001.
- [14] T. L. Erwin. How many species are there?: Revisited. *Conservation Biology*, 5(3):330–333, 1991.
- [15] K. J. Gaston. The magnitude of global insect species richness. *Conservation Biology*, 5(3):283–296, 1991.
- [16] R. C. Gauthier and C. Ross. Theoretical and experimental considerations for a single-mode fiber-optic bend-type sensor. *Applied optics*, 36(25):6264–6273, 1997.
- [17] D. A. Grimaldi and M. S. Engel. *Evolution of the Insects*. Cambridge University Press, 40 West 20th Street, New York, NY 10011, May 2005.
- [18] L. D. Harmon. Automated Tactile Sensing. *The International Journal of Robotics Research*, 1(2):3–32, 1982.

- [19] K. Ilango. Morphological characteristics of the antennal flagellum and its sensilla chaetica with character displacement in the sandfly *Phlebotomus argentipes* Annandale and Brunetti sensu lato (Diptera: Psychodidae). *J. Biosci*, 25(2):163–172, 2000.
- [20] M. Kaneko, N. Kanayama, and T. Tsuji. Active antenna for contact sensing. *Robotics and Automation, IEEE Transactions on*, 14(2):278–291, Apr 1998.
- [21] D. Kindersley. Overhead view of an american cockroach. <http://www.dkimages.com/discover/DKIMAGES/Discover/Home/Animals/Invertebrates/Arthropods/Insects/Cockroaches/Common-Cockroaches/American-Cockroach/American-Cockroach-4.html>, 2009.
- [22] R. L. Klatzky and S. J. Lederman. Touch. In A. F. Healy, R. W. Proctor, and I. B. Weiner, editors, *Experimental Psychology*, volume 4, pages 147–176. Wiley, 5 edition, January 2003.
- [23] B. L. Kutcher. Mapping and following walls using a mobile robot equipped with an antenna-like tactile sensor. Master’s thesis, Johns Hopkins University, 2004.
- [24] A. G. Lamperski, O. Y. Loh, B. L. Kutscher, and N. J. Cowan. Dynamical wall following for a wheeled robot using a passive tactile sensor. In *ICRA*, pages 3838–3843, 2005.
- [25] J. Lee. *Identifying Feedback Control Strategies Of Running Cockroaches and Humans*. PhD thesis, Johns Hopkins University, 2009.
- [26] J. Lee, O. Y. Loh, and Cowan N. J. A hierarchy of neuromechanical and robotic models of antenna-based wall following in cockroaches. In *Proceedings of the IEEE/RSJ International Conference on Intelligent Robots and Systems (IROS)*, 2007.
- [27] J. Lee, S. N. Sponberg, O. Y. Loh, A. G. Lamperski, and N. J. Cowan. Templates and anchors for antenna-based wall following in cockroaches and robots. *IEEE Transactions on Robotics*, 24(1):130–143, 2008.
- [28] M. H. Lee. Tactile sensing: new directions, new challenges. *The International Journal of Robotics Research*, 19(7):636, 2000.

- [29] M. H. Lee and H. R. Nicholls. Review article tactile sensing for mechatronics—a state of the art survey. *Mechatronics*, 9(1):1–31, 1999.
- [30] J. M. Loomis and S. J. Lederman. Tactual perception. In K. R. Boff, Kaufman L., and Thomas J. P., editors, *Cognitive Processes and Performance*, volume 2. Wiley-Interscience, 5 edition, January 1986.
- [31] J. C. Mankins. Technology Readiness Levels. Technical report, NASA, 1995.
- [32] R. M. May. How many species are there on earth? *Science*, 241(4872):1441–1449, 1988.
- [33] Melexis. *PMLX90316, Rotary Position Sensor IC*.
- [34] M. A. Neimark, M. L. Andermann, J. J. Hopfield, and C. I. Moore. Vibrissa resonance as a transduction mechanism for tactile encoding. *Journal of Neuroscience*, 23(16):6499–6509, 2003.
- [35] H. R. Nicholls and M. H. Lee. A survey of robot tactile sensing technology. *The International Journal of Robotics Research*, 8(3):3–30, 1989.
- [36] H. Nishino, M. Nishikawa, F. Yokohari, and M. Mizunami. Dual, multilayered somatosensory maps formed by antennal tactile and contact chemosensory afferents in an insect brain. *The Journal of Comparative Neurology*, 493(2), 2005.
- [37] J. Okada, Y. Morimoto, and Y. Toh. Antennal motor activity induced by pilocarpine in the American cockroach. *Journal of Comparative Physiology A: Neuroethology, Sensory, Neural, and Behavioral Physiology*, 195(4):351–363, 2009.
- [38] J. Okada and Y. Toh. Antennal system in cockroaches: a biological model of active tactile sensing. *International Congress Series*, 1269:57–60, 2004. Brain-Inspired IT I. Invited papers of the 1st Meeting entitled Brain IT 2004.
- [39] Philips Semiconductors. *P89LPC932A1 8-bit microcontroller with two-clock 80C51 core*.

- [40] Soennichsen R. In-system programming (isp) with the philips p89lpc932 microcontroller. Technical report, Philips Semiconductors.
- [41] D. C. Sandeman. Physical properties, sensory receptors and tactile reflexes of the antenna of the australian freshwater crayfish *cherax destructor*. *Journal of Experimental Biology*, 141(1):197–217, 1989.
- [42] R. Schafer and T. V. Sanchez. Antennal sensory system of the cockroach, *periplaneta americana*: postembryonic development and morphology of the sense organs. *The Journal of Comparative Neurology*, 149(3), 1973.
- [43] R. Schafer and T. V. Sanchez. The nature and development of sex attractant specificity in cockroaches of the genus *Periplaneta*. I. Sexual dimorphism in the distribution of antennal sense organs in five species. *Journal of Morphology*, 149(2):139–157, 1976.
- [44] D. Schneider. Insect antennae. *Annual Review of Entomology*, 9(1):103–122, 1964.
- [45] G. Seelinger and T. R. Tobin. Sense organs. In W. J. Bellm and K. G. Adiyodi, editors, *The American Cockroach*. Springer, 1 edition, December 1981.
- [46] L. Shyamal. Insect antenna forms. <http://bugguide.net/node/view/110081>, 2007.
- [47] E.M. Staudacher, M. Gebhardt, and V. Dürr. Antennal movements and mechanoreception: Neurobiology of active tactile sensors. In S. J. Simpson, editor, *Advances in Insect Physiology*. Academic Press, 1 edition, December 2005.
- [48] N. Ueno, M. M. Svinin, and M. Kaneko. Dynamic contact sensing by flexible beam. *Mechatronics, IEEE/ASME Transactions on*, 3(4):254–264, Dec 1998.
- [49] Y. Wang and G. S. Chirikjian. Large kinematic error propagation in revolute manipulators. In J. Lenarcic and R. B., editors, *Advances in robot kinematics: mechanisms and motion*. Springer, 1 edition, July 2006.
- [50] S. Ye, V. Leung, A. Khan, Y. Baba, and C. M. Comer. The antennal system and cockroach evasive behavior. I. Roles for visual and mechanosensory cues in the response.

Journal of Comparative Physiology A: Neuroethology, Sensory, Neural, and Behavioral Physiology, 189(2):89–96, 2003.

- [51] C. Zimmer. A pair of wings took evolving insects on a nonstop flight to domination. *The New York Times*, November 2005.

Appendix A

Notes

- All CAD models are designed and exported to u3d using *PTC's Pro Engineer Wildfire 4* through Johns Hopkins University educational licence.
- Exported 3D objects were converted in the pdf-ready U3D format with *PTC's Pro Engineer Wildfire 4* and assembled in a pdf with pdf \LaTeX and the movie15 package.
- The sensor characterization figures were generated and manipulated as vector graphics using *MATLAB R2007b*.
- This research is sponsored partially through a Summer 2006 PURA¹ grant and mainly by Professor Noah J. Cowan.
- This essay itself was prepared in *TeXnicCenter 1 Beta 7.5* using $\LaTeX 2_{\epsilon}$ typesetter through *MiKTeX 2.7*.

¹Provosts Undergraduate Research Award

Appendix B

Segment Part Models

(Aluminum Bottom Shell part)

Aluminum Bottom Shell part.

3D transformations are allowed when viewed with Acrobat Reader 7 or above.

(Aluminum Top Shell part)

Aluminum Top Shell part. Note that the slot has not been machined during the actual CNC operation to ease the manufacturing process

3D transformations are allowed when viewed with Acrobat Reader 7 or above.

(Aluminum Shell Assembly)

Aluminum Shell assembly (Exploded view).

3D transformations are allowed when viewed with Acrobat Reader 7 or above.

(Vertical Section of the Electronic Sub-assembly)

Vertical section of the electronic sub-assembly.

3D transformations are allowed when viewed with Acrobat Reader 7 or above.

(Horizontal Section of the Electronic Sub-assembly)

Horizontal section of the electronic sub-assembly.

3D transformations are allowed when viewed with Acrobat Reader 7 or above.

(Complete Segment (without hairs))

Complete Segment (without hairs).

3D transformations are allowed when viewed with Acrobat Reader 7 or above.

(2-Segment Antenna (without hairs))

2-Segment Antenna (without hairs).

3D transformations are allowed when viewed with Acrobat Reader 7 or above.

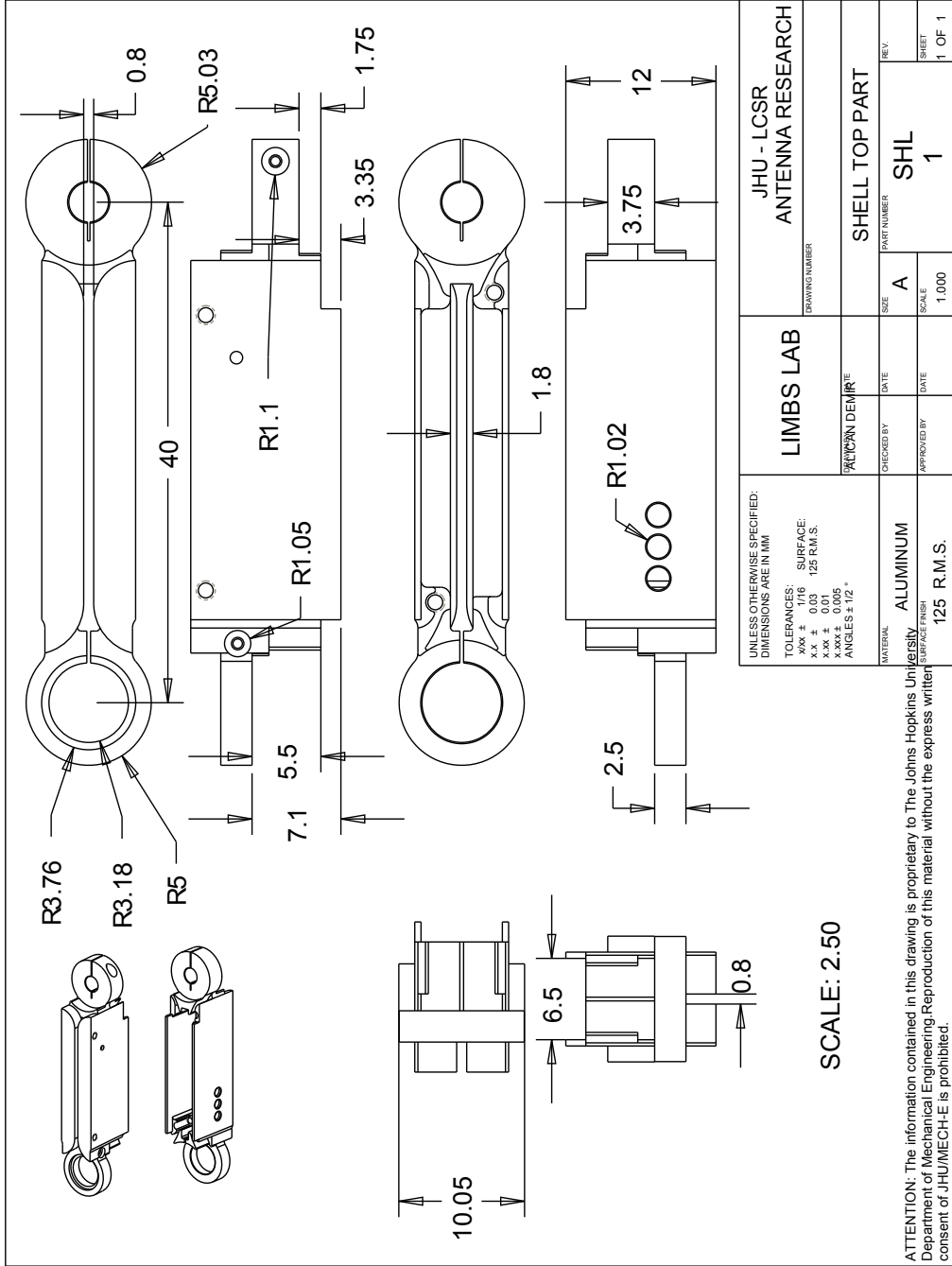
(Exploded view of the Segment Antenna (without hairs))

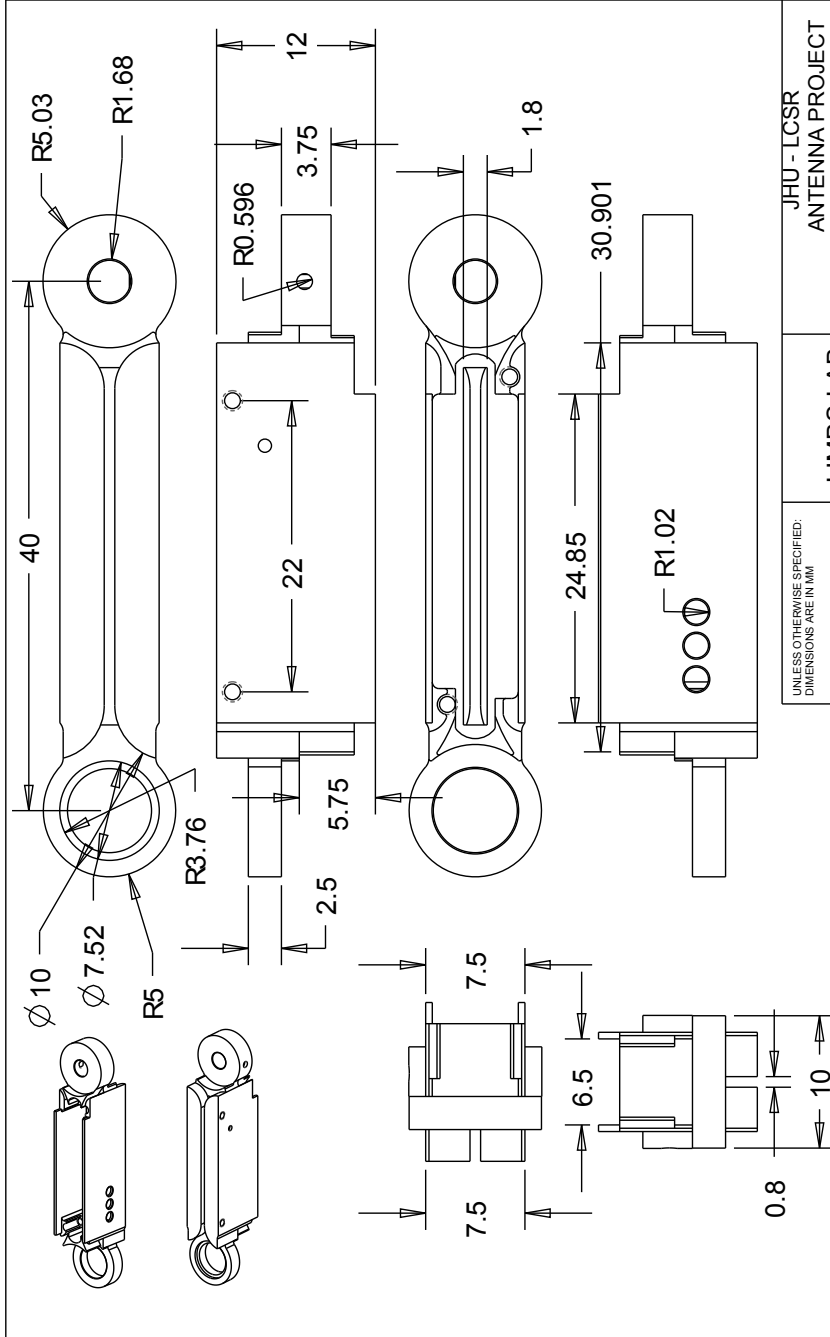
Exploded view of the Segment Antenna (without hairs).

3D transformations are allowed when viewed with Acrobat Reader 7 or above.

Appendix C

Segment - Engineering Drawings

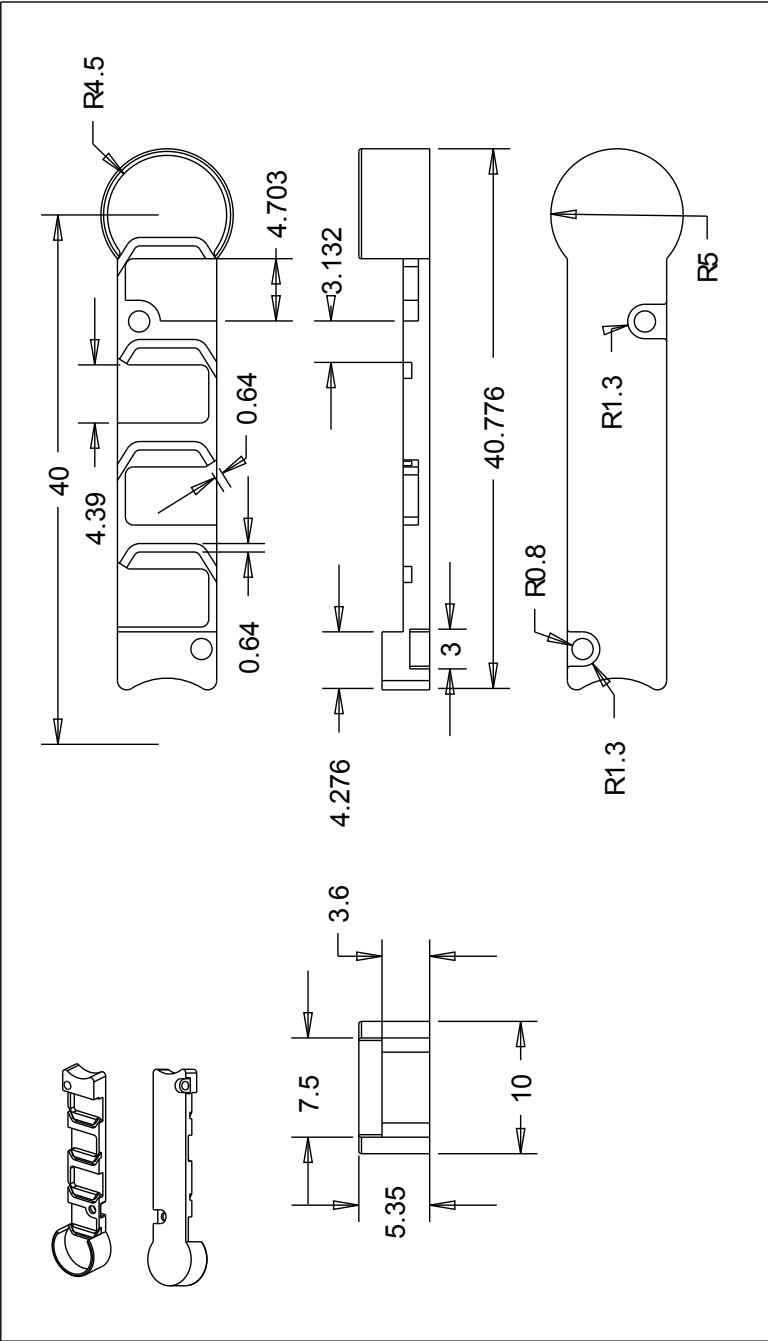




SCALE 2.500

UNLESS OTHERWISE SPECIFIED: DIMENSIONS ARE IN MM		JHU - LCSR ANTENNA PROJECT	
TOLERANCES: x.x ±0.03 SURFACE x.xx ±0.116 125 R.M.S. x.xxx ±0.005 x.xxxx ±0.005 ANGLES ± 1/2 °		DRAWING NUMBER 01	
MATERIAL ALUMINIUM		SHELL TOP PART revised	
DESIGNED BY ALICAN DEMIR	DATE	SIZE A	PART NUMBER SHL2
APPROVED BY	DATE	SCALE 1.000	SHEET 1 OF 1

ATTENTION: The information contained in this drawing is proprietary to The Johns Hopkins University Department of Mechanical Engineering. Reproduction of this material without the express written consent of JHU/MECH-E is prohibited.

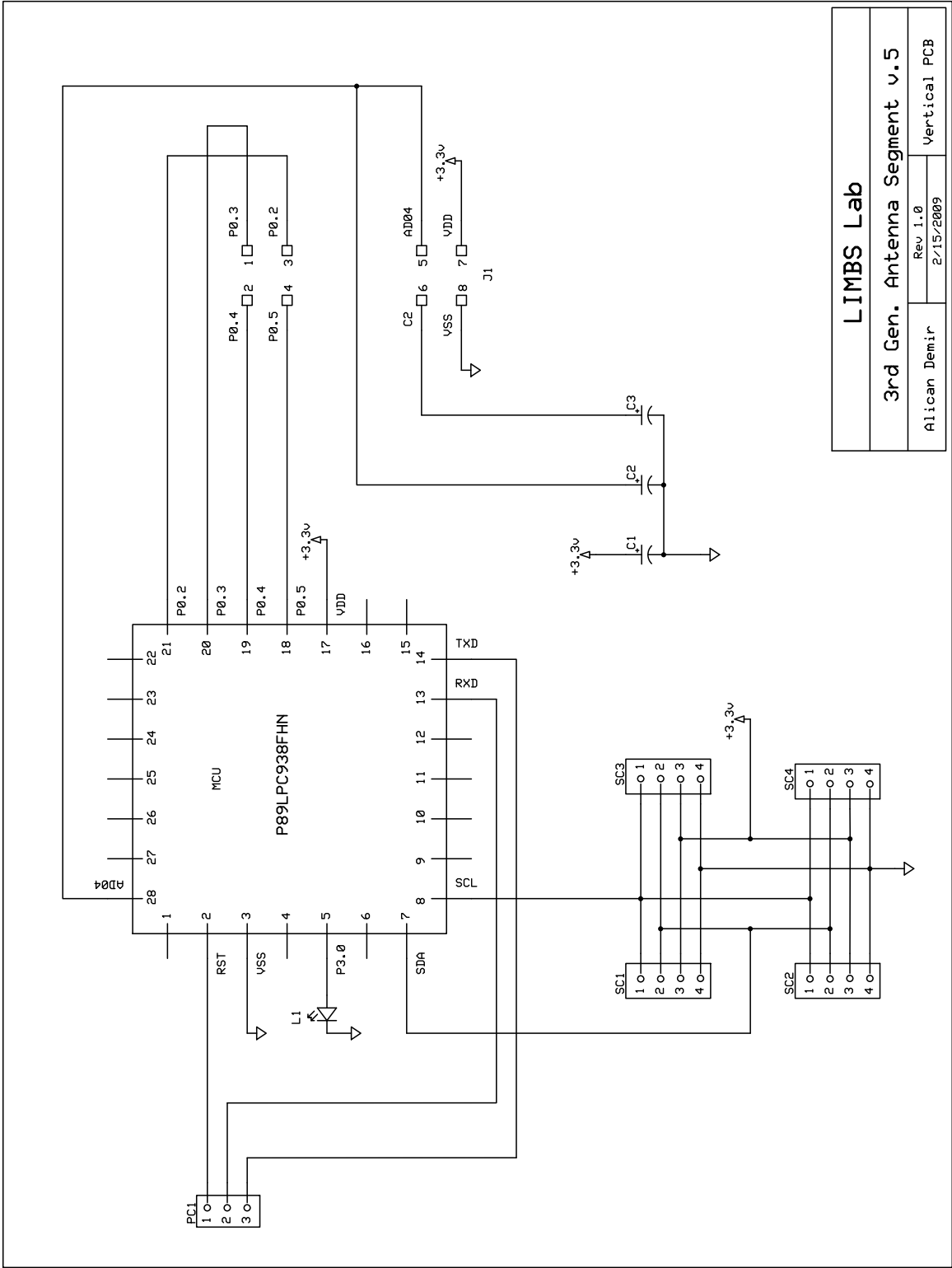


UNLESS OTHERWISE SPECIFIED: DIMENSIONS ARE IN INCHES TOLERANCES: XXX ±1/16 SURFACE X.X ±0.03 125 R.M.S. X.XX ±0.005 X.XXX ±0.0005 ANGLES ± 1/2 °	LIMBS LAB		JHU SR. DESIGN PROJECT 530.403	
	DRAWING NUMBER 01		DRAWING NUMBER 01	
MATERIAL ALUMINUM SURFACE FINISH 125 R.M.S.	DESIGNED BY ALICAN DEMIR	DATE	SIZE A	PART NUMBER SHL1
	APPROVED BY	DATE	SCALE 1,000	SHEET 1 OF 1

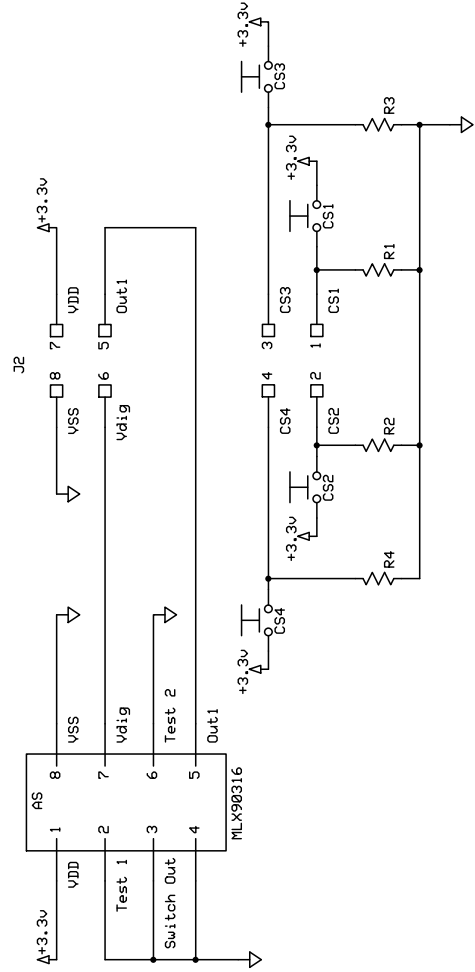
ATTENTION: The information contained in this drawing is proprietary to The Johns Hopkins University Department of Mechanical Engineering. Reproduction of this material without the express written consent of JHU/MECH-E is prohibited.

Appendix D

Segment - Circuit Diagram



LIMBS Lab	
3rd Gen. Antenna Segment v.5	
Alican Demir	Rev 1.0 2/15/2009
Vertical PCB	



LIMBS Lab	
3rd Gen. Antenna Segment v.5	
Alican Demir	Rev 1.0 2/14/2009
Horizontal PCB	

Appendix E

Segment - PCB Layouts

E.1 Vertical Section

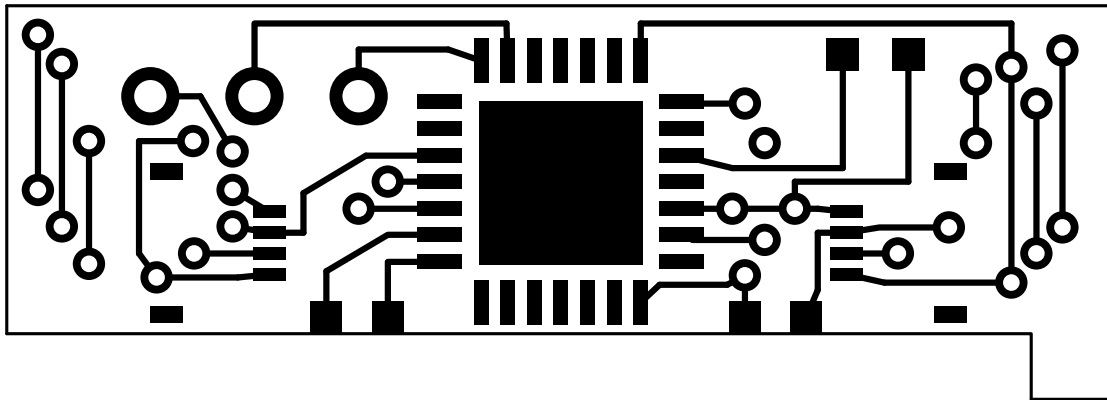


Figure E.1: PCB top layout of the vertical section of the segment.

E.2 Horizontal Section

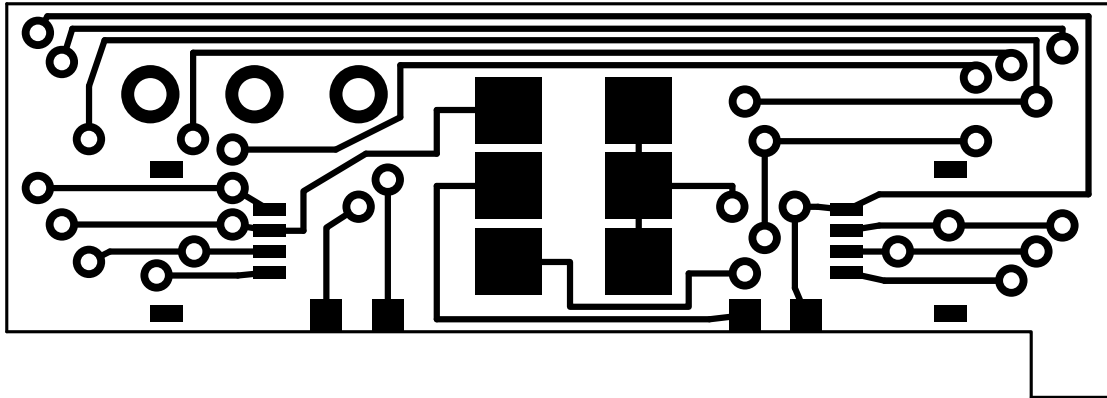


Figure E.2: PCB bottom layout of the vertical section of the segment.

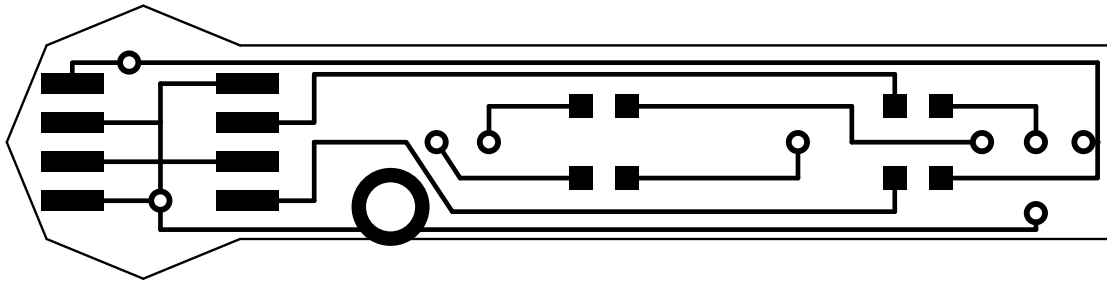


Figure E.3: PCB top layout of the horizontal section of the segment.

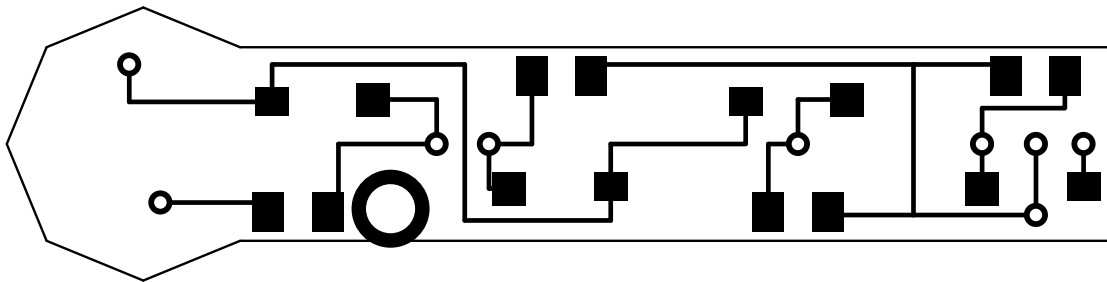


Figure E.4: PCB bottom layout of the horizontal section of the segment

Appendix F

Segment - Firmware

```
1 // Alican Demir
2 //
3 // 3rd Generation Antenna v.5
4 // Segment Code
5 //
6 // NXP (founded by Philips) P89LPC938-FHN
7 //
8 // v.3.0: 03.22.2009
9 // v.3.1: 03.23.2009
10 // v.3.2: 03.24.2009
11 // v.3.3: 04.20.2009
12 // v.3.4: 07.31.2009
13 // -----
14
15
16 #include <reg938.h>
17 #include <stdio.h>
18 /*=====ADC & Calibration Variables=====*/
19 // Highest ADC output (calibration)
20 unsigned int ADCmaxReading = 908;
21 // Lowest ADC output (calibration)
22 unsigned int ADCminReading = 109;
23 // Adjusted ADC output corresponding to 0 degrees
```

```

24 unsigned long ADCzeroOffset;
25 // ADC to Degree conversion factor
26 unsigned long ADCtoAngle;
27 // Segment angle in degrees
28 unsigned long angle;
29 // ADC 10-bit combined storage
30 unsigned long ADCreading = 0;
31
32
33 /*=====Touch Sensor Variables=====*/
34 // Touch Sensor Values Array
35 int Touch;
36
37 /*=====I2C Variables=====*/
38 // Set own 8-bit slave address. started: 11 (7bit 5),13,15...
39 int i2cSlaveAddr = 47;
40 // Command to be received
41 int i2cDataReceived = 0;
42 // Degree&Touch data LSB 8bits
43 unsigned short i2cDataLSB = 0;
44 // Degree&Touch data MSB 8bits
45 unsigned short i2cDataMSB = 0;
46 unsigned short segmentStatus;
47
48 int DEBUG = 0;
49
50 /*=====Delay Function=====*/
51 // The delay C function
52 static void delay (void) {
53     unsigned long i;
54     // waste timea and do nothing
55     for (i = 0; i < 6000; i++) {
56         ;
57     }
58 }
59

```

```

60
61 // Main Code
62 // -----
63 //
64 main()
65 {
66 unsigned int angleProblem = 0;
67 // binary converter counter
68 unsigned int i;
69 // SDA and SCL as Open-Drain
70 P1M1 = 0x0C;
71 P1M2 = 0x0C;
72 // INFO:
73 // The blue LED is connected to Pin      5 (P3.0) (XTAL2) (CLKOUT)
74 // Set the port to the Push-Pull mode to make it a current source.
75 // There are 4 modes:
76 //             - P3M1=0,P3M2=0 : Quasi-bidirectional
77 //             - P3M1=0,P3M2=1 : Push-Pull
78 //             - P3M1=1,P3M2=0 : Input Only (High Impedance)
79 //             - P3M1=1,P3M2=1 : Open Drain
80 // P3M1: Port 3 output mode 1
81 // P3M2: Port 3 output mode 2
82 P3M1 = 0;
83 P3M2 = 1;
84 // Source current to the LED from P3.0
85 P3 = 1;
86 for (i = 0; i < 10; i++) {
87 // waste timea and do nothing
88     delay();
89 }
90 // Cut current to the LED from P3.0
91 P3 = 0;
92 for (i = 0; i < 10; i++) {
93     delay();
94 }
95 // Enable general interrupt

```

```

96 EA = 1;
97
98 //          Serial Configuration
99 //
100 // initialize UART
101 SCON  = 0x52;
102 // 9600 baud, 8 bit, no parity, 1 stop bit      (C0 for TSSOP, F0 for PLCC)
103 BRGR0 = 0xF0;
104 // 9600 baud, 8 bit, no parity, 1 stop bit
105 BRGR1 = 0x02;
106 // Baud rate generator control
107 BRGCON = 0x03;
108
109
110 //          Angle Sensing Configuration
111 //
112 // INFO: The angle sensor is connected to Pin 28 (P1.7)(AD04)
113 //
114 // Special Function Register (SFR) "AD0INS" (ADC0 input select)
115 // bits :    7    6    5    4    3    2    1    0
116 // AD0INS: ADI07 ADI06 ADI05 ADI04 ADI03 ADI02 ADI01 ADI00
117 // Used  :      0    0    0    1    0    0    0    0 = 0x10
118 AD0INS = 0x10;
119 // Enable the Analog to Digital Converter (ENADC0 = 1)
120 // SFR "AD0CON" (ADC0 control register)
121 // bits :    7    6    5    4    3    2    1    0
122 // AD0CON: ENBI0 ENADCI TMM0 EDGE0 ADCI0 ENADC0 ADCS01 ADCS00
123 // Used  :      0    0    0    1    0    1    0    0 = 0x04
124 AD0CON = 0x04;
125 // A/D Converter Mode configuration B (bin: 01000000)
126 // bits :    7    6    5    4    3    2    1    0
127 // ADMODB: CLK2  CLK1  CLK0  -  ENDAC1 ENDAC0 BSA1  BSA0
128 // Used  :    0    1    0    0    0    0    0    0 = 0x40
129 ADMODB = 0x40;
130 // EAD maps to the bit function EIEE (bit 7) in the IEN1*
131 // (Interrupt Enable 1) SFR and allows the A/D converter values to

```

```

132 // be read
133 EAD = 1;
134
135
136 //          Contact Sensing Configuration
137 //
138 // INFO:  --          1      3
139 //      / \ --/-----/-----
140 //      | -----|          Segment
141 //      \--/      \      \          v.5
142 //          2      4
143 //
144 // The 4 pins connected to the contact sensors are:
145 // - #4 : Pin 18 (P0.5) Port 0, bit 5.      KBI5  Keyboard input 5.
146 // - #2 : Pin 19 (P0.4) Port 0, bit 4.      KBI4  Keyboard input 4.
147 // - #1 : Pin 20 (P0.3) Port 0, bit 3.      KBI3  Keyboard input 3.
148 // - #3 : Pin 21 (P0.2) Port 0, bit 2;      KBI2  Keyboard input 2.
149 // bits:  7    6    5    4    3    2    1    0
150 // P0 : KB7 KB6 KB5 KB4 KB3 KB2 KB1 KB0
151 // Used:  0    0    1    1    1    1    0    0      = 0x3C
152 // Get the contact information from the relevant pins
153 // Reset array
154 Touch = P0 & 0x3C;
155
156
157 // I2C Configuration
158 // -----
159 //
160 // INFO:
161 // When the internal SCL generator is selected for the
162 // I2C interface by setting CRSEL = 0 in the I2CON register
163 // (0th bit), the user must set values for registers I2SCLL
164 // and I2SCLH to select the data rate. I2SCLH defines the
165 // number of PCLK cycles for SCL = high, I2SCLL defines the
166 // number of PCLK cycles for SCL = low.
167 // The frequency is determined by the following formula:

```

```

168 // Bit Frequency = fPCLK / (2*(I2SCLH + I2SCLL))
169 // Where fPCLK is the frequency of PCLK.
170 // Where PCLK is "CPU Clock (CCLK)/2"
171 //
172 // Set to 369 Kbit/sec (I2SCLH = 5, I2SCLL 5)
173 // For internal clock: 7.373 MHz
174 I2SCLH = 5;
175 I2SCLL = 5;
176 // Set initial I2C configuration
177 I2CON = 0x44;
178 // Set own slave address (started 11,13,15...)
179 I2ADR = i2cSlaveAddr;
180 // Enable I2C interrupt
181 EI2C = 1;
182 // Initialize mode to send garbage
183 segmentStatus = 0;
184 // ADC to Degree conversion factor
185 ADCtoAngle = ((ADCmaxReading-ADCminReading)*10)/360;
186 // Calculate base ADC value
187 ADCzeroOffset = ADCminReading*10;
188
189 while(1)
190     {
191         // Immediate start of A/D converter 1
192         AD0CON = AD0CON | 0x01;
193         // Combine low and high bits in one variable: "ad"
194         ADCreading = ((ADCreading | AD0DAT4L) << 2) | AD0DAT4R;
195         // Convert ADC to degrees
196         angle = ((ADCreading*10)-ADCzeroOffset)/ADCtoAngle;
197         // Hall Effect Sensor sanity check
198         if (angle > 360 && angleProblem == 0) {
199             P3 = 1;
200             // Source current to the LED from P3.0
201             angleProblem = 1;
202         }
203         else if (angle < 500 && angleProblem == 1) {

```

```

204         P3 = 0;
205         angleProblem = 0;
206     }
207     // Set I2C start condition
208     I2CON = 0x44;
209
210     if (DEBUG == 1) {
211         // Set ucActEncVal to new encoder position and get touch data
212         Touch = P0 & 0x3C;
213         Touch >>= 1;
214         // DEBUG: Print:
215         //     - I2C Status
216         //     - Angle measurement
217         //     - 4-pin contact sensor daya in decimal
218         //     - 4-pin contact sensor data in binary form
219         printf ("I2C Address: %d Angle: %lu Touch: %d-", i2cSlaveAddr,
                angle, Touch);
220         for(i = 4; i>=1; i--)
221         {
222             if((1<<i)&Touch) printf("1");
223             else printf("0");
224         }
225         printf("\n");
226     }
227     delay ();
228     // Clear "ad"
229     ADCreading=0;
230     // Clear received command
231     i2cDataReceived = 0;
232 }
233 }
234
235
236 /*=====ADC Interrupt=====*/
237 void v_ADInt (void) interrupt 14
238 {

```

```

239 // clear ADC complete flag
240 ADOCON = ADOCON & 0xF7;
241 }
242
243
244 /*=====I2C Interrupt=====*/
245 void vI2C.Interrupt(void) interrupt 6
246 {
247 // check value of I2STAT
248 switch(I2STAT)
249 {
250 case 0x78:
251     I2CON = 0x44;
252     break;
253 case 0x80:
254     i2cDataReceived = I2DAT;
255     I2CON = 0x44;
256     break;
257 case 0x88:
258     I2CON = 0x44;
259     break;
260 case 0x90:
261     I2CON = 0x44;
262     break;
263 case 0x98:
264     I2CON = 0x44;
265     break;
266 case 0xA0:
267 // Identification command "19" detected
268 if (i2cDataReceived == 19)
269     {
270         // Light up LED
271         P3 = 1;
272 // Changing response mode
273         segmentStatus = 3;
274 // Clear received command

```

```

275             i2cDataReceived = 0x00;
276         }
277     // LED turn off command "100" detected
278     else if (i2cDataReceived == 100)
279     {
280         // turn off LED
281         P3 = 0;
282         // Clear received command
283         i2cDataReceived = 0x00;
284     }
285     // LED light up command "101" detected
286     else if (i2cDataReceived == 101)
287     {
288         // turn on LED
289         P3 = 1;
290         // Clear received command
291         i2cDataReceived = 0x00;
292     }
293     else
294     {
295         // Change mode to not to send anything
296         segmentStatus = 0;
297     }
298     I2CON = 0x44;
299     break;
300 case 0x60:
301 case 0x68:
302 case 0x70:
303     I2CON = 0x44;
304     break;
305 // Bus Error has occurred
306 case 0x00:
307     I2CON = 0x54;
308     break;
309 case 0x08:
310 case 0x10:

```

```

311     // slave address
312     I2DAT = 0x04;
313     I2CON = 0x44;
314     break;
315 case 0x18:
316 case 0x28:
317     // continue if not
318     I2CON = 0x44;
319     break;
320 case 0x20:
321 case 0x48:
322     I2CON = 0x54;
323     break;
324 case 0x30:
325     I2CON = 0x54;
326     break;
327 case 0x38:
328     I2CON = 0x64;
329     break;
330 /* IF ADDRESSED AS A SLAVE TRANSMITTER – (somebody wants to read something)
331    */
331 case 0xA8:
332     // Received the first SLAVE READ flag. ACK returned
333     if (segmentStatus == 1)
334     {
335         // Set ucActEncVal to new encoder position and get touch data
336         Touch = (P0 & 0x3C) >> 1;
337         // Start binary encoding
338         // Get the 8-bit LSB of the 16-bit angle+touch data
339         i2cDataLSB = (((angle*100)+Touch) & 0xFF) | i2cDataLSB;
340         // Get the 8-bit MSB of the 16-bit angle+touch data
341         i2cDataMSB = (((angle*100)+Touch) >> 8) | i2cDataMSB;
342         // Master wants me to load Data 1st part
343         I2DAT = i2cDataMSB;
344         segmentStatus = 2;
345         i2cDataMSB = 0;

```

```

346         // Done transmitting first byte, ready to send the second
347         I2CON = 0x44;
348         break;
349     }
350     // Garbage mode
351     else if (segmentStatus == 0)
352     {
353         segmentStatus = 0;
354         // Load Garbage response 0
355         I2DAT = 0x00;
356         // That's it! no more loading
357         I2CON = 0x40;
358         break;
359     }
360     // Identification mode
361     else if (segmentStatus == 3)
362     {
363         segmentStatus = 1;
364         // Load identification response
365         I2DAT = 0xBB;
366         // That's it! no more loading
367         I2CON = 0x40;
368         break;
369     }
370     break;
371     // Tried to be master but failed, Received SLAVE READ flag
372     case 0xB0:
373     case 0xB8:
374         // Continuing to send data, 2 consecutive bytes will be send, Received
375         // SLAVE READ flag
376         if (segmentStatus == 2)
377         {
378             segmentStatus = 1;
379             // Master wants me to load Data 2nd byte
380             I2DAT = i2cDataLSB;
381             i2cDataLSB = 0;

```

```
381         // That's it! no more loading
382         I2CON = 0x40;
383         break;
384     }
385 case 0xC0:
386 case 0xC8:
387     I2CON = 0x44;
388     break;
389 default:
390     // set IC stop condition (STO =1)
391     I2CON = 0x54;
392     break;
393 }
394 }
```

Appendix G

Segment - Bill of Materials

25 Segment - Tactile Antenna

Bill of Materials

#	Component Name	Comp. ID	Manufacturer Part #	Retailer	Retailer Part #	Unit Price	Price Break	Qty	Extended Price
1	Angle Sensor	AS	MLX90316	Digikey	MLX90316KDC-PPA-ND	\$8.17	25.00	1.0	\$204.25
2	Capacitor 100nF	C1	F921V104MAA	Digikey	493-2336-1-ND	\$0.18	100.00	1.0	\$17.78
3	Capacitor 100nF	C2	F921V104MAA	Digikey	493-2336-1-ND				
4	Capacitor 100nF	C3	F921V104MAA	Digikey	493-2336-1-ND				
5	Contact Sensor (left)	CS1	D3SH-A0L	Digikey	SW1048CT-ND	\$1.02	50.00	1.0	\$50.91
7	Contact Sensor (left)	CS3	D3SH-A0L	Digikey	SW1048CT-ND				
6	Contact Sensor (right)	CS2	D3SH-A0R	Digikey	SW1044CT-ND	\$1.02	50.00	1.0	\$50.91
8	Contact Sensor (right)	CS4	D3SH-A0R	Digikey	SW1044CT-ND				
9	LED	L1	598-8091-107F	Digikey	350-2037-1-ND	\$0.50	25.00	1.0	\$12.58
10	Microcontroller	MCU	P89LPC938FHN	Digikey	568-3226-ND	\$2.58	25.00	1.0	\$64.42
11	Programming Connector	PC1	SL-103-T-12	Digikey	SAM1107-03-ND	\$2.10	10.00	2.5	\$52.58
12	Pull-down Resistor	R1	ERJ-6ENF4753V	Digikey	P475KCCT-ND	\$0.05	50.00	2.0	\$4.88
13	Pull-down Resistor	R2	ERJ-6ENF4753V	Digikey	P475KCCT-ND				
14	Pull-down Resistor	R3	ERJ-6ENF4753V	Digikey	P475KCCT-ND				
15	Pull-down Resistor	R4	ERJ-6ENF4753V	Digikey	P475KCCT-ND				
16	Segment Connector	SC1	FH34S-4S-0.5SH(10)	Digikey	HFT04CT-ND	\$1.85	100.00	1.0	\$184.80
17	Segment Connector	SC2	FH34S-4S-0.5SH(10)	Digikey	HFT04CT-ND				
18	Segment Connector	SC3	FH34S-4S-0.5SH(10)	Digikey	HFT04CT-ND				
19	Segment Connector	SC4	FH34S-4S-0.5SH(10)	Digikey	HFT04CT-ND				
20	Coupling Cable	FFC1	050R04-76B	Digikey	HFF-04U-03-ND	\$3.71	10.00	2.5	\$92.83
21	Diametrical Cylinder Magnet	MGN	D24DIA	K&J Magnetics		\$0.20	25.00	1.0	\$5.00
22	Precision Ball Bearing	BB		McMaster-Carr	4259T6	\$11.95	1.00	25.0	\$298.75
23	0-80 Socket Screw	S1		McMaster-Carr	91251A056	\$0.16	50.00	1.0	\$8.08
24	0-80 Socket Screw	S2		McMaster-Carr	91251A056				
25	PCB Board (Vertical)	PCB1	NBJJ-4805-E	ExpressPCB		\$3.86	26.00	1.0	\$100.48
26	PCB Board (Horizontal)	PCB2	XGNW-4805-A	ExpressPCB		\$3.82	26.00	1.0	\$99.21
27	Aluminum Shell - Top	SHL1		Richard Middlestadt				20.0	\$2,350.00
28	Aluminum Shell - Bottom	SHL2							
29	Hairs (stainless steel) .024"	H1		McMaster-Carr	9495K68	\$8.00	1.00	1.0	\$8.00
30	0-80 Set Screw	SS1		McMaster-Carr	91375A052	\$0.48	25.00	2.0	\$24.1
31	0-80 Set Screw	SS2		McMaster-Carr	91375A052				
32	PCB Assembly - Horizontal	ASM1		ScreamingCircuits	4222-1508			25.0	\$462.4
33	PCB Assembly - Vertical	ASM2		ScreamingCircuits	7563-5879			25.0	\$797.4
Total Price									\$4,889.30

Appendix H

Segment - Component Datasheets

- Only relevant pages of these 3rd party drawings and datasheets have been included

2. Description

The MLX90316 is a monolithic sensor IC featuring the Tria \otimes is™ Hall technology. Conventional planar Hall technology is only sensitive to the flux density applied orthogonally to the IC surface. The Tria \otimes is™ Hall sensor is also sensitive to the flux density applied parallel to the IC surface. This is obtained through an Integrated Magneto-Concentrator (IMC®) which is deposited on the CMOS die (as an additional back-end step).

The MLX90316 is only sensitive to the flux density coplanar with the IC surface. This allows the MLX90316 with the correct magnetic circuit to decode the absolute rotary (angular) position from 0 to 360 Degrees. It enables the design of novel generation of non-contacting rotary position sensors that are frequently required for both automotive and industrial applications.

In combination with the appropriate signal processing, the magnetic flux density of a small magnet (diametral magnetization) rotating above the IC can be measured in a non-contacting way (Figure 3). The angular information is computed from both vectorial components of the flux density (i.e. B_x and B_y). MLX90316 produces an output signal proportional to the decoded angle. The output is selectable between Analog, PWM and Serial Protocol.

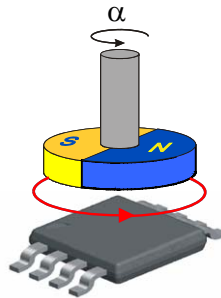


Figure 3 - Typical application of MLX90316

3. Glossary of Terms – Abbreviations – Acronyms

- Gauss (G), Tesla (T): Units for the magnetic flux density – 1 mT = 10 G
- TC: Temperature Coefficient (in ppm/Deg.C.)
- NC: Not Connected
- PWM: Pulse Width Modulation
- %DC: Duty Cycle of the output signal i.e. $T_{ON} / (T_{ON} + T_{OFF})$
- ADC: Analog-to-Digital Converter
- DAC: Digital-to-Analog Converter
- LSB: Least Significant Bit
- MSB: Most Significant Bit
- DNL: Differential Non-Linearity
- INL: Integral Non-Linearity
- RISC: Reduced Instruction Set Computer
- ASP: Analog Signal Processing
- DSP: Digital Signal Processing
- ATAN: trigonometric function: arctangent (or inverse tangent)
- IMC: Integrated Magneto-Concentrator (IMC®)
- CoRDIC: Coordinate Rotation Digital Computer (i.e. iterative rectangular-to-polar transform)
- EMC: Electro-Magnetic Compatibility

4. Pinout

Pin #	SOIC-8		TSSOP-16	
	Analog / PWM	Serial Protocol	Analog / PWM	Serial Protocol
1	VDD	VDD	VDIG ₁	VDIG ₁
2	Test 0	Test 0	VSS ₁ (Ground ₁)	VSS ₁ (Ground ₁)
3	Switch Out	/SS	VDD ₁	VDD ₁
4	Not Used	SCLK	Test 0 ₁	Test 0 ₁
5	Out	MOSI / MISO	Switch Out ₂	/SS ₂
6	Test 1	Test 1	Not Used ₂	SCLK ₂
7	VDIG	VDIG	Out ₂	MOSI ₂ / MISO ₂
8	Vss (Ground)	Vss (Ground)	Test 1 ₂	Test 1 ₂
9			VDIG ₂	VDIG ₂
10			VSS ₂ (Ground ₂)	VSS ₂ (Ground ₂)
11			VDD ₂	VDD ₂
12			Test 0 ₂	Test 0 ₂
13			Switch Out ₁	/SS ₁
14			Not Used ₁	SCLK ₁
15			Out ₁	MOSI ₁ / MISO ₁
16			Test 1 ₁	Test 1 ₁

For optimal EMC behavior, it is recommended to connect the unused pins (Not Used and Test) to the Ground (see section 17).

5. Absolute Maximum Ratings

Parameter	Value
Supply Voltage, VDD (overvoltage)	+ 20 V
Reverse Voltage Protection	- 10 V
Positive Output Voltage – Standard Version (Analog or PWM)	+ 10 V + 14 V (200 s max – T _A = + 25°C)
Positive Output Voltage – SPI Version	VDD + 0.3V
Positive Output Voltage (Switch Out)	+ 10 V + 14 V (200 s max – T _A = + 25°C)
Output Current (I _{OUT})	± 30 mA
Reverse Output Voltage	- 0.3 V
Reverse Output Current	- 50 mA
Operating Ambient Temperature Range, T _A	- 40°C ... + 150°C
Storage Temperature Range, T _S	- 40°C ... + 150°C
Magnetic Flux Density	± 700 mT

Exceeding the absolute maximum ratings may cause permanent damage. Exposure to absolute-maximum-rated conditions for extended periods may affect device reliability.

6. Detailed Description

As described on the block diagram (Figure 1 and Figure 2), the magnetic flux density parallel to the IC surface (i.e. B_{||}) is sensed through the Tria^ois™ sensor front-end. This front-end consists into two orthogonal pairs (for each of the two directions parallel with the IC surface i.e. X and Y) of conventional planar Hall plates (blue area on Figure 4) and an Integrated Magneto-Concentrator (IMC^o yellow disk on Figure 4).

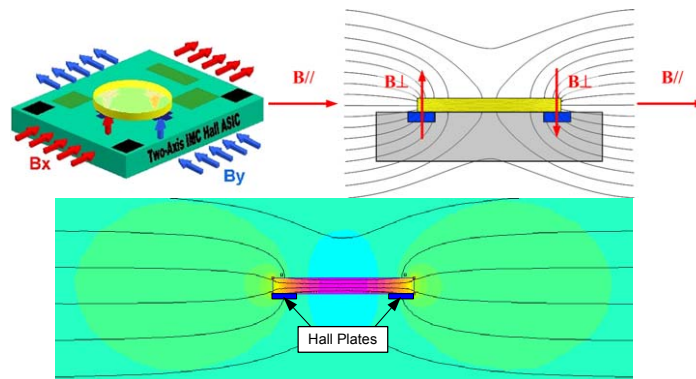


Figure 4 - Tria^ois™ sensor front-end (4 Hall plates + IMC^o disk)

Both components of the applied flux density $B_{//}$ are measured individually i.e. $B_{X//}$ and $B_{Y//}$. Two orthogonal components (respectively $B_{X\perp}$ and $B_{Y\perp}$) proportional to the parallel components (respectively $B_{X//}$ and $B_{Y//}$) are induced through the IMC and can be measured by both respective pairs of conventional planar Hall plates as those are sensitive to the flux density applied orthogonally to them and the IC surface.

While a magnet (diametrically magnetized) rotates above the IC as described on Figure 3, the sensing stage provides two differential signals in quadrature (sine and cosine – Figure 5 and Figure 6)

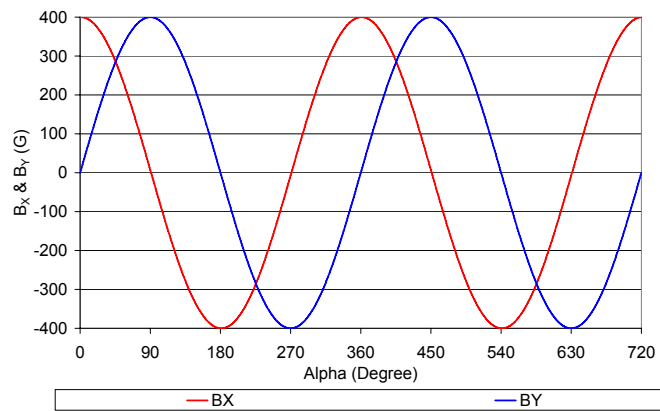


Figure 5 – Magnetic Flux Density – $B_x \propto \cos(\alpha)$ & $B_y \propto \sin(\alpha)$

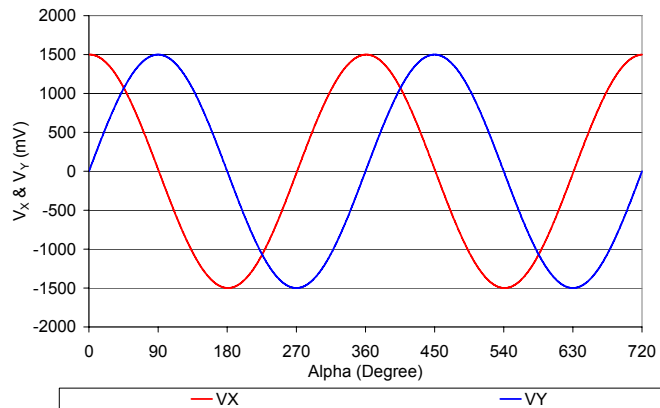


Figure 6 – Triaxis™ sensor front-end – Output signals – $V_x \propto B_x \propto \cos(\alpha)$ & $V_y \propto B_y \propto \sin(\alpha)$

Those Hall signals are processed through a fully differential analog chain featuring the classic offset cancellation technique (Hall plate quadrature spinning and chopper-stabilized amplifier).

The conditioned analog signals are converted through an ADC (configurable – 14 or 15 bits) and provided to a DSP block for further processing. The DSP stage is based on a 16 bit RISC micro-controller whose primary function is the extraction of the angular position from the two raw signals (after so-called front-end compensation steps) through the following operation:

$$\alpha = ATAN\left(\frac{V_y}{V_x}\right)$$

The DSP functionality is governed by the micro-code (firmware – F/W) of the micro-controller which is stored into the ROM (mask programmable). In addition to the “ATAN” function, the F/W controls the whole analog chain, the output transfer characteristic, the output protocol, the programming/calibration and also the self-diagnostic modes.

In the MLX90316, the “ATAN” function is computed via a look-up table (i.e. it is not obtained through a CoRDiC algorithm).

Due to the fact that the “ATAN” operation is performed on the ratio “ V_y/V_x ”, the angular information is intrinsically self-compensated vs. flux density variations (due to airgap change, thermal or ageing effects) affecting both signals. This feature allows therefore an improved thermal accuracy vs. rotary position sensor based on conventional linear Hall sensors.

In addition to the improved thermal accuracy, the realized rotary position sensor is capable of measuring a complete revolution (360 Degrees) and the linearity performances are excellent taking into account typical manufacturing tolerances (e.g. relative placement between the Hall IC and the magnet).

Once the angular information is computed (over 360 degrees), it is further conditioned (mapped) vs. the target transfer characteristic and it is provided at the output(s) as:

- an analog output level through a 12 bit DAC followed by a buffer
- a digital PWM signal with 12 bit depth (programmable frequency 100 Hz ... 1 kHz)
- a digital Serial Protocol (SP – 14 bits computed angular information available)

For instance, the analog output can be programmed for offset, gain and clamping to meet any rotary position sensor output transfer characteristic:

$$\begin{aligned} V_{out}(\alpha) &= \text{ClampLo} && \text{for } \alpha \leq \alpha_{min} \\ V_{out}(\alpha) &= V_{offset} + \text{Gain} \times \alpha && \text{for } \alpha_{min} \leq \alpha \leq \alpha_{max} \\ V_{out}(\alpha) &= \text{ClampHi} && \text{for } \alpha \geq \alpha_{max} \end{aligned}$$

where V_{offset} , Gain, ClampLo and ClampHi are the main adjustable parameters for the end-user.

The linear part of the transfer curve can be adjusted through either a 2 point or a 3 point calibration depending on the linearity requirement.

A digital output is also available and used as a programmable angular switch.

The calibration parameters are stored in EEPROM featuring a Hamming Error Correction Coding (ECC).

The programming steps do not require any dedicated pins. The operation is done using the supply and output nodes of the IC. The programming of the MLX90316 is handled at both engineering lab and production line levels by the Melexis Programming Unit PTC-04 with the dedicated MLX90316 daughterboard and software tools (DLL – User Interface).

10. MLX90316 Accuracy Specification

DC Operating Parameters at $V_{DD} = 5V$ (unless otherwise specified) and for T_A as specified by the Temperature suffix (S, E, K or L).

Parameter	Symbol	Test Conditions	Min	Typ	Max	Units
ADC Resolution on the raw signals sine and cosine	R_{ADC}	Slow Mode ⁽¹⁶⁾		15		bits
		Fast Mode ⁽¹⁶⁾		14		bits
Thermal Offset Drift #1 ⁽¹⁷⁾		Thermal Offset Drift at the DSP input (excl. DAC and output stage)				
		Temperature suffix S, E and K	-60		+60	LSB ₁₅
		Temperature suffix L	-90		+90	LSB ₁₅
Thermal Offset Drift #2 (to be considered only for the analog output mode)		Thermal Offset Drift of the DAC and Output Stage				
		Temperature suffix S, E and K	-0.3		+0.3	%V _{DD}
		Temperature suffix L	-0.4		+0.4	%V _{DD}
Thermal Drift of Sensitivity Mismatch ⁽¹⁸⁾		Temperature suffix S, E and K	-0.3		+0.3	%
		Temperature suffix L	-0.5		+0.5	%
Intrinsic Linearity Error ⁽¹⁹⁾	Le	$T_A = 25^\circ C$	-1		1	Deg
Analog Output Resolution	R_{DAC}	12 bits DAC (Theoretical – Noise free)		0.025		%V _{DD} /LSB
		INL	-4		+4	LSB
		DNL	0.05	1	2	LSB
Output stage Noise		Clamped Output		0.05		%V _{DD}
Noise pk-pk ⁽²⁰⁾		RG = 9, Slow mode, Filter=5		0.03	0.06	Deg
		RG = 9, Fast mode, Filter=0		0.1	0.2	Deg
Ratiometry Error			-0.1	0	0.1	%V _{DD}
PWM Output Resolution	R_{PWM}	12 bits (Theoretical – Jitter free)		0.025		%DC/LSB
PWM Jitter ⁽²¹⁾	J_{PWM}	RG = 6, $F_{PWM} = 250 \text{ Hz} - 800 \text{ Hz}$			0.2	%DC
Serial Protocol Output Resolution	R_{SP}	14 bits – 360 Deg. mapping (Theoretical – Jitter free)		0.022		Deg/LSB

¹⁶ 15 bits corresponds to 14 bits + sign and 14 bits corresponds to 13 bits + sign. After angular calculation, this corresponds to 0.005Deg/LSB₁₅ in Low Speed Mode and 0.01Deg/LSB₁₄ in High Speed.

¹⁷ For instance, Thermal Offset Drift #1 equal $\pm 60\text{LSB}_{15}$ yields to max. ± 0.3 Deg. angular error for the computed angular information (output of the DSP). See Front End Application Note for more details. This is only valid if automatic gain is set (See Section 14.4.2)

¹⁸ For instance, Thermal Drift of Sensitivity Mismatch equal $\pm 0.4\%$ yields to max. ± 0.1 Deg. angular error for the computed angular information (output of the DSP). See Front End Application Note for more details.

¹⁹ The Intrinsic Linearity Error refers to the IC itself (offset, sensitivity mismatch, orthogonality) taking into account an ideal rotating field. Once associated to a practical magnetic construction and the associated mechanical and magnetic tolerances, the output linearity error increases. However, it can be improved with the multi point end-user calibration that is available on the MLX90316.

²⁰ The application diagram used is described in the recommended wiring. For detailed information, refer to section Filter in application mode (Section 14.5).

²¹ Jitter is defined by $\pm 3 \sigma$ for 1000 successive acquisitions and the slope of the transfer curve is 100%DC/360 Deg.

17. Recommended Application Diagrams

17.1. Analog Output Wiring with the MLX90316 in SOIC Package

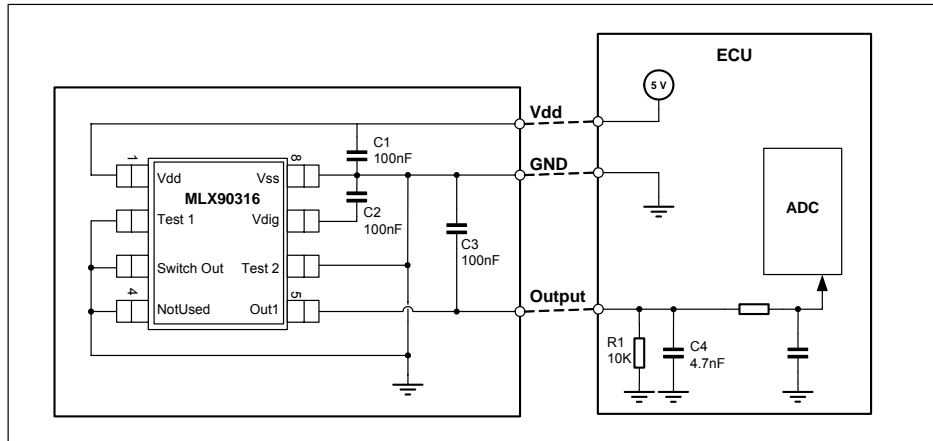


Figure 13 – Recommended wiring for the MLX90316 in SOIC8 package⁽²⁸⁾.

17.2. Analog Output Wiring with the MLX90316 in TSSOP Package

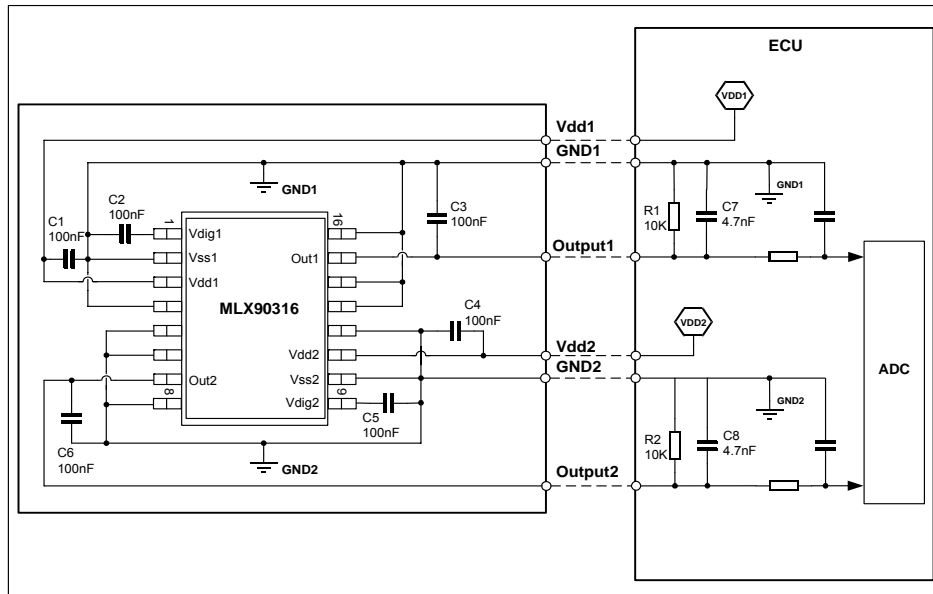
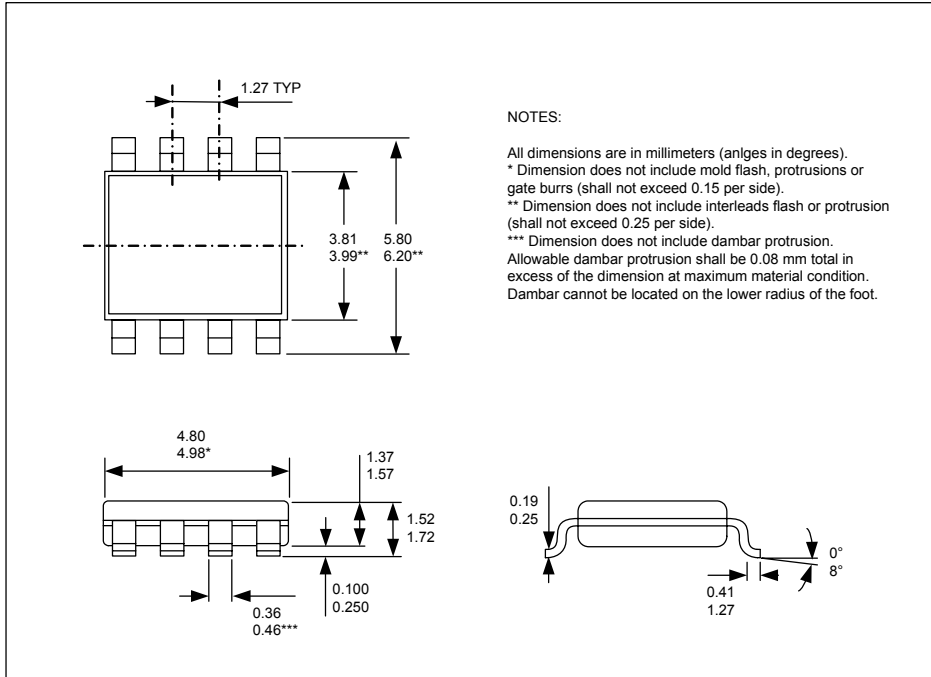


Figure 14 – Recommended wiring for the MLX90316 in TSSOP16 package (dual die).

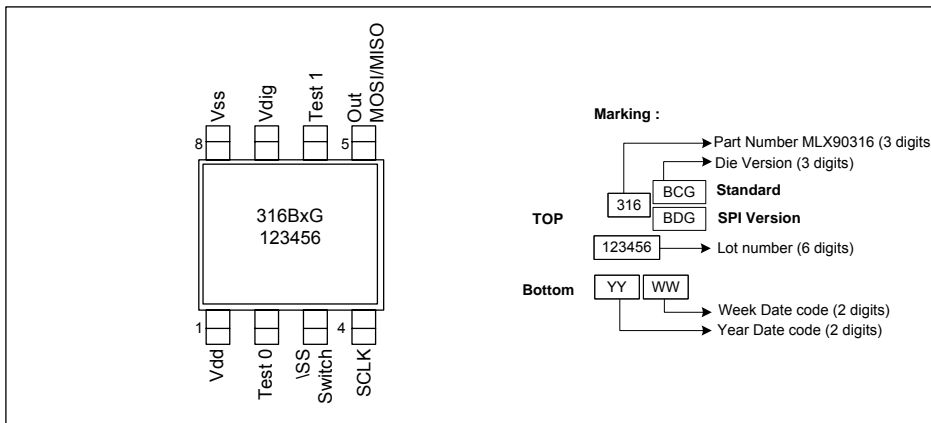
²⁸ See section 14.1.4 if the Switch Output feature is used.

20. Package Information

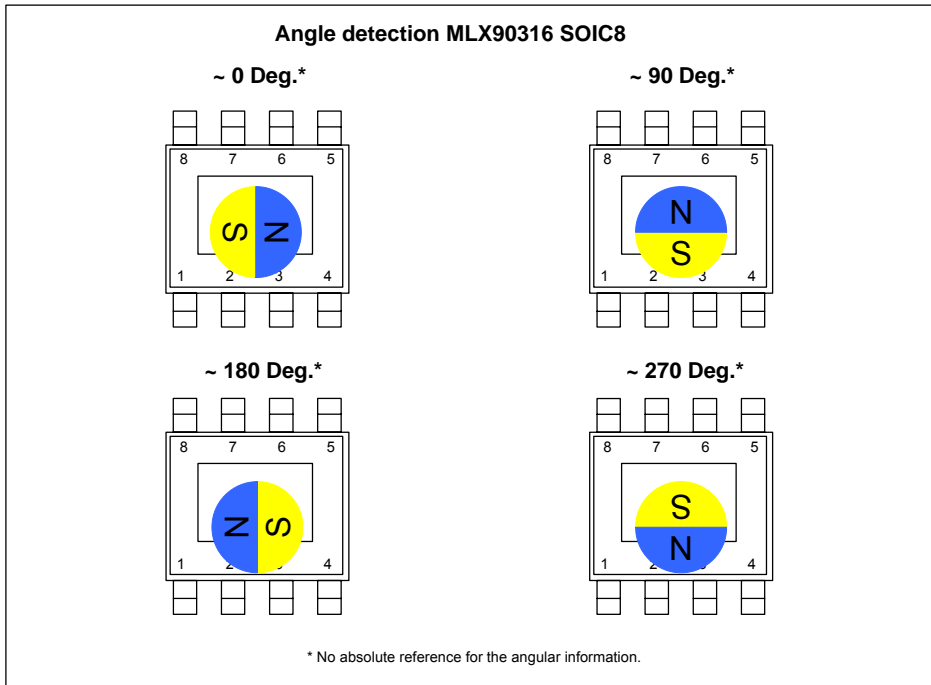
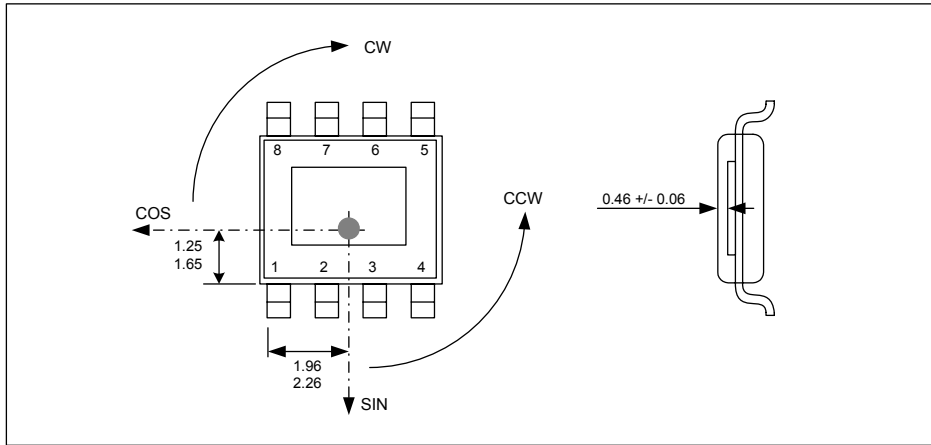
20.1. SOIC8 - Package Dimensions



20.2. SOIC8 - Pinout and Marking

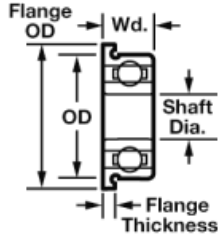


20.3. SOIC8 - IMC Positioning

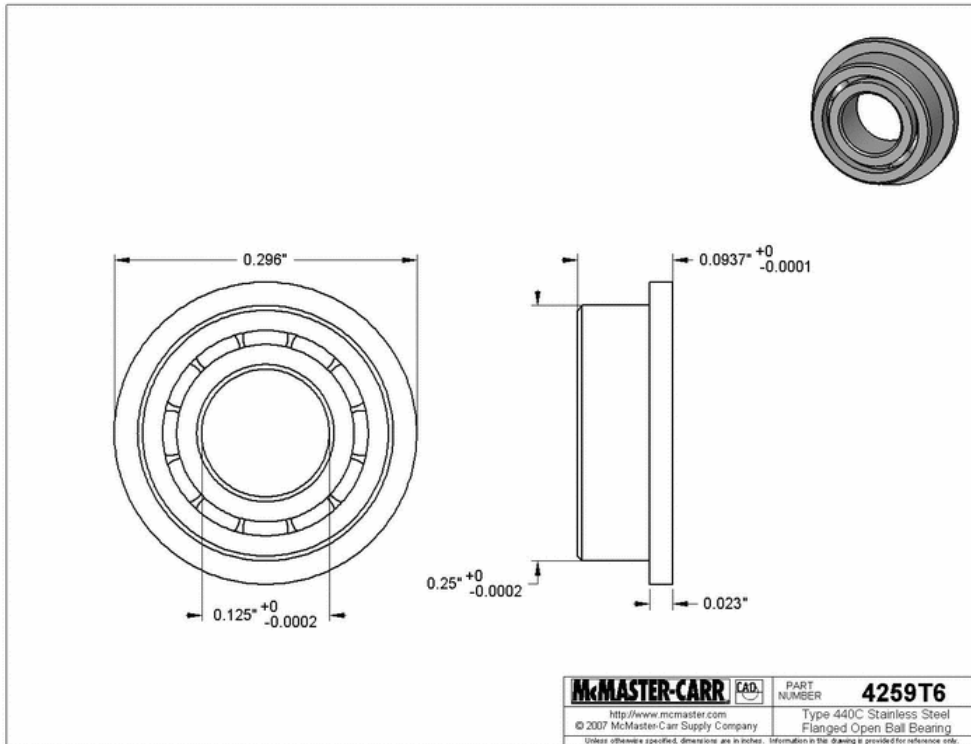


The MLX90316 is an absolute angular position sensor but the linearity error (Le – See Section 10) does not include the error linked to the absolute reference 0 Deg (which can be fixed in the application through the discontinuity point – See 14.2.2).

Ball and Roller Bearings



Part Number:	4259T6	\$11.95 Each
Type	Ball Bearings	
Ball Bearing Style	Flanged Open	
Ball Bearing Type	General Purpose	
System of Measurement	Inch	
For Shaft Diameter	1/8"	
Outside Diameter	1/4"	
Width	3/32"	
Flange Outside Diameter	.296"	
Flange Thickness	.023"	
ABEC Precision Bearing Rating	ABEC-7	
Dynamic Radial Load Capacity, lbs.	31	
Dynamic Radial Load Capacity Range, lbs.	6 to 250 lbs.	
Maximum rpm	80,000	
Maximum rpm Range	Above 60,000	
Temperature Range	-13° to +248° F	
Bearing Material	Stainless Steel	
Stainless Steel Material Type	Type 440C Stainless Steel	
Specifications Met	Not Rated	
Note	Bearings are lubricated.	



McMASTER-CARR CAD	PART NUMBER	4259T6
http://www.mcmaster.com	Type 440C Stainless Steel	
© 2007 McMaster-Carr Supply Company	Flanged Open Ball Bearing	
<small>Unless otherwise specified, dimensions are in inches. Information in the drawing is provided for reference only.</small>		

SOLID TANTALUM ELECTROLYTIC CAPACITORS

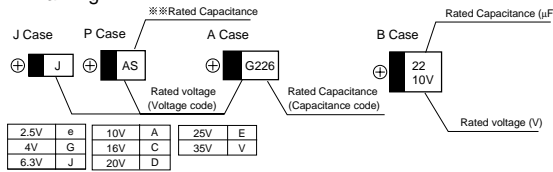
nichicon

F92

Resin-molded Chip,
Compact Series



■ Marking

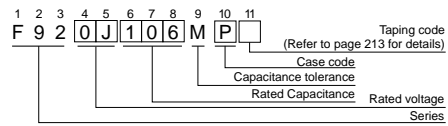


※ Capacitance code of "P" case products are as shown below.

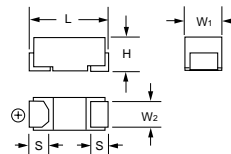
■ Specifications

Item	Performance Characteristics	
	J · P Case	A · B Case
Category	-55 ~ +125°C (Rated temperature : 85°C)	
Temperature Range	-55 ~ +125°C (Rated temperature : 85°C)	
Capacitance Tolerance	±20% (at 120Hz)	
Dissipation Factor (120Hz)	refer to P.216	
E.S.R. (100kHz)	refer to P.216	
Leakage Current	<ul style="list-style-type: none"> After 1 minute's application of rated voltage, leakage current at 20°C is not more than 0.01CV or 0.5μA, whichever is greater. After 1 minute's application of rated voltage, leakage current at 85°C is not more than 0.1CV or 5μA, whichever is greater. After 1 minute's application of derated voltage, leakage current at 125°C is not more than 0.125CV or 6.3μA, whichever is greater. 	
Capacitance Change by Temperature	+20% Max. (at +125°C) +15% Max. (at +85°C) -15% Max. (at -55°C)	+15% Max. (at +125°C) +10% Max. (at +85°C) -10% Max. (at -55°C)
Damp Heat (No voltage applied)	At 40°C 90 ~ 95% R.H. 240 hours Capacitance Change... Within ±20% of initial value Dissipation Factor...150% or less of initial specified value Leakage Current... Initial specified value or less	At 40°C 90 ~ 95% R.H. 500 hours Within ±10% of initial value Initial specified value or less Initial specified value or less
Temperature Cycles	-55°C / +125°C 30 minutes each 5 cycles Capacitance Change... Within ±10% of initial value (J case Within ±20%) Dissipation Factor...150% of less of initial specified value *1 Leakage Current... Initial specified value or less	Within ±5% of initial value Initial specified value or less Initial specified value or less

■ Type numbering system (Example: 6.3V 10μF)



■ Drawing



■ Dimensions

Case code	L	W ₁	W ₂	H	S
J	1.6 ± 0.1	0.8 ± 0.1	0.6 ± 0.1	0.8 ± 0.1	0.4 ± 0.1
P	2.0 ± 0.2	1.25 ± 0.1	0.9 ± 0.1	1.1 ± 0.1	0.5 ± 0.2
A	3.2 ± 0.2	1.6 ± 0.2	1.2 ± 0.1	1.1 ± 0.1	0.8 ± 0.2
B	3.4 ± 0.2	2.8 ± 0.2	2.3 ± 0.1	1.1 ± 0.1	0.8 ± 0.2

Resistance to Soldering Heat	5 seconds immersion at 260°C, 10 seconds reflow at 260°C Capacitance Change... Within ±10% of initial value (J case within ±20%) Dissipation Factor...150% of less of initial specified value*1 Leakage Current... Initial specified value or less		Within ±5% of initial value Initial specified value or less Initial specified value or less
Surge*	After application of surge voltage in series with a 33Ω (For "J" "P" case: 1kΩ) resistor at the rate of 30 seconds ON, 30 seconds OFF, for 1000 successive test cycles at 85°C, capacitors meet the characteristics requirements listed below. Capacitance Change... Within ±10% of initial value (J case within ±20%) Dissipation Factor...150% or less of initial specified value*1 Leakage Current... Initial specified value or less		Within ±5% of initial value Initial specified value or less Initial specified value or less
Endurance*	After 1000hours' application of rated voltage in series with a 3Ω resistor at 85°C, or derated voltage in series with a 3Ω resistor at 125°C, capacitors meet the characteristic requirements listed below. Capacitance Change... Within ±10% of initial value (J case within ±20%) Dissipation Factor...150% or less of initial specified value*1 Leakage Current... Initial specified value or less (J case 2 times value or less)	After 2000hours' application of rated voltage in series with a 3Ω resistor at 85°C, or derated voltage in series with a 3Ω resistor at 125°C, capacitors meet the characteristic requirements listed below. Capacitance Change... Within ±10% of initial value Dissipation Factor... Initial specified value or less Leakage Current... Initial specified value or less	
Shear Test	After applying the pressure load of 5N for 10±1 seconds horizontally to the center of capacitor side body which has no electrode and has been soldered beforehand on an aluminum substrate, there shall be found neither exfoliation nor its sign at the terminal electrode.		 5N (0.51kg · f) For 10 ± 1seconds
Terminal Strength	Keeping a capacitor surface-mounted on a substrate upside down and supporting the substrate at both of the opposite bottom points 45mm apart from the center of the capacitor, the pressure strength is applied with a specified jig at the center of the substrate so that the substrate may bend by 1mm as illustrated. Then, there shall be found no remarkable abnormality on the capacitor terminals.		 R230 20 45 45 1mm

* As for the surge and derated voltage at 125°C, refer to page 212 for details.

■ Standard ratings

Cap.(μF)	V	2.5	4	6.3	10	16	20	25	35	※ ※ Capacitance code
0.1	104	0E	0G	0J	1A	1C	1D	1E	1V	
0.15	154								A	
0.22	224						P · A	A	A	J
0.33	334						P · A	A	A	N
0.47	474					P	P · A	A	B	S
0.68	684						A	B	B	W
1	105			P	P	J · P · A	P · A	P · A · B	(A)	A
1.5	155			P	P · A	P · A	A · B	A · B		E
2.2	225		P	J · P · A	J · P · A	P · A · B	A · B	(B)	(B)	J
3.3	335		P · A	P · A	P · A	A · B	B			N
4.7	475	P	J · P · A	J · P · A	P · A	A · B	B			S
6.8	685	P	J · P · A	P · A	P · A	B				w
10	106	J · P · A	J · P · A	J · P · A	P · A · B	(A) · B				a
15	156	P · A	P · A	P · A	A · B					e
22	226	P · A	P · A	P · A · B	(A) · B	(B)				j
33	336	P · A	(P) · A · B	(A) · B	B					n
47	476	B	(A) · B	B						
68	686	B	B							
100	107	B	B	(B)						

() The series in parentheses are being developed.
Please contact to your local Nichicon sales office when these series are being designed in your application.

CAT.8100S

SOLID TANTALUM ELECTROLYTIC CAPACITORS

F92

■ Standard ratings

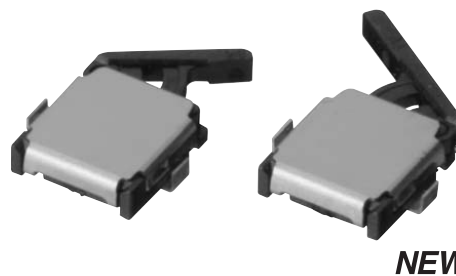
Rated Volt (V)	Rated Capacitance (μF)	Case size	Part Number	Leakage Current (μA)	Dissipation Factor (%@120Hz)	E. S. R. (Ω@100kHz)
2.5V	4.7	P	F920E475MPA	0.5	8	6.0
	6.8	P	F920E685MPA	0.5	10	6.0
	10	J	F920E106MJA	0.5	20	6.5
	10	P	F920E106MPA	0.5	10	6.0
	10	A	F920E106MAA	0.5	8	4.0
	15	P	F920E156MPA	0.5	10	5.0
	15	A	F920E156MAA	0.5	8	4.0
	22	P	F920E226MPA	0.6	20	4.0
	22	A	F920E226MAA	0.6	12	2.8
	33	P	F920E336MPA	0.8	20	4.0
	33	A	F920E336MAA	0.8	12	2.8
	47	B	F920E476MBA	1.2	12	1.7
	68	B	F920E686MBA	1.7	12	1.5
	100	B	F920E107MBA	2.5	18	1.3
4V	2.2	P	F920G225MPA	0.5	8	12.0
	3.3	P	F920G335MPA	0.5	8	12.0
	3.3	A	F920G335MAA	0.5	6	7.0
	4.7	J	F920G475MJA	0.5	20	8.5
	4.7	P	F920G475MPA	0.5	8	6.0
	4.7	A	F920G475MAA	0.5	6	4.0
	6.8	J	F920G685MJA	0.5	20	7.5
	6.8	P	F920G685MPA	0.5	10	6.0
	6.8	A	F920G685MAA	0.5	6	4.0
	10	J	F920G106MJA	0.5	20	6.5
	10	P	F920G106MPA	0.5	10	6.0
	10	A	F920G106MAA	0.5	8	4.0
	15	P	F920G156MPA	0.6	10	5.0
	15	A	F920G156MAA	0.6	8	4.0
22	P	F920G226MPA	0.9	20	5.0	
22	A	F920G226MAA	0.9	12	2.8	
33	A	F920G336MAA	1.3	12	2.8	
33	B	F920G336MBA	1.3	12	1.7	
47	B	F920G476MBA	1.9	12	1.7	
68	B	F920G686MBA	2.7	18	1.5	
100	B	F920G107MBA	4.0	18	1.3	
6.3V	1	P	F920J105MPA	0.5	8	12.0
	1.5	P	F920J155MPA	0.5	8	12.0
	2.2	J	F920J225MJA	0.5	20	17.5
	2.2	P	F920J225MPA	0.5	8	12.0
	2.2	A	F920J225MAA	0.5	6	7.0
	3.3	P	F920J335MPA	0.5	8	12.0
	3.3	A	F920J335MAA	0.5	6	7.0
	4.7	J	F920J475MJA	0.5	20	8.5
	4.7	P	F920J475MPA	0.5	8	6.0
	4.7	A	F920J475MAA	0.5	6	4.0
	6.8	P	F920J685MPA	0.5	10	6.0
	6.8	A	F920J685MAA	0.5	6	4.0
	10	J	F920J106MJA	0.6	20	8.5
	10	P	F920J106MPA	0.6	10	6.0
10	A	F920J106MAA	0.6	8	4.0	
15	P	F920J156MPA	0.9	10	6.0	
15	A	F920J156MAA	0.9	8	4.0	
22	P	F920J226MPA	1.4	20	5.0	
22	A	F920J226MAA	1.4	12	2.8	
22	B	F920J226MBA	1.4	8	1.9	
33	B	F920J336MBA	2.1	12	1.7	
47	B	F920J476MBA	3.0	12	1.7	
10V	1	P	F921A105MPA	0.5	8	12.0
	1.5	P	F921A155MPA	0.5	8	12.0
	1.5	A	F921A155MAA	0.5	6	7.4
	2.2	J	F921A225MJA	0.5	20	17.5
	2.2	P	F921A225MPA	0.5	8	12.0
	2.2	A	F921A225MAA	0.5	6	7.0
	3.3	P	F921A335MPA	0.5	8	12.0
	3.3	A	F921A335MAA	0.5	6	7.0
	4.7	P	F921A475MPA	0.5	8	6.0
	4.7	A	F921A475MAA	0.5	6	4.0
	6.8	P	F921A685MPA	0.7	8	6.0
	6.8	A	F921A685MAA	0.7	6	4.0
	10	P	F921A106MPA	1.0	14	6.0
	10	A	F921A106MAA	1.0	8	4.0
10	B	F921A106MBA	1.0	6	2.0	
15	A	F921A156MAA	1.5	8	4.0	
15	B	F921A156MBA	1.5	6	2.0	
22	B	F921A226MBA	2.2	8	1.9	
33	B	F921A336MBA	3.3	12	1.9	
16V	0.47	P	F921C474MPA	0.5	8	20.0
	0.68	P	F921C684MPA	0.5	8	12.0
	1	J	F921C105MJA	0.5	20	25.5
	1	P	F921C105MPA	0.5	8	12.0
	1	A	F921C105MAA	0.5	4	10.0
	1.5	P	F921C155MPA	0.5	8	12.0
	1.5	A	F921C155MAA	0.5	6	7.4
	2.2	P	F921C225MPA	0.5	8	12.0
	2.2	A	F921C225MAA	0.5	6	7.0
	2.2	B	F921C225MBA	0.5	6	3.0
	3.3	A	F921C335MAA	0.5	6	7.0
	3.3	B	F921C335MBA	0.5	6	3.0
	4.7	A	F921C475MAA	0.8	6	7.0
	4.7	B	F921C475MBA	0.8	6	3.0
6.8	B	F921C685MBA	1.1	6	3.0	
10	B	F921C106MBA	1.6	6	2.0	
20V	0.22	P	F921D224MPA	0.5	8	20.0
	0.22	A	F921D224MAA	0.5	4	10.0
	0.33	P	F921D334MPA	0.5	8	20.0
	0.33	A	F921D334MAA	0.5	4	10.0
	0.47	P	F921D474MPA	0.5	8	20.0
	0.47	A	F921D474MAA	0.5	4	10.0
	0.68	A	F921D684MAA	0.5	4	10.0
	1	P	F921D105MPA	0.5	8	20.0
	1	A	F921D105MAA	0.5	4	10.0
	1.5	A	F921D155MAA	0.5	6	7.4
	1.5	B	F921D155MBA	0.5	6	4.0
	2.2	A	F921D225MAA	0.5	6	7.0
	2.2	B	F921D225MBA	0.5	6	3.0
	3.3	B	F921D335MBA	0.7	6	3.0
4.7	B	F921D475MBA	0.9	6	3.0	
25V	0.22	A	F921E224MAA	0.5	4	10.0
	0.33	A	F921E334MAA	0.5	4	10.0
	0.47	A	F921E474MAA	0.5	4	10.0
	0.68	B	F921E684MBA	0.5	4	4.0
	1	P	F921E105MPA	0.5	8	20.0
	1	A	F921E105MAA	0.5	6	10.0
35V	1	B	F921E105MBA	0.5	4	4.0
	0.1	A	F921V104MAA	0.5	4	10.0
	0.15	A	F921V154MAA	0.5	4	10.0
	0.22	A	F921V224MAA	0.5	4	10.0
	0.33	A	F921V334MAA	0.5	4	10.0
	0.47	B	F921V474MBA	0.5	4	4.0
0.68	B	F921V684MBA	0.5	4	4.0	

CAT.8100S

Surface Mount Detection Switch D3SH

The smallest detection switch in the world. (OMRON's data as of June 2006.)

- Ultra small size and ultra low profile contributing to down-sizing of sets devices. (3.0 x 3.4 x 0.9 mm (W x D x H))
- A unique mechanism enables high contact reliability and high precision operation.
- Horizontal 2-way detection and long stroke for easy installation are available.
- Meet a variety of applications by contact and lever variations.



Ordering Information

Model Number Legend

D3SH-
1 2 3

1. Contact Form

- A: SPST-NO
- B: SPST-NC

2. Boss for Positioning

- 0: without Boss
- 1: with Boss

3. Lever and Direction of Operation

- R : Right operating with standard lever
- L : Left operating with standard lever
- R1: Right operating with long lever
- L1: Left operating with long lever

List of Models

Standard Lever Models

Contact form	Direction of Operation	Boss of Positioning	Model	Packing form
SPST-NO	Right	With Boss	D3SH-A1R	Embossed tape packing (see note)
		Without Boss	D3SH-A0R	
	Left	With Boss	D3SH-A1L	
		Without Boss	D3SH-A0L	
SPST-NC	Right	With Boss	D3SH-B1R	Embossed tape packing (see note)
		Without Boss	D3SH-B0R	
	Left	With Boss	D3SH-B1L	
		Without Boss	D3SH-B0L	

Note: Minimum packing unit is 1,000 pcs./reel.

Long Lever Models

Contact form	Direction of Operation	Boss of Positioning	Model	Packing form
SPST-NO	Right	With Boss	D3SH-A1R1	Embossed tape packing (see note)
		Without Boss	D3SH-A0R1	
	Left	With Boss	D3SH-A1L1	
		Without Boss	D3SH-A0L1	
SPST-NC	Right	With Boss	D3SH-B1R1	Embossed tape packing (see note)
		Without Boss	D3SH-B0R1	
	Left	With Boss	D3SH-B1L1	
		Without Boss	D3SH-B0L1	

Note: Minimum packing unit is 1,000 pcs./reel.

Specifications

■ Ratings

Rated voltage	Resistive load
5 VDC	1 mA

Note: The ratings values apply under the following test conditions:
 Ambient temperature : 20± 2°C
 Ambient humidity: 65± 5%
 Operating frequency: 30 operations/min.

■ Characteristics

Operating speed	1 mm to 300 mm/s
Operating frequency	Mechanical: 20 operations/min max. Electrical: 20 operations/min max.
Insulation resistance	100 MΩ min. (at 100 VDC)
Contact resistance (initial value)	3Ω max.
Dielectric strength	100 VAC for 1 min between terminals of same polarity
Vibration resistance (see note 2)	Malfunction: 10 to 55 Hz, 1.5-mm double amplitude
Shock resistance (see note 2)	Destruction: 1000 m/s ² {approx. 100 G} max. Malfunction: 300 m/s ² {approx. 30 G} max.
Durability (see note 3)	Mechanical: 150,000 operations min. (20 operations/min.) Electrical: 100,000 operations min. (20 operations/min.)
Ambient operating temperature	-25°C to 85°C (at ambient humidity of 60% max.) (with no icing or condensation)
Ambient operating humidity	85% max. (for 5°C to 35°C)
Weight	Approx. 0.02 g

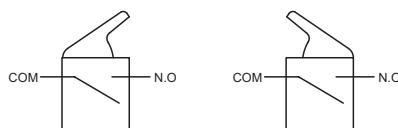
Note: 1. The data given above are initial values.
 2. The values apply at the total travel position. Contact opening or closing time is within 1ms.
 3. For testing conditions, consult your OMRON sales representative.

■ Contact Specifications

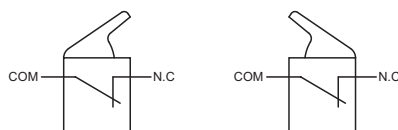
Contact Specification	Slide
Minimum applicable load	15 μ A at 3 VDC

■ Contact form

SPST-NO



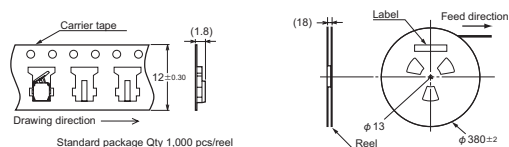
SPST-NC



Note: The cover connects with COM terminal inside.

Dimensions

■ Packaging Specifications



Standards	Conforms to JEITA
Package	Qty 1,000 pcs/reel

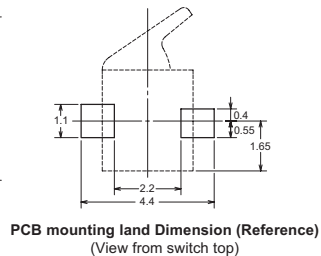
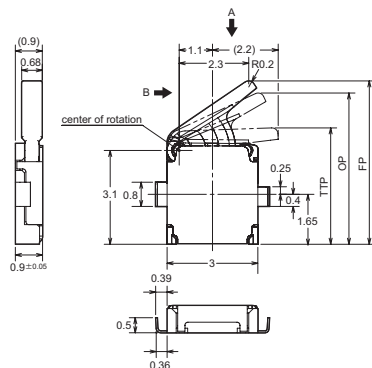
■ Dimensions and Operating Characteristics

- Note:** 1. All units are in millimeters unless otherwise indicated.
 2. Unless otherwise specified, a tolerance of ± 0.15 mm applies to all dimensions.
 3. The operating characteristics are for operation in the A direction (\downarrow) and B direction (\rightarrow , \leftarrow).

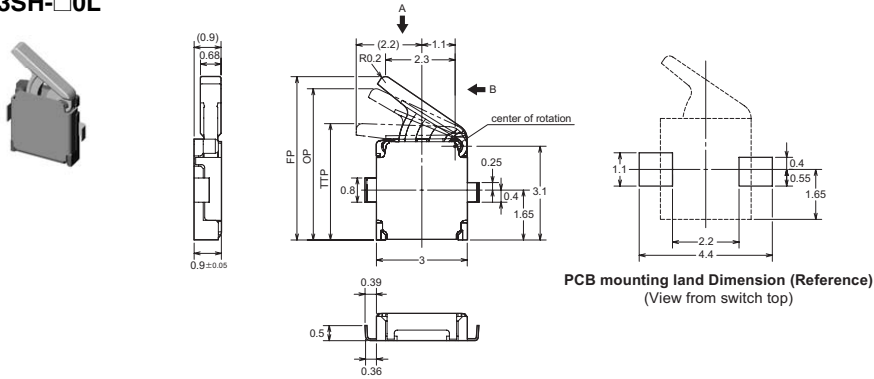
Standard Lever Models

Model	D3SH-□□R D3SH-□□L
Operating force (OF) max.	0.3 N (31 gf)
Free position (FP)	5.4 ± 0.2 mm
Operating position (OP)	5.0 ± 0.2 mm
Total travel position (TTP)	3.8 ± 0.15 mm

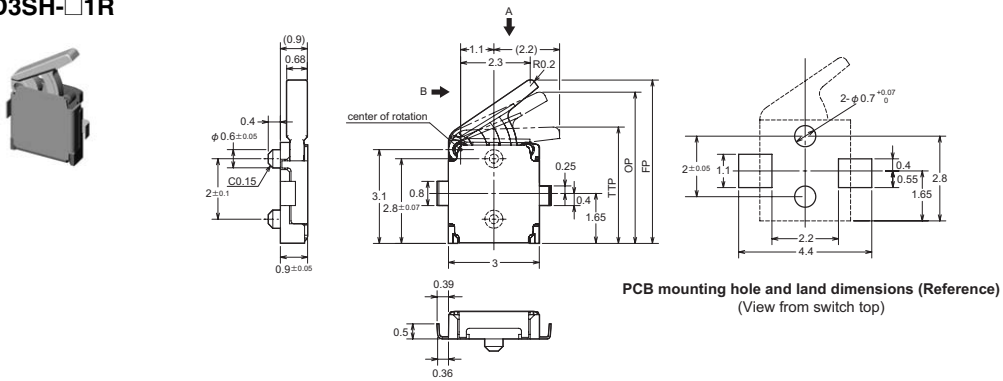
Right operating – without Boss D3SH-□0R



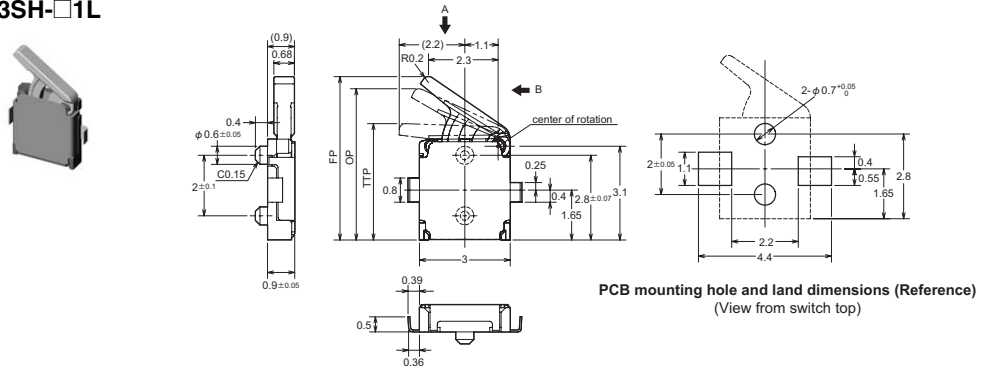
Left operating – without Boss
D3SH-□0L



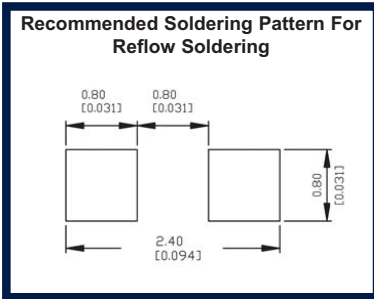
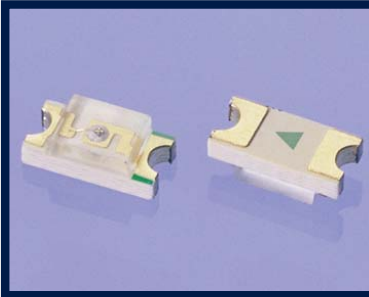
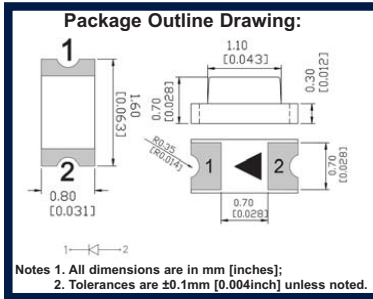
Right operating – with Boss
D3SH-□1R



Left operating – with Boss
D3SH-□1L

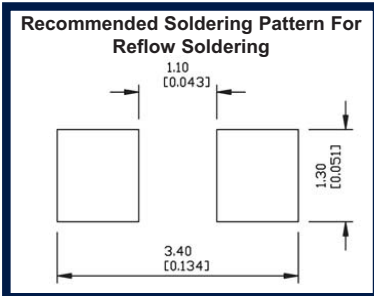
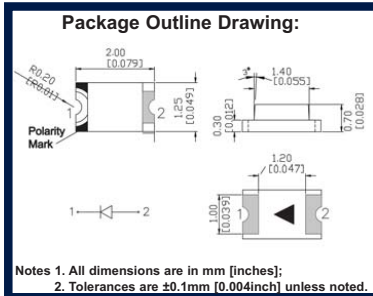


0603 SERIES PACKAGE (1.6MM X 0.8MM X 0.7MM) SINGLE COLOR



DIALIGHT P/N	EMITTED COLOR	MATERIAL	LENS COLOR	LUMINOUS INTENSITY (mcd)			DOMINANT WAVELENGTH (nm)			FORWARD VOLTAGE (V)			VIEWING ANGLE ° DEGREES
				If = 20 ma			If = 20 ma			If = 20 ma			
				MIN	TYP	MAX	MIN	TYP	MAX	MIN	TYP	MAX	
598-8010-107F	RED	AlInGaP	Water Clear	30	40	80	630	635	642	1.7	2.2	2.4	140
598-8020-107F	RED-ORANGE	AlInGaP	Water Clear	120	150	200	620	625	630	1.7	2	2.4	140
598-8030-107F	ORANGE	AlInGaP	Water Clear	70	-	150	600	-	610	1.7	2	2.4	140
598-8040-107F	YELLOW	AlInGaP	Water Clear	100	130	160	590	-	595	1.7	2	2.2	140
598-8050-107F	YELLOW	AlInGaP	Water Clear	100	130	160	583	-	590	1.7	2	2.4	140
598-8060-107F	YELLOW-GREEN	AlInGaP	Water Clear	20	40	60	570	-	575	1.8	2	2.4	140
598-8070-107F	GREEN	GaP	Water Clear	10	20	40	562	-	570	1.8	2	2.4	140
598-8081-107F	GREEN	InGaN	Water Clear	220	300	400	520	523	525	3	3.2	3.5	140
598-8091-107F	BLUE	InGaN	Water Clear	90	140	160	470	473	475	2.8	3.2	3.5	140

0805 SERIES PACKAGE (2.0MM X 1.25MM X 0.70MM) SINGLE COLOR



DIALIGHT P/N	EMITTED COLOR	MATERIAL	LENS COLOR	LUMINOUS INTENSITY (mcd)			DOMINANT WAVELENGTH (nm)			FORWARD VOLTAGE (V)			VIEWING ANGLE ° DEGREES
				If = 20 ma			If = 20 ma			If = 20 ma			
				MIN	TYP	MAX	MIN	TYP	MAX	MIN	TYP	MAX	
598-8110-107F	RED	AlInGaP	Water Clear	30	40	80	630	635	642	1.7	2.2	2.4	140
598-8120-107F	RED-ORANGE	AlInGaP	Water Clear	120	150	200	620	625	630	1.7	2	2.4	140
598-8130-107F	ORANGE	AlInGaP	Water Clear	70	-	150	600	-	610	1.7	2	2.4	140
598-8140-107F	YELLOW	AlInGaP	Water Clear	100	130	160	590	-	595	1.7	2	2.4	140
598-8150-107F	YELLOW	AlInGaP	Water Clear	100	130	160	583	-	590	1.7	2	2.4	140
598-8160-107F	YELLOW-GREEN	AlInGaP	Water Clear	20	40	60	570	-	575	1.8	2	2.4	140
598-8170-107F	GREEN	GaP	Water Clear	10	20	40	562	-	570	1.8	2	2.4	140
598-8181-107F	GREEN	InGaN	Water Clear	220	300	400	520	523	525	3	3.2	3.5	140
598-8191-107F	BLUE	InGaN	Water Clear	90	140	160	470	473	475	2.8	3.2	3.5	140



UPS Orders placed online by noon ET (M-F) will be shipped the same day

[home](#) | [products](#) | [search](#) | [checkout](#) | [policies](#) | [contact](#) | [UPS tracking](#)

Wednesday January 21st 2009

PRODUCT DETAIL

- [Home](#)
- [Products](#)
- [Neo Mag Safety](#)
- [Neo Mag Info](#)
- [Order/Ship Info](#)
- [Uses](#)
- [Neo Mag Specs](#)
- [FAQ](#)
- [Links](#)
- [About Us](#)

Shopping cart
 0 Products in cart
 Total \$0.00
[» Checkout](#)

- Quick Links**
- Discs
 - Cylinders
 - Blocks
 - Rings
 - Spheres
 - Plastic/Rubber Coated
 - Mounting Magnets
 - Surplus
 - Other Items
 - Grade N50/N52
 - Custom Magnets



[Home](#) » **NEODYMIUM CYLINDER MAGNETS**

[Checkout](#)

news
January Specials

D24DIA

- **Dimensions:** 1/8" dia. x 1/4" thick
- **Tolerances:** ±0.002" x ±0.002"
- **Material:** NdFeB, Grade N42
- **Plating/Coating:** Ni-Cu-Ni (Nickel)
- **Magnetization Direction:** Diametrical
- **Weight:** 0.0133 oz. (0.377 g)
- **Pull Force:** 1.45 lbs
- **Surface Field:** 3840 Gauss
- **Brmax:** 13,200 Gauss
- **BHmax:** 42 MGOe



These small diametrically magnetized cylinders are great for use with Hall Effect Sensors or just making chains of magnets for bracelets or necklaces. The poles are located on the sides of the cylinders, so they will attract each other as shown in the bottom picture.

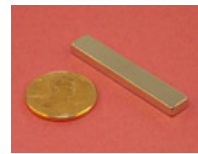
D24DIA:

Quantity:

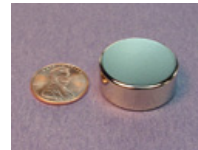
[Add to cart](#)

[« Previous](#) | [Next »](#)

[Tell a Friend](#)



15% Off
 1 1/2" x 1/4" x 1/8" Neodymium Block



20% Off
 1" dia. x 3/8" discs Strong & Sturdy!

Order by phone:
1-888-SHOP-KJM
(1-888-746-7556)
or 215-766-8055
 Order online for fastest shipping!

NO MINIMUM ORDER



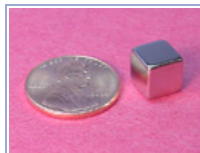
Our secure shopping cart is able to process credit cards quickly, easily and **securely**.

K&J Magnetics, Inc.
 Your online source for incredibly powerful neodymium magnets

Customers who purchased this item also purchased:



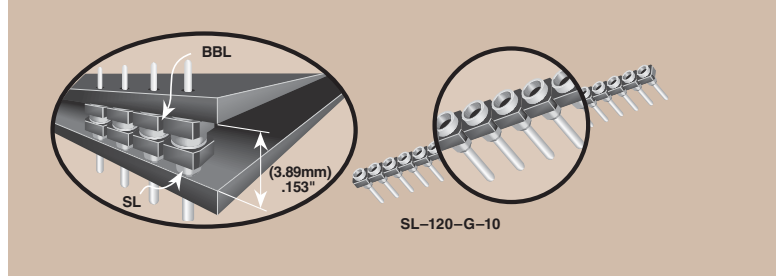
BC62
 3/4" x 3/8" x 1/8" thick
 Grade N42 - Nickel Plated



B555
 5/16" x 5/16" x 5/16" thick
 Grade N42 - Nickel Plated



DE3
 7/8" dia. x 3/16" thick
 Grade N42 - Nickel Plated



LOW PROFILE SOCKET STRIPS SL & SDL SERIES

- FEATURES**
- Achieve low profile without sacrificing insertion depth!
 - Choice of four precision screw machined lead styles.
 - Exceptionally low profile, down to (2,11mm) .083" off of board.
 - Mates with BBL or BDL for board stacking spaces down to (3,89mm) .153"

SPECIFICATIONS

For complete specifications see www.samtec.com?SL or www.samtec.com?SDL

Insulator Material: Black Glass Filled Polyester

Contact/Shell Materials: BeCu/Brass

Plating: Au or Sn over 50µ" (1,27µm) Ni

Operating Temp Range: -55°C to +125°C with Gold
-55°C to +105°C with Tin

Current Rating: 1A

Contact Resistance: 10 mΩ max

Insertion Force: (Single contact only)
Standard = 9 oz (2,50N) avg., 16oz (4,45N) max ((0,43mm) .017" DIA probe)

Low Insertion Force = 2.5oz (0,70N) avg., 5.5oz (1,53N) max ((0,43mm) .017" DIA probe except Style 30 (0,46mm) .018" DIA probe)

Withdrawal Force: (Single contact only)
Standard = 2.5oz (0,70N) avg., 1.5oz (0,42N) min ((0,43mm) .017" DIA probe)

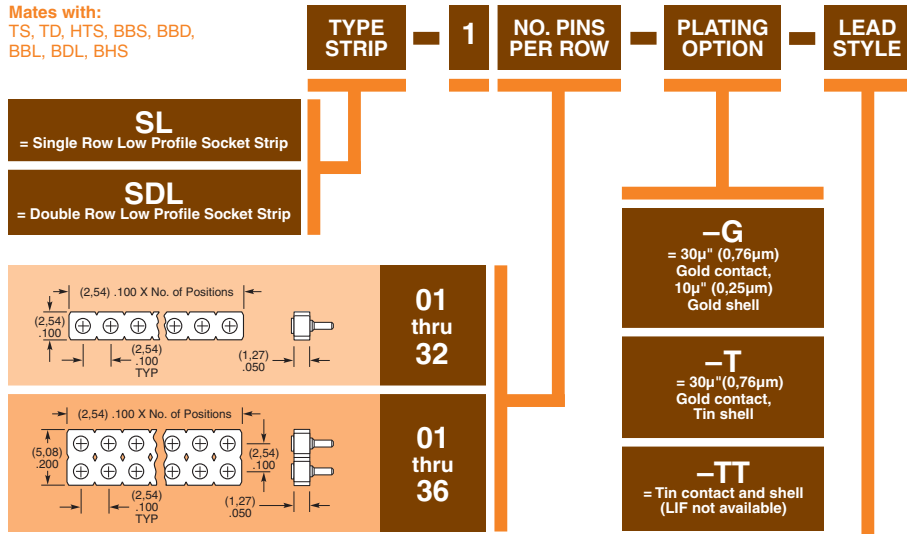
Low Insertion Force = 2.0oz (0,56N) avg., 0.5oz min ((0,43mm) .017" DIA probe except Style 30 is 2.0oz (0,56N) avg., .35oz (0,10N) min (0,46mm) .018" DIA probe)

RoHS Compliant: Yes

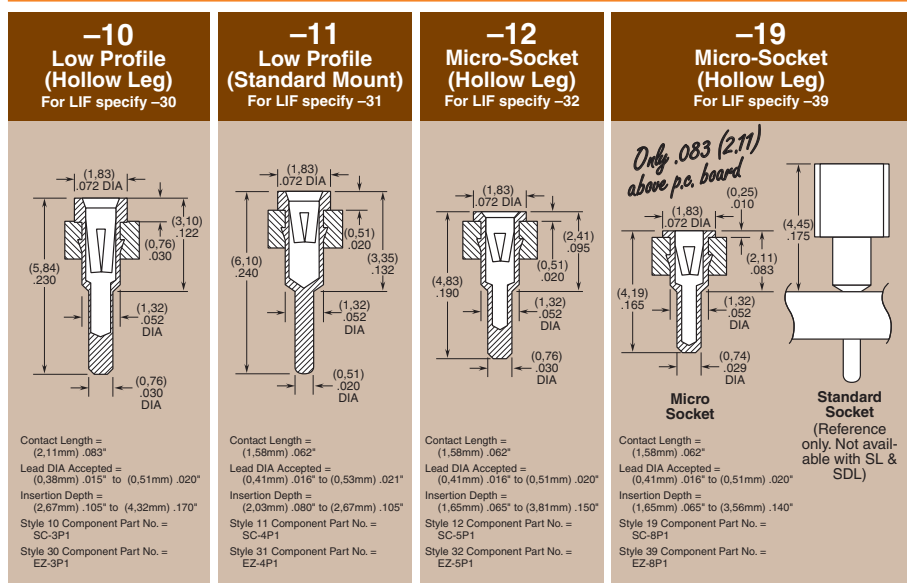
Lead-Free Solderable: Wave only

Note: Some lengths, styles and options are non-standard, non-returnable.

Mates with: TS, TD, HTS, BBS, BBD, BBL, BDL, BHS



Low Insertion Force (LIF) Available

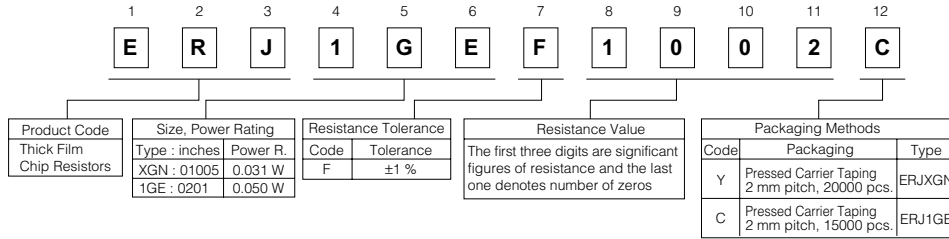


Due to technical progress, all designs, specifications and components are subject to change without notice.

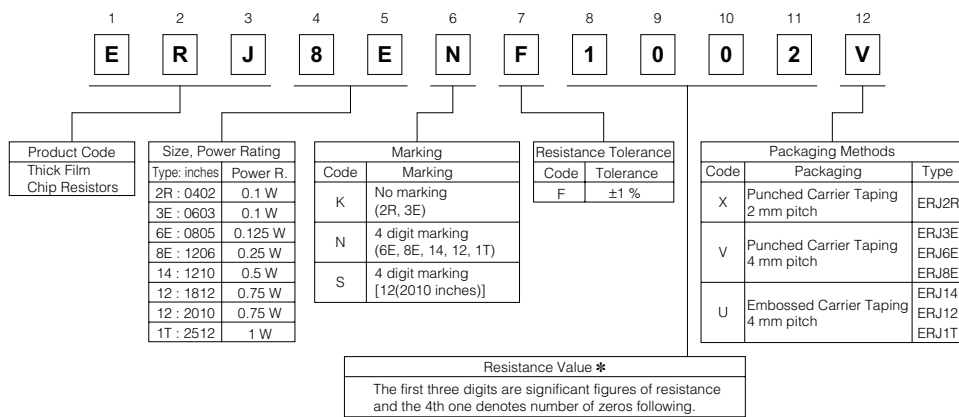
WWW.SAMTEC.COM

SAMTEC USA • Tel: 1-800-SAMTEC-9 or 812-944-6733 • Fax: 812-948-5047
 SAMTEC GERMANY • Tel: +49 (0) 89 / 89460-0 • Fax: +49 (0) 89 / 89460-299
 SAMTEC NORRICH/BALTIC • Tel: +46-84477280 • Fax: +46-87420413
 SAMTEC JAPAN • Tel: 045-475-1385 • Fax: 045-475-1340
 SAMTEC CHINA • Tel: 86-21-61103766 • Fax: 86-21-5423 4575
 SAMTEC TAIWAN • Tel: 886-2-2735-6109 • Fax: 886-2-2735-5036
 SAMTEC ASIA PACIFIC • Tel: 65 6745-5955 • Fax: 65 6841-1502
 SAMTEC HONG KONG • Tel: 852-26904658 • Fax: 852-26904842
 SAMTEC KOREA • Tel: 82-31-717-5685 • Fax: 82-31-717-5681
 SAMTEC SOUTH AFRICA • Tel: 27 11 452 8112 • Fax: 27 86 6714432
 SAMTEC UK • Tel: 01236 739292 • Fax: 01236 727113
 SAMTEC FRANCE • Tel: 01 60 95 06 60 • Fax: 01 60 95 06 61
 SAMTEC ITALY • Tel: 39 039 6890337 • Fax: 39 039 6890315
 SAMTEC INDIA • Tel: +91-80-3272 1612 • Fax: +91-80-4152 8187

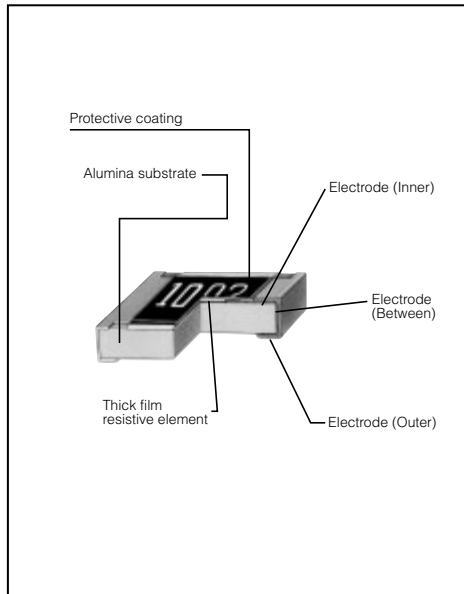
● ERJXG, 1G Series, ±1 % type



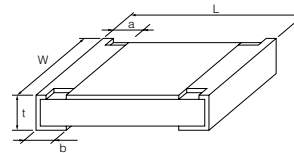
● ERJ2R, 3E, 6E, 8E, 14, 12, 1T Series, ±1 % type



■ Construction



■ Dimensions in mm (not to scale)



Type (inches)	Dimensions (mm)					Mass (Weight) [g/1000pcs.]
	L	W	a	b	t	
ERJXG (01005)	0.40 ^{+0.02}	0.20 ^{+0.02}	0.10 ^{+0.03}	0.10 ^{+0.03}	0.13 ^{+0.02}	0.04
ERJ1G, 1R (0201)	0.60 ^{+0.03}	0.30 ^{+0.03}	0.10 ^{+0.05}	0.15 ^{+0.05}	0.23 ^{+0.03}	0.15
ERJ2R□ (0402)	1.00 ^{+0.05}	0.50 ^{+0.05}	0.20 ^{+0.10}	0.25 ^{+0.05}	0.35 ^{+0.05}	0.8
ERJ3R□ (0603)	1.60 ^{+0.15}	0.80 ^{+0.15}	0.30 ^{+0.20}	0.30 ^{+0.15}	0.45 ^{+0.10}	2
ERJ6R□ (0805)	2.00 ^{+0.20}	1.25 ^{+0.10}	0.40 ^{+0.20}	0.40 ^{+0.20}	0.60 ^{+0.10}	4
ERJ3EK (0603)	1.60 ^{+0.15}	0.80 ^{+0.15}	0.30 ^{+0.20}	0.30 ^{+0.15}	0.45 ^{+0.10}	2
ERJ6EN (0805)	2.00 ^{+0.20}	1.25 ^{+0.10}	0.40 ^{+0.20}	0.40 ^{+0.20}	0.60 ^{+0.10}	4
ERJ8EN (1206)	3.20 ^{+0.05}	1.60 ^{+0.05}	0.50 ^{+0.20}	0.50 ^{+0.20}	0.60 ^{+0.10}	10
ERJ14N (1210)	3.20 ^{+0.20}	2.50 ^{+0.20}	0.50 ^{+0.20}	0.50 ^{+0.20}	0.60 ^{+0.10}	16
ERJ12N (1812)	4.50 ^{+0.20}	3.20 ^{+0.20}	0.50 ^{+0.20}	0.50 ^{+0.20}	0.60 ^{+0.10}	27
ERJ12S (2010)	5.00 ^{+0.20}	2.50 ^{+0.20}	0.60 ^{+0.20}	0.60 ^{+0.20}	0.60 ^{+0.10}	27
ERJ1TN (2512)	6.40 ^{+0.20}	3.20 ^{+0.20}	0.65 ^{+0.20}	0.60 ^{+0.20}	0.60 ^{+0.10}	45

Design and specifications are each subject to change without notice. Ask factory for the current technical specifications before purchase and/or use. Should a safety concern arise regarding this product, please be sure to contact us immediately.

Jul. 2008

■ Ratings
<±0.5 %>

Type (inches)	Power Rating at 70 °C (W)	Limiting Element Voltage (Maximum RCWV) ⁽¹⁾ (V)	Maximum Overload Voltage ⁽²⁾ (V)	Resistance Tolerance (%)	Resistance Range (Ω)	T.C.R. [$\times 10^{-6}/^{\circ}\text{C}$ (ppm/ $^{\circ}\text{C}$)]	Category Temperature Range (Operating Temperature Range) ($^{\circ}\text{C}$)
ERJ1RH (0201)	0.05	15	30	±0.5	1 k to 100 k (E24, E96)	±50	-55 to +125
ERJ1RK (0201)	0.05	15	30	±0.5	100 to 976 (E24, E96)	±100	-55 to +125
ERJ2RH (0402)	0.063	50	100	±0.5	100 to 100 k (E24, E96)	±50	-55 to +125
ERJ2RK (0402)	0.063	50	100	±0.5	10 to 97.6 102 k to 1 M (E24, E96)	±100	-55 to +125
ERJ3RB (0603)	0.063	50	100	±0.5	100 to 100 k (E24, E96)	±50	-55 to +125
ERJ3RE (0603)	0.063	50	100	±0.5	10 to 97.6 102 k to 1 M (E24, E96)	±100	-55 to +125
ERJ6RB (0805)	0.1	150	200	±0.5	100 to 100 k (E24, E96)	±50	-55 to +125
ERJ6RE (0805)	0.1	150	200	±0.5	10 to 97.6 102 k to 1 M (E24, E96)	±100	-55 to +125

<±1 %>

Type (inches)	Power Rating at 70 °C (W)	Limiting Element Voltage (Maximum RCWV) ⁽¹⁾ (V)	Maximum Overload Voltage ⁽²⁾ (V)	Resistance Tolerance (%)	Resistance Range (Ω)	T.C.R. [$\times 10^{-6}/^{\circ}\text{C}$ (ppm/ $^{\circ}\text{C}$)]	Category Temperature Range (Operating Temperature Range) ($^{\circ}\text{C}$)
ERJXG (01005)	0.031	15	30	±1	10 to 1 M (E24, E96)	<100 Ω : ±300 100 Ω ≤ : ±200	-55 to +125
ERJ1G (0201)	0.05	25	50	±1	10 to 1 M ⁽³⁾ (E24, E96)	±200	-55 to +125
ERJ2RK (0402)	0.1	50	100	±1	10 to 1 M (E24, E96)	±100	-55 to +155
ERJ3EK (0603)	0.1	75	150	±1	10 to 1 M (E24, E96)	±100	-55 to +155
ERJ6EN (0805)	0.125	150	200	±1	10 to 2.2 M (E24, E96)	±100	-55 to +155
ERJ8EN (1206)	0.25	200	400	±1	10 to 2.2 M (E24, E96)	±100	-55 to +155
ERJ14N (1210)	0.5	200	400	±1	10 to 1 M (E24, E96)	±100	-55 to +155
ERJ12N (1812)	0.75	200	500	±1	10 to 1 M (E24, E96)	±100	-55 to +155
ERJ12S (2010)	0.75	200	500	±1	10 to 1 M (E24, E96)	±100	-55 to +155
ERJ1TN (2512)	1	200	500	±1	10 to 1 M (E24, E96)	±100	-55 to +155

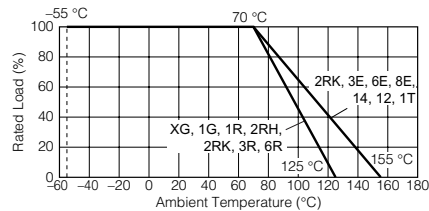
(1) Rated Continuous Working Voltage (RCWV) shall be determined from $\text{RCWV} = \sqrt{\text{Power Rating} \times \text{Resistance Values}}$, or Limiting Element Voltage (max. RCWV) listed above, whichever less.

(2) Overload (Short-time Overload) Test Voltage (SOTV) shall be determined from $\text{SOTV} = 2.5 \times \text{Power Rating}$ or max. Overload Voltage listed above whichever less.

(3) Please contact us when you need a type with a resistance of less than 10 Ω.

Power Derating Curve

For resistors operated in ambient temperatures above 70 °C, power rating shall be derated in accordance with the figure on the right.



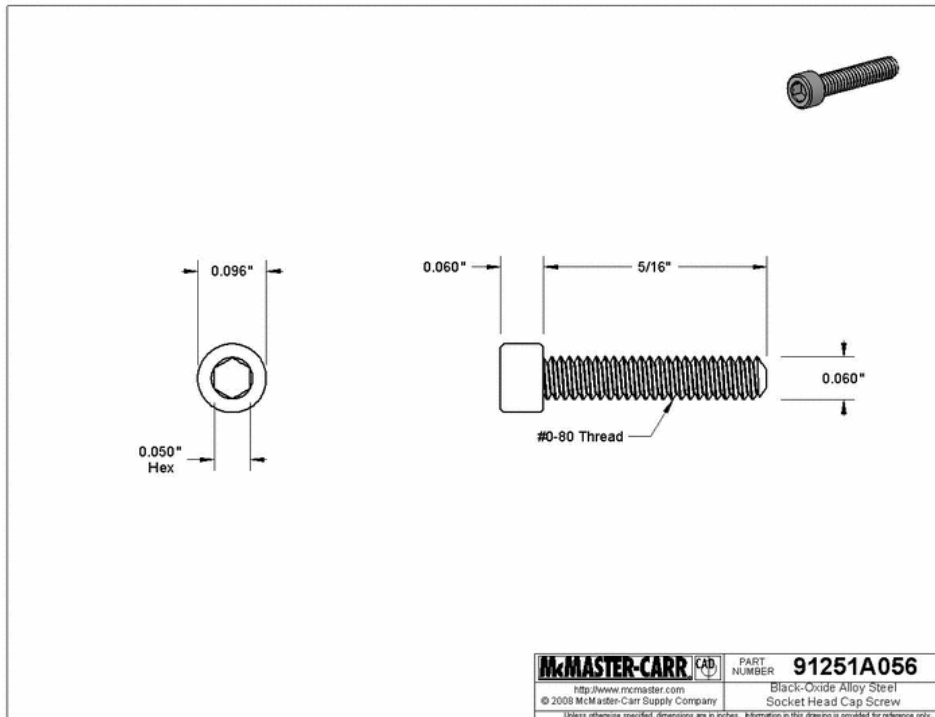
Design and specifications are each subject to change without notice. Ask factory for the current technical specifications before purchase and/or use. Should a safety concern arise regarding this product, please be sure to contact us immediately.

Jul. 2008

Socket Cap Screws



Part Number: 91251A056	\$8.08 per Pack of 50
Head Style	Standard
Standard Head Style	Standard
Material Type	Steel
Finish	Black-Oxide
Class	Not Rated
Drive Style	Hex Socket
Inch Thread Size	0-80
Length	5/16"
Thread Length	Fully Threaded
Thread Direction	Right Handed
Tip Type	Plain
Self-Locking Method	None
Screw Quantity	Individual Screw
Hex Size	.050"
Head Diameter	.096"
Head Height	.060"
Rockwell Hardness	Minimum C39
Minimum Tensile Strength	180,000 psi
Thread Fit	Class 3A
Specifications Met	American Society for Testing and Materials (ASTM)
ASTM Specification	ASTM A574

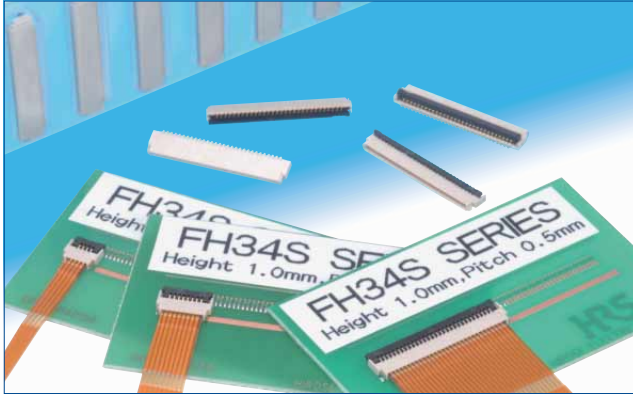


The product information in this catalog is for reference only. Please request the Engineering Drawing for the most current and accurate design information.
 All non-RoHS products have been discontinued, or will be discontinued soon. Please check the products status on the Hirose website RoHS search at www.hirose-connectors.com, or contact your Hirose sales representative.

0.5 mm Pitch, 1.0 mm above the board Top Contact, Back-Flip actuator Flexible Printed Circuit & Flexible Flat Cable ZIF Connectors

FH34(S)Series

Increased FPC/FFC holding force



Features

1. Low-profile

With the 1.0 mm above the board and width of 3.8 mm the connectors are used in space saving applications.

2. Increased FPC/FFC retention

As compared with existing similar construction connectors:

- * In horizontal direction: Approximately 2.6 times
- * In vertical direction: Approximately 2 times

3. Unique Back-Flip rotating actuator

The rotating actuator opens from the back of the connector, assuring reliable electrical and mechanical connection.

4. Easy FPC/ FFC insertion

Entry chamfers at all sides of the FPC/FFC insertion slot assure correct insertion and positioning of the FPC/FFC.

5. Delivered with the actuator open

FPC/FFC can be immediately inserted without the need for the opening of the actuator.

6. Standard FPC/FFC thickness

Reliable connection with the use of ready available 0.3 mm thick FPC/FFC.

7. Compatible with existing connectors.

FPC/FFC and PCB mounting patterns are the same as for the FH19SC Series (bottom contact), allowing the use of both connectors for interconnections between two boards or replacement of the connectors.

8. Conductive traces on the PCB can run under the connector

No exposed contacts on the bottom of the connector.

9. Board placement with automatic equipment

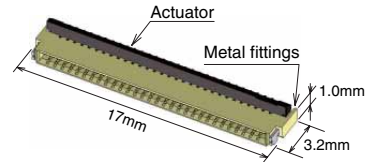
Flat top surface and packaging on the tape-and-reel allows use of vacuum nozzles.

Standard reel contains 5,000 pieces.

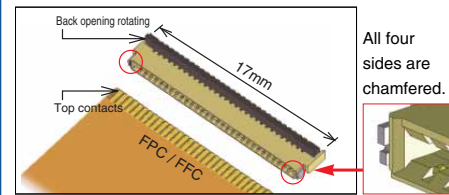
Applications

Mobile phones, PDA's, digital cameras, digital camcorders, camera modules and other compact devices requiring Flexible Printed Circuit connections using high reliability extremely small profile connectors.

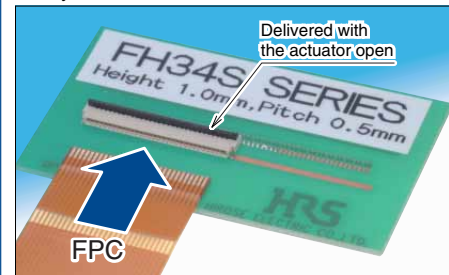
Space saving (30 pos. shown)



Easy FPC/FFC insertion



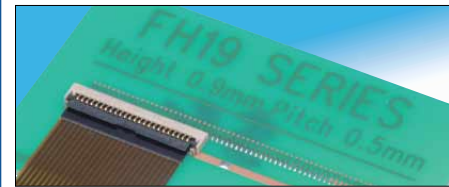
Ready to insert FPC/FFC



FPC/FFC inserted and retained.
Completed electrical and mechanical connection.



Compatible with existing connectors.(FH19SC SERIES)



The product information in this catalog is for reference only. Please request the Engineering Drawing for the most current and accurate design information.
 All non-RoHS products have been discontinued and will be discontinued soon. Please check the product's status on the Hirsch website. RoHS search at www.hirsch-connectors.com or contact your Hirsch sales representative.

■ Specifications

Ratings	Current rating 0.5 A	Operating temperature range: -55 to +85°C (Note 1)	Storage temperature range: -10 to +50°C (Note 2)
	Voltage rating 50 Vrms AC	Operating humidity range: Relative humidity 90% max. (No condensation)	Storage humidity range: Relative humidity 90% max. (No condensation)

Recommended FPC/FFC	Thickness: 0.3 +/- 0.03 mm, Gold plated contact pads
---------------------	--

Item	Specification	Conditions
1. Insulation resistance	500 MΩ min.	100 V DC
2. Withstanding voltage	No flashover or insulation breakdown	250 Vrms AC / one minute
3. Contact resistance	100 mΩ max. * Including FPC and FFC conductor resistance	1 mA, AC / DC 20mV max (AC: 1kHz)
4. Durability	Contact resistance: 100 mΩ max. No damage, cracks, or parts dislocation	20 cycles
5. Vibration	No electrical discontinuity of 1μs or longer Contact resistance: 100 mΩ max. No damage, cracks, or parts dislocation	Frequency: 10 to 55 Hz, single amplitude of 0.75 mm, 10 cycles in each of the 3 axis
6. Shock	No electrical discontinuity of 1μs or longer Contact resistance: 100 mΩ max. No damage, cracks, or parts dislocation	Acceleration of 981m/s ² , 6 ms duration, sine half-wave, 3 cycles in each of the 3 axis
7. Humidity (Steady state)	Contact resistance: 100 mΩ max. Insulation resistance: 50 MΩ min. No damage, cracks, or parts dislocation	96 hours at 40°C and humidity of 90 to 95%
8. Temperature cycle	Contact resistance: 100 mΩ max. Insulation resistance: 50 MΩ min. No damage, cracks, or parts dislocation	Temperature : -55°C → +15°C → +35°C → +85°C → +15°C → +35°C Time: 30 → 2 to 3 → 30 → 2 to 3 minutes 5 cycles
9. Resistance to soldering heat	No deformation of components affecting performance	Reflow: At the recommended temperature profile Manual soldering: 350°C ±5°C for 5 seconds (Note 3)

Note1: Includes temperature rise caused by current flow.

Note2: The term "storage" refers to products stored for a long period prior to mounting and use.

The operating temperature and humidity range covers the non-conducting condition of installed connectors in storage, shipment or during transportation after board mounting.

Note3: Small blisters of the molding compounds in small areas will not affect form, fit or function.

Note4: Information contained in this catalog represents general requirements for this Series.

Contact us for the drawings and specifications for a specific part number shown.

■ Materials

Part	Material	Finish	Remarks
Insulator	LCP	Color: Beige	UL94V-0
Actuator	PA	Color: Black	
Contacts	Phosphor bronze	Gold plating	—
Metal fittings	Phosphor bronze	Pure tin reflow plating	—

■ Ordering information

FH34 S - 30S - 0.5 SH (50)

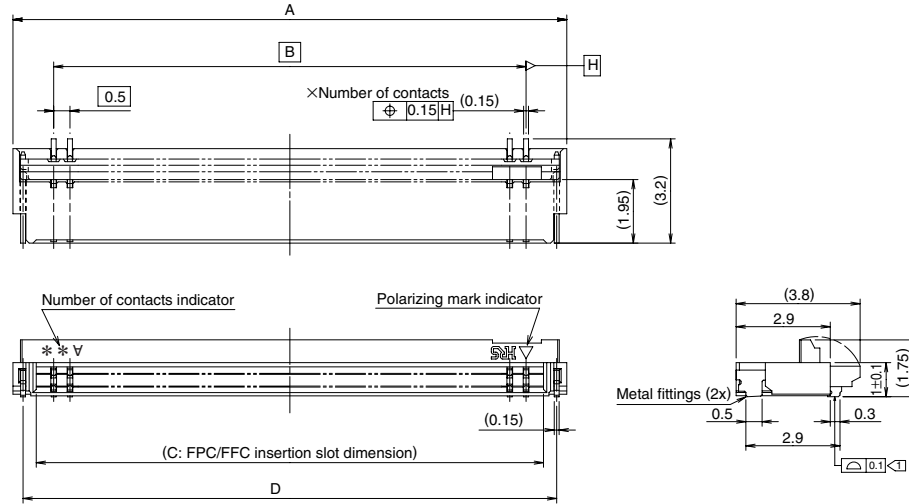
① ② ③ ④ ⑤ ⑥

① Series name : FH34	⑤ Termination type : SH : SMT horizontal mounting type
② S : FPC/FFC 0.3 mm thick	⑥ Plating specifications (50)...Gold plating with nickel barrier
③ Number of positions : 4, 8, 11, 14, 16, 22 26, 30, 32, 34	5,000 pieces / reel
④ Contact pitch : 0.5mm	

The product information in this catalog is for reference only. Please request the Engineering Drawing for the most current and accurate design information.
 All non-RoHS products have been discontinued and will be discontinued soon. Please check the products status on the Hirose website. RoHS search at www.hirose-connectors.com or contact your Hirose sales representative.

FH34(S) Series 0.5 mm Pitch, 1.0 mm above the Board Top Contact, Back Flip-actuator Flexible Printed Circuit & Flexible Flat Cable ZIF Connectors

Connector Dimensions



Note 1: The coplanarity of each terminal lead is within 0.1.

Note 2: Slight variations in color of the plastic compounds do not affect form, fit or function of the connector.

All dimensions: mm

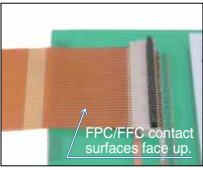
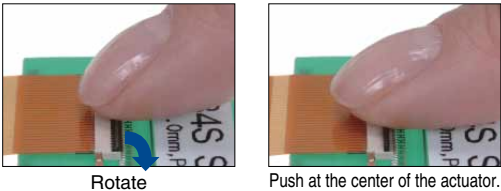
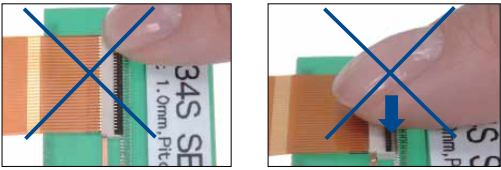
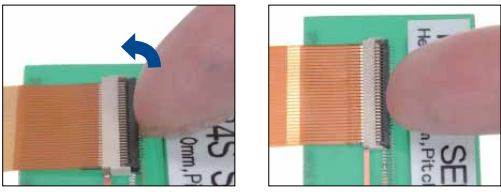
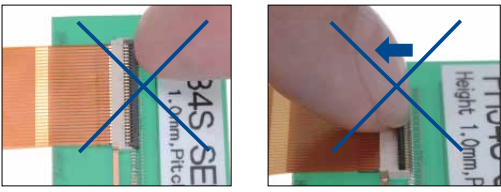
Part Number	CL No.	Number of Contacts	A	B	C	D	RoHS
FH34S- 4S-0.5SH(50)	580-1203-2-50	4	4	1.5	2.53	3.38	YES
FH34S- 6S-0.5SH(50)	Reserved for product expansion	6	5	2.5	3.53	4.38	
FH34S- 8S-0.5SH(50)	580-1204-5-50	8	6	3.5	4.53	5.38	
FH34S- 9S-0.5SH(50)	Reserved for product expansion	9	6.5	4	5.03	5.88	
FH34S-11S-0.5SH(50)	580-1213-6-50	11	7.5	5	6.03	6.88	
FH34S-12S-0.5SH(50)	Reserved for product expansion	12	8	5.5	6.53	7.38	
FH34S-14S-0.5SH(50)	580-1206-0-50	14	9	6.5	7.53	8.38	
FH34S-16S-0.5SH(50)	580-1211-0-50	16	10	7.5	8.57	9.38	
FH34S-20S-0.5SH(50)	Reserved for product expansion	20	12	9.5	10.57	11.38	
FH34S-22S-0.5SH(50)	580-1216-4-50	22	13	10.5	11.57	12.38	
FH34S-24S-0.5SH(50)	Reserved for product expansion	24	14	11.5	12.57	13.38	
FH34S-26S-0.5SH(50)	580-1212-3-50	26	15	12.5	13.57	14.38	
FH34S-28S-0.5SH(50)	Reserved for product expansion	28	16	13.5	14.57	15.38	
FH34S-30S-0.5SH(50)	580-1201-7-50	30	17	14.5	15.57	16.38	
FH34S-32S-0.5SH(50)	580-1208-6-50	32	18	15.5	16.57	17.38	
FH34S-34S-0.5SH(50)	580-1207-3-50	34	19	16.5	17.57	18.38	

Tape and reel packaging (5,000 pieces/reel).

Order by number of reels.

◆ Operation and Precautions

Exercise care when handling connectors. Follow recommendations given below.

Operation	Precautions
<p>1. As delivered</p> <p>Delivered with the actuator open. There is no need to operate the actuator prior to inserting the FPC/FFC.</p> 	<ul style="list-style-type: none"> Do not close the actuator without the FPC/FFC inserted.
<p>2. FPC/FFC insertion</p> <p>Insert the FPC/FFC with the conductive surfaces facing up. Align the FPC/FFC straight with the connector and insert it firmly all the way.</p> 	<ul style="list-style-type: none"> This connector is of the top contact specification. The contacts are making connection with the FPC/FFC pads from the top. Do not insert the FPC/FFC with the pads facing down. When inserting the FPC/FFC do not twist it. Insert straight. Improper insertion may cause deformation of the contacts and connection failures. Be sure to insert the FPC/FFC when the actuator is fully open.
<p>3. Locking</p> <p>After FPC/FFC insertion, rotate the actuator down to a full stop, pushing it at the center.</p> 	<ul style="list-style-type: none"> Do not operate the actuator by only one end. Open or close by pushing at the center. Do not try to rotate the actuator past the fully open 90° position. This will damage the connector, preventing it from use. Do not apply excessive force to the connector when the actuator is closed. 
<p>4. FPC/FFC removal (Lock release)</p> <p>Carefully rotate the actuator up to 90°, lifting it at the center.</p> 	<ul style="list-style-type: none"> Do not operate the actuator from one end only. The actuator opens only 90°. Do not attempt to open it past this angle or grasp it. During the opening of the actuator do not press it toward the connector body. Rotate up at the center. 

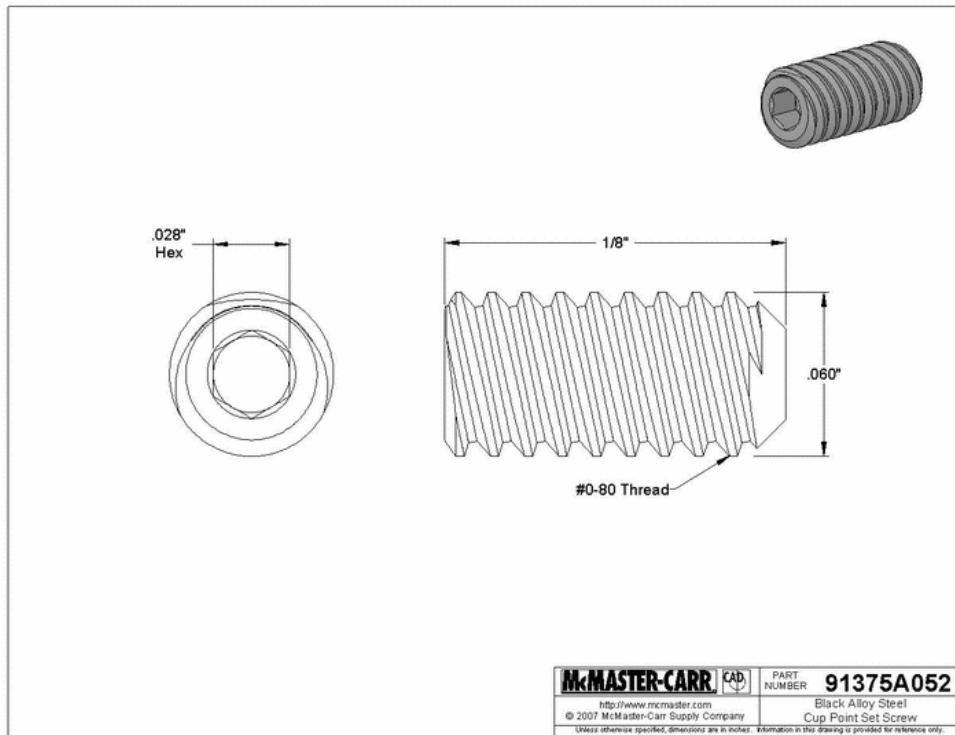
Set Screws



Part Number: **91375A052**

\$12.05 per Pack of 25

Screw Style	Standard Socket
Material Type	Steel
Finish	Black-Finish
Point	Cup
System of Measurement	Inch
Inch Thread Size	0-80
Decimal Equivalent	.060"
Hex Size	.028"
Length	1/8"
Thread Fit	Class 3A
Rockwell Hardness	Minimum C45
Specifications Met	American Society of Mechanical Engineers (ASME), American Society for Testing and Materials (ASTM)
ASME Specification	ASME B18.3
ASTM Specification	ASTM F912
Set Screw Quantity	Individual Screw



McMASTER-CARR © McMaster-Carr Supply Company. All rights reserved.

Appendix I

Antenna - Accessories

I.1 Power+I²C Dongle

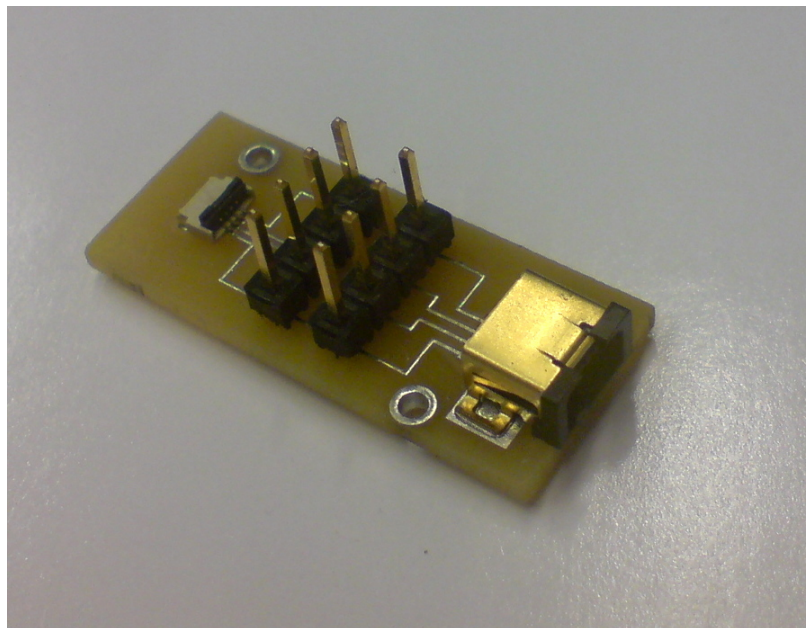


Figure I.1: Power+I²C Dongle.

pagecommand = , scale = 0.8]Appendix/Circuit-Dongle.pdf

I.2 Programming Dongle

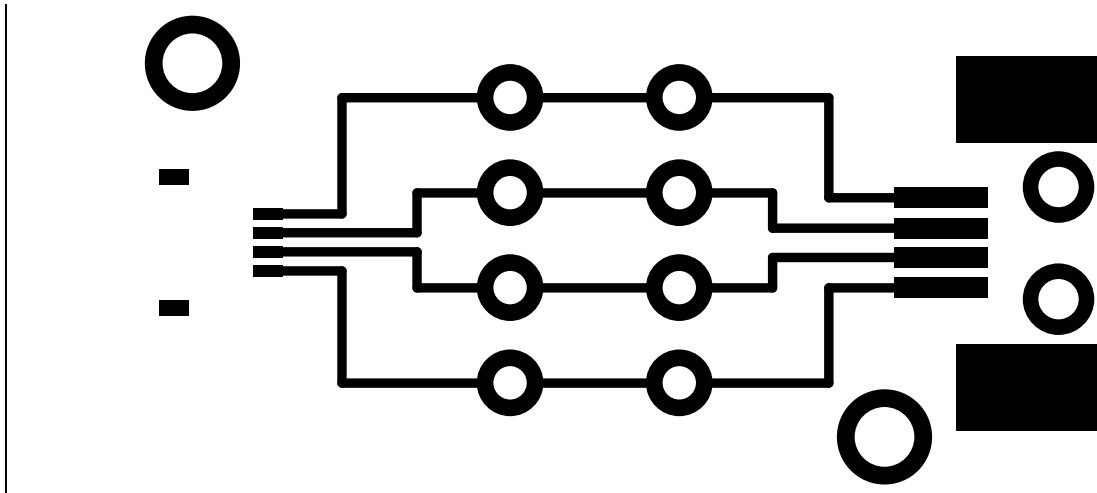


Figure I.2: PCB layout of the I²C + Power Dongle.

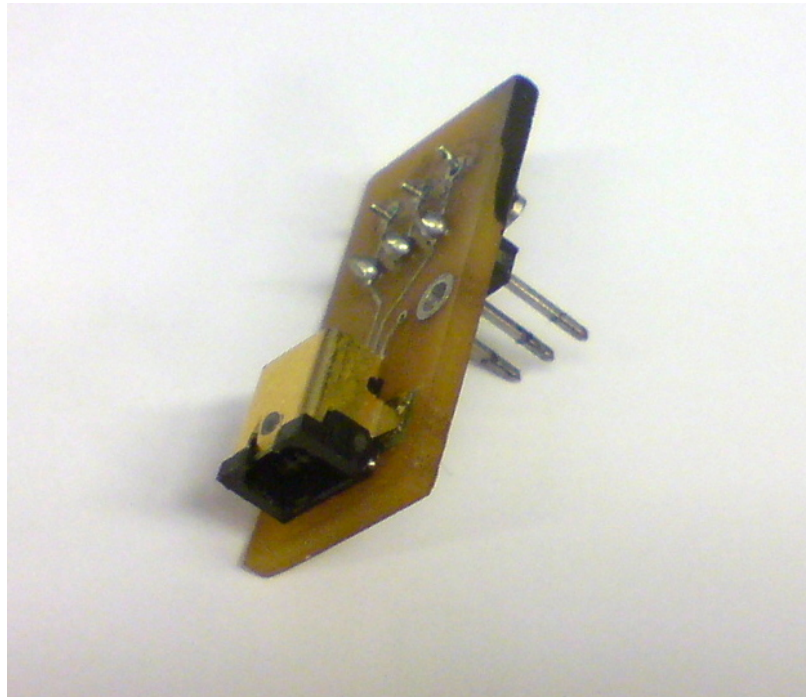


Figure I.3: Programming Dongle.

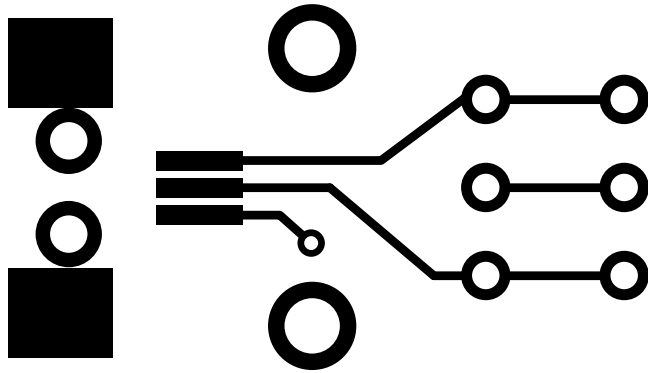


Figure I.4: PCB top layout of the Programming Dongle.

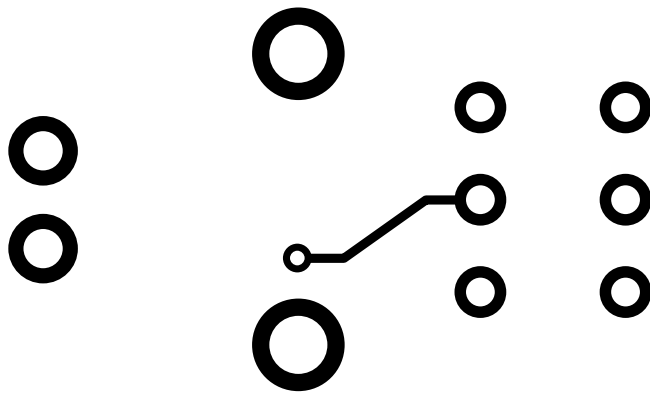


Figure I.5: PCB bottom layout of the Programming Dongle.

Appendix J

Antenna - Users Manual

J.1 Assembling antenna

The assembly stages of a two segment antenna is depicted here step by step.

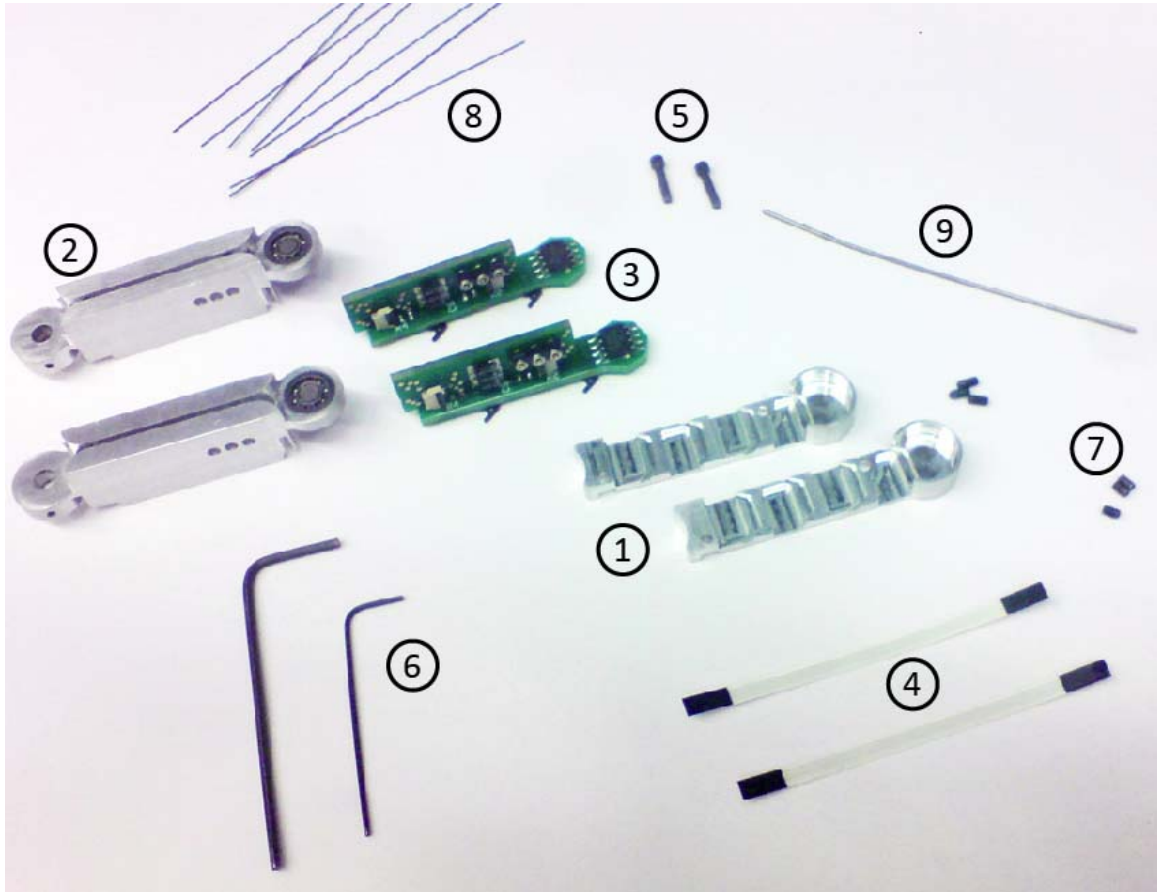
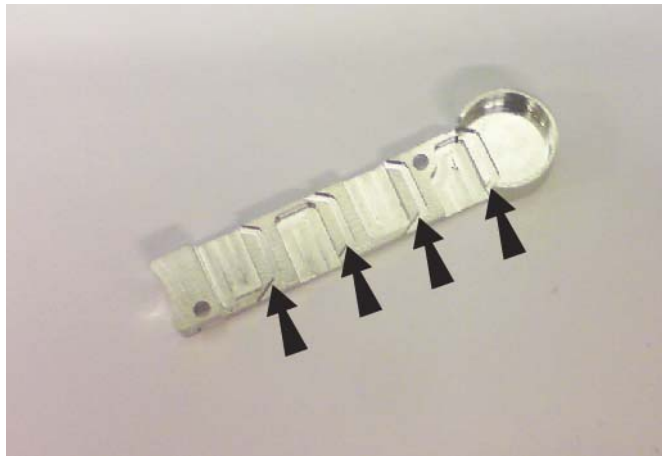


Figure J.1: 1 Aluminum bottom shell, 2 Aluminum top shell with bearing+magnet assembly, 3 Segment electronic sub-assembly, 4 Coupling cable, 5 0-80 Socket cap screw $\times 4$, 6 0.050" and 0.028" allen keys, 7 0-80 set screws $\times 3$, 8 various NiTi hairs, 9 NiTi backbone.



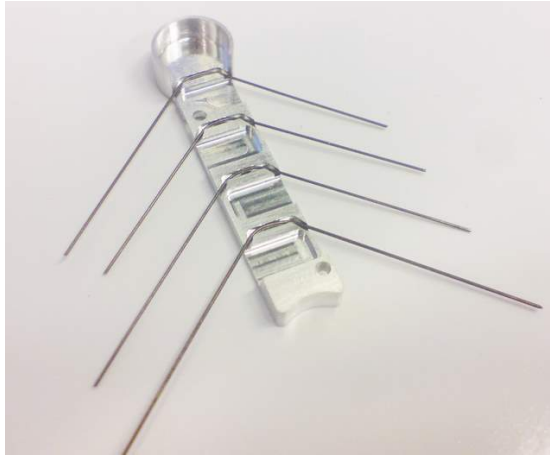
(h)

(a) We start from the bottom piece. Notice the periodic narrow channels carved on the top surface indicated by arrows. These channels hold the hairs.



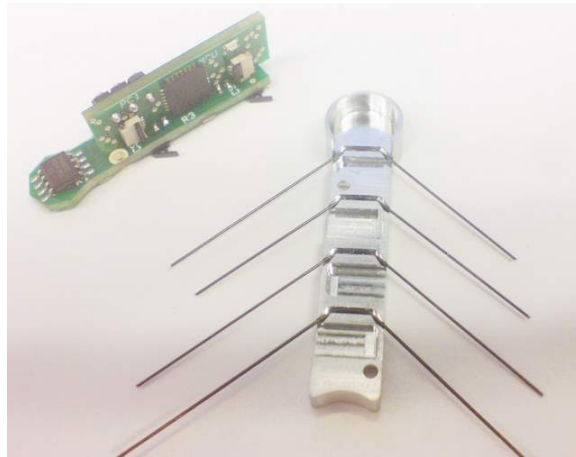
(b) Place the hairs by bending them. Their restoring stiffnesses should hold them in place.

Figure J.2: Assembly Stages - Placing hairs.



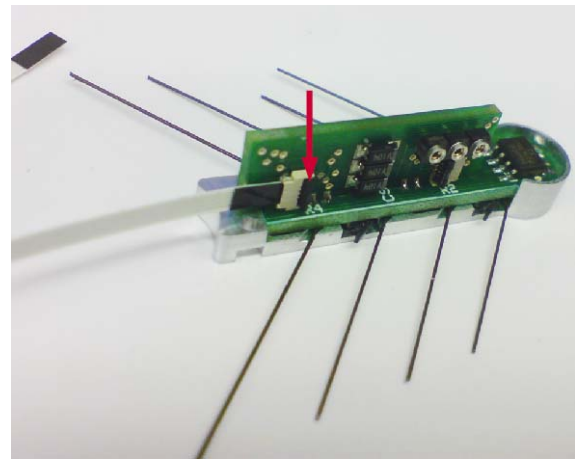
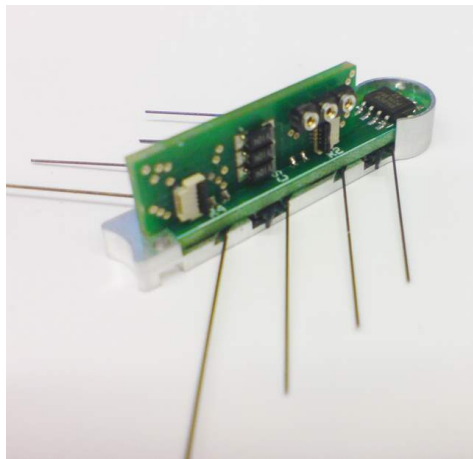
(h)

(a) The hairs should look like this after occupying all channels



(b) Next we take one of the electronic assemblies

Figure J.3: Assembly Stages - Placing the electronic sub-assembly.

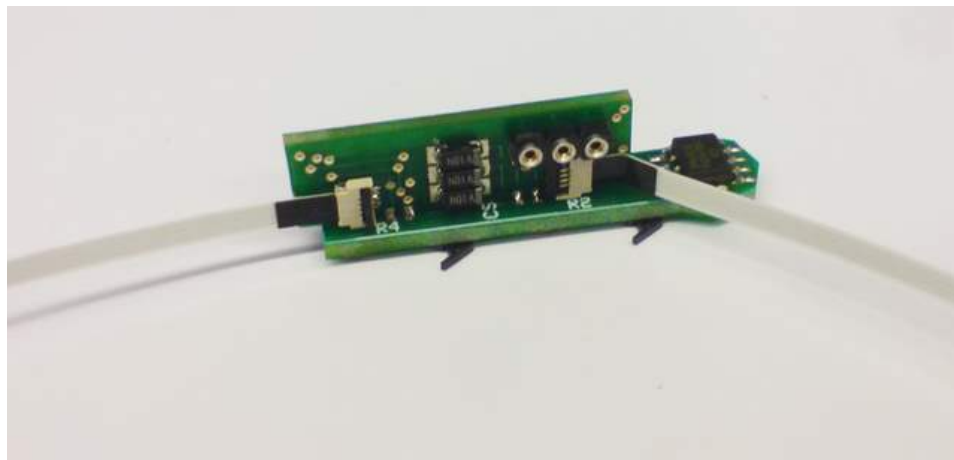
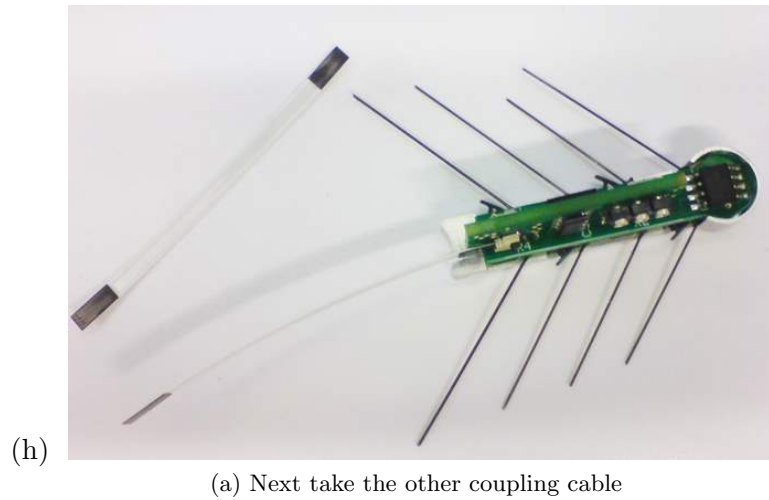


(h)

(a) Place the electronic sub-assembly such that the detector switches land on the gaps. There is only one way that the sub-assembly can sit on the bottom piece comfortably.

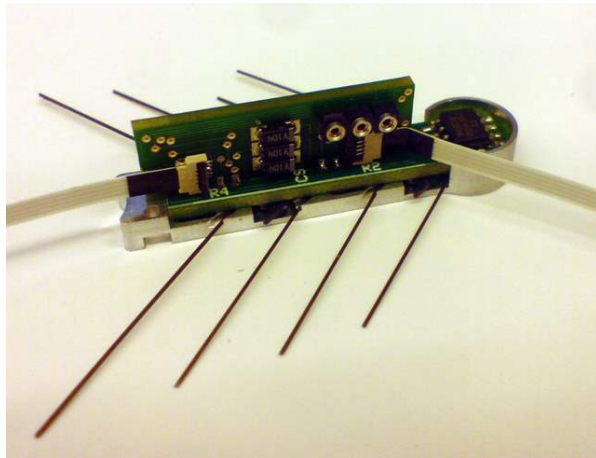
(b) Next, take one coupling FFC (Flat Flex Cable) cable and insert to one of the segment connectors. Make sure that while inserting the actuator part of the connector is raised (depicted by a red arrow). Check Appendix H for the segment connector operation for more details.

Figure J.4: Assembly Stages - Coupling Cables.



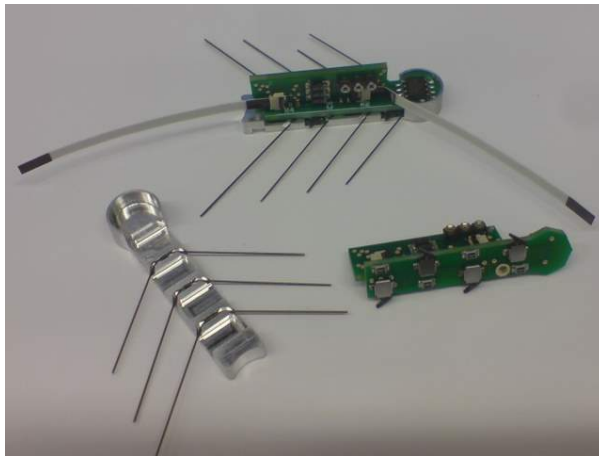
(b) Insert the second coupling cable to the opposite end of the electronic sub-assembly

Figure J.5: Assembly Stages - Coupling Cables.



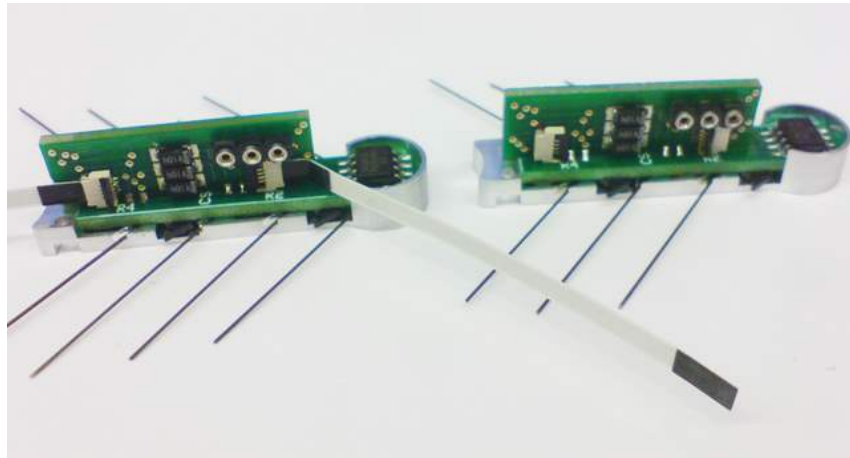
(h)

(a) The segment should look like this after inserting both coupling cables



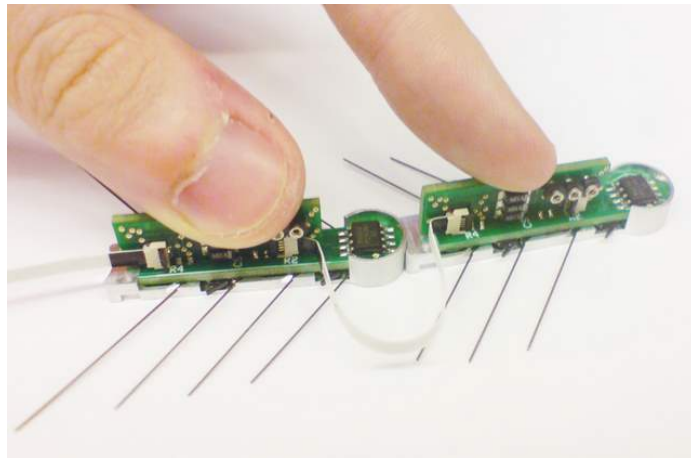
(b) Take the second aluminum bottom piece and place its hairs.

Figure J.6: Assembly Stages - Second segment.



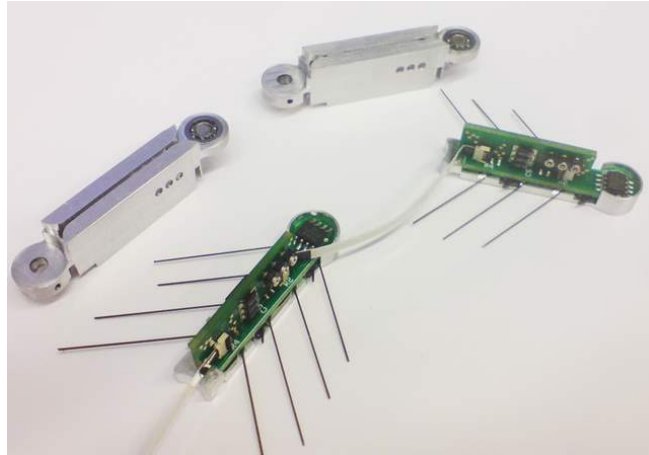
(h)

(a) Take the other electronic sub-assembly and place it on the second bottom piece with hairs



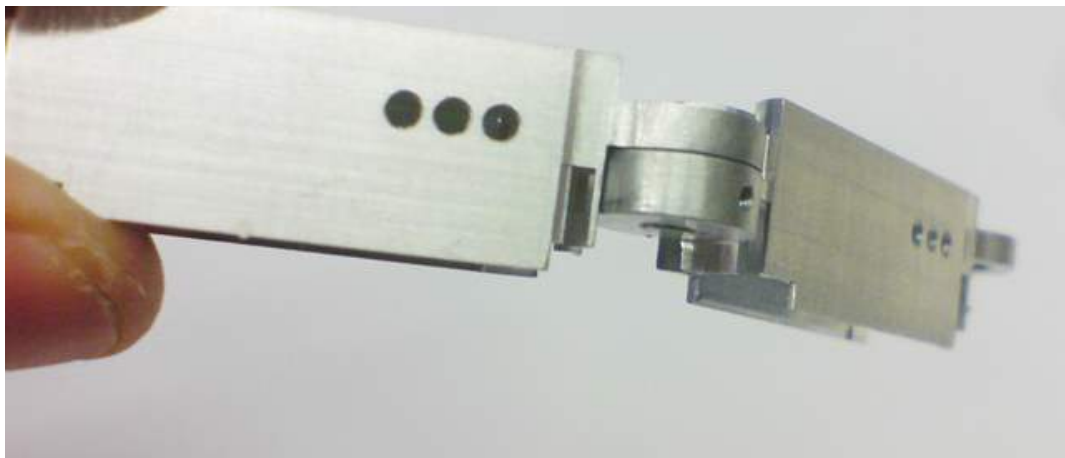
(b) Insert the free end of the closest coupling cable to the closest connector of the second segment

Figure J.7: Assembly Stages - Second segment.



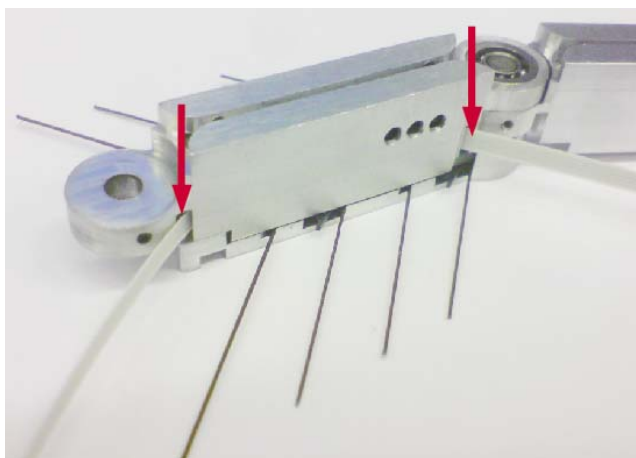
(h)

(a) Now take the aluminum top shells



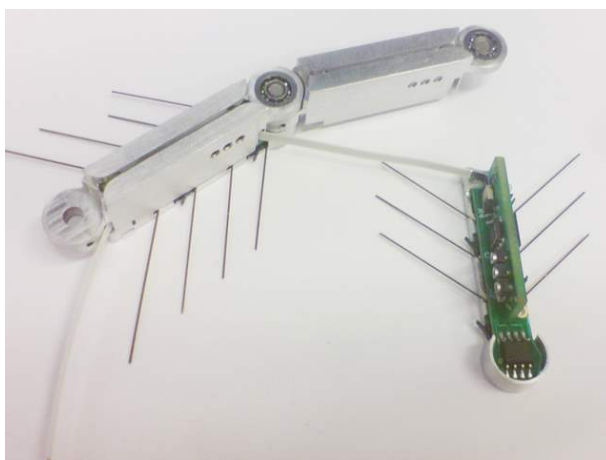
(b) Attach the top aluminum shells together. This is done by inserting the shaft magnet of one shell into the hinge-end of the second shell

Figure J.8: Assembly Stages - Integrating segments.



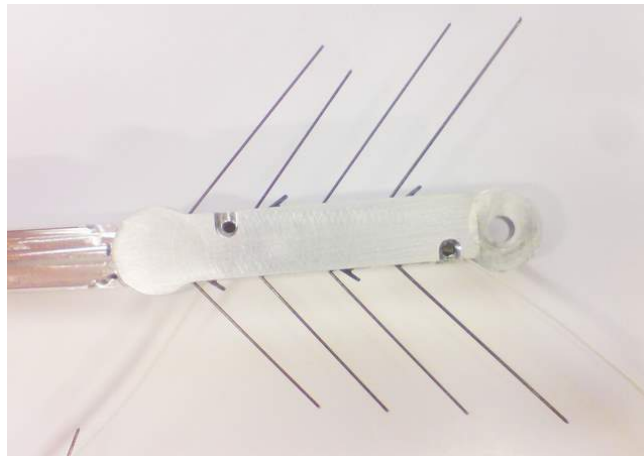
(h)

(a) Combine the top and bottom parts of one of the segments. During this operation make sure that both coupling cables are passing through the slits (see arrows) of the top shell. Do not press the shells together in the hopes that the cables will automatically get into these slits. Failing to do so will create an excessive force on the segment connectors and most likely detach from its surface mount footprint.



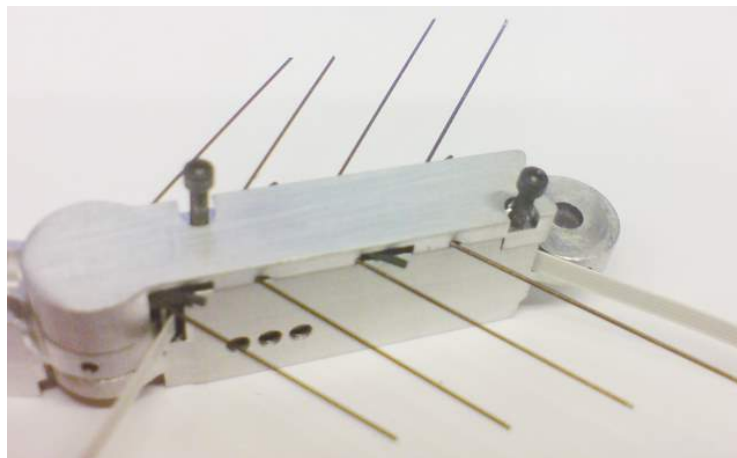
(b) Your assembly should look like this at this point

Figure J.9: Assembly Stages - Integrating segments.



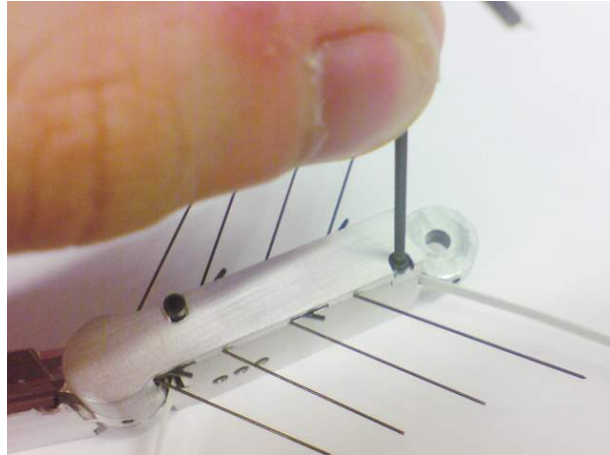
(h)

(a) Now turn the entire partial assembly upside down. You will notice two holes for the cap screws.



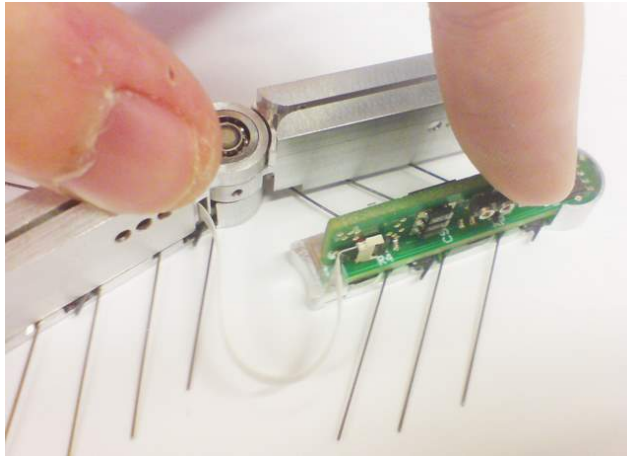
(b) Insert two 0-80 socket cap screws into the holes. Again do not press the screws hard. They may be hitting the coupling cables underneath. Instead slowly rotate the screws and push gently downward.

Figure J.10: Assembly Stages - Integrating segments.



(h)

(a) When you come to the point where the screws won't go in more, just take the 0.050" allen key and tighten the screws. Note that it will take only a few revolutions to fully tighten them.

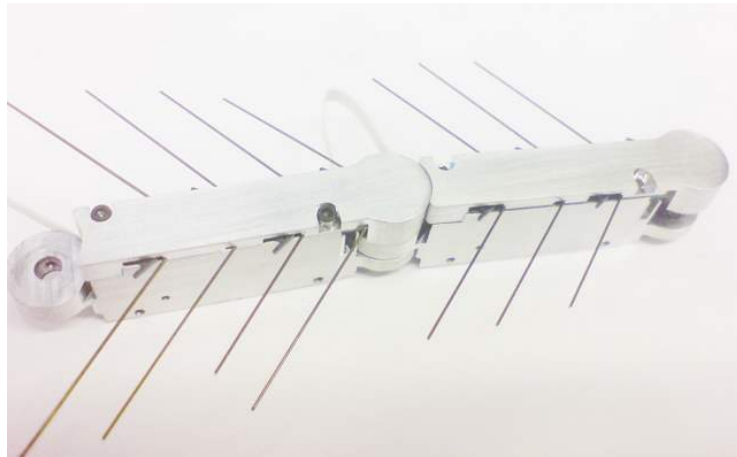


(b) Now bring the segments together again and get ready to insert the second piece.

Figure J.11: Assembly Stages - Integrating segments.

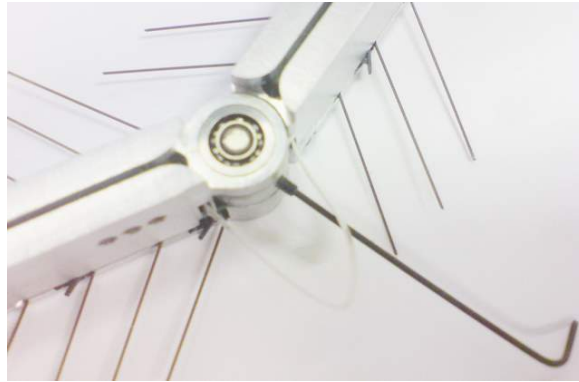


- (h)
- (a) Carefully insert the second piece. Again make sure the coupling cable is passing through the associated slit.



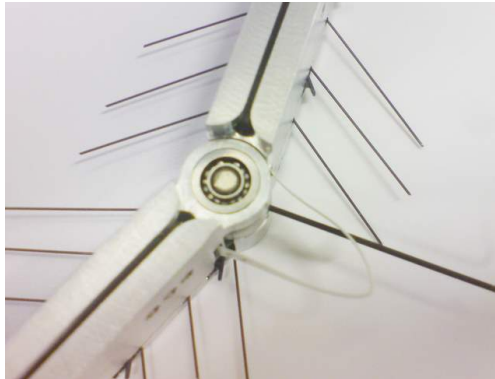
- (b) We are now ready to put the cap screws for this segment as well.

Figure J.12: Assembly Stages - Integrating segments.



(h)

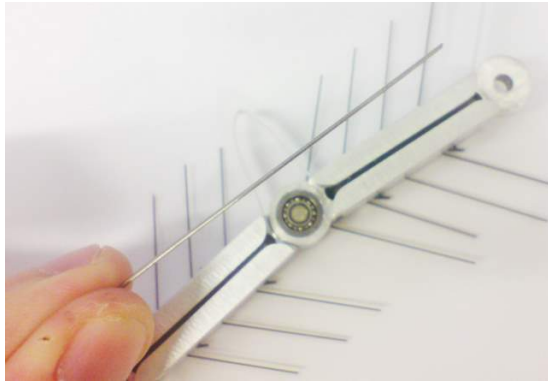
(a) Next we take a 0-80 set screw. Using the 0.028" allen key, tighten the magnet that is passing through the bearing.



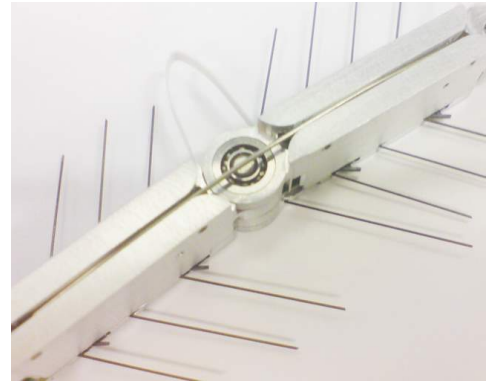
(b) This will make sure that the magnet is fixed with respect to the second segment but free to rotate with respect to the first segment. Thus when the second segment turns, the magnet will turn with it. This effectively will cause the Hall-effect sensor to register the angular change

Figure J.13: Assembly Stages - Fixing the magnet.

(h)

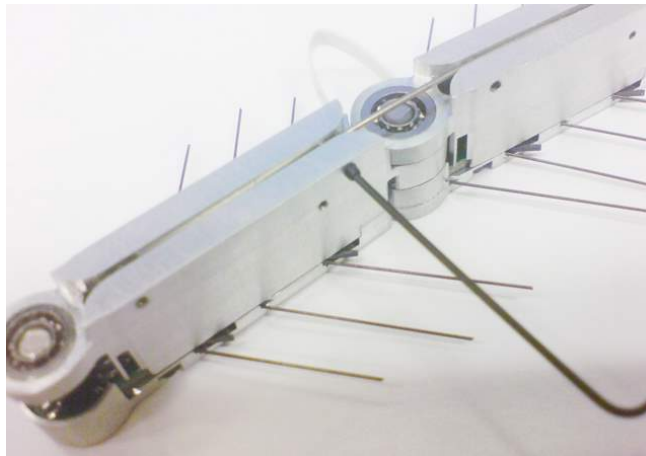


(a) Now take the NiTi backbone.



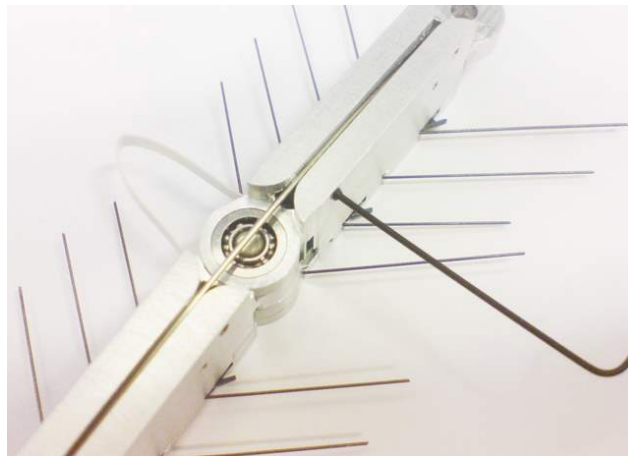
(b) Center the NiTi wire around the joint and place it inside the channel, which traverses the entire top side of the assembly.

Figure J.14: Assembly Stages - NiTi backbone.



(h)

(a) Now take a 0-80 set screw and insert it to the threaded hole on the side close to the joint. Tighten the screw such that it pinches the NiTi backbone



(b) Repeat the previous action across the joint, such that the NiTi backbone is pinched from two ends

Figure J.15: Assembly Stages - NiTi backbone.

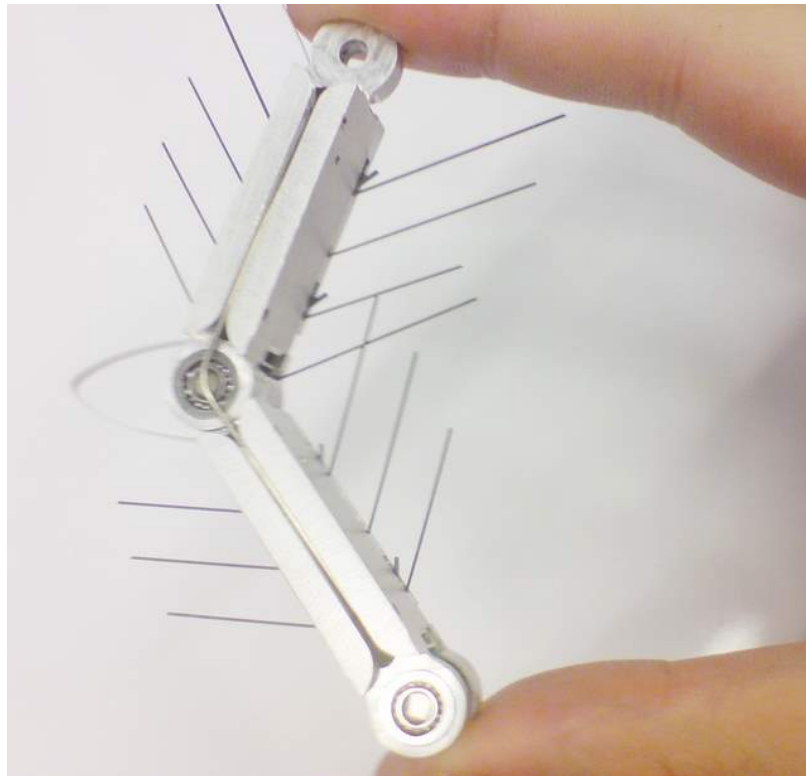


Figure J.16: This concludes the assembly of a two segment joint. Adding more segments simply follow the same procedure. Refer to maintenance section for troubleshooting specific problems and additional assembly steps.

J.2 Firmware update

This appendix contains a tutorial on how to use the Keil μ vision software to compile and upload a firmware into the program memory of the P89LPC938 microcontroller.

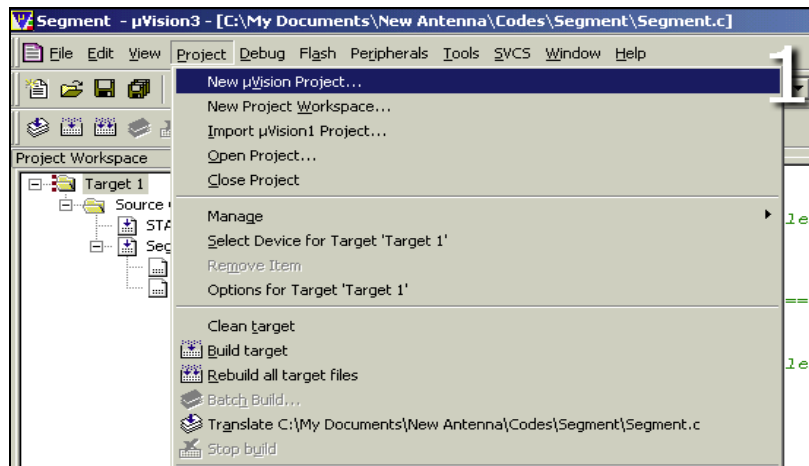
Programming P89LPC938 Microcontroller with Keil μ Vision 3

I- Starting a New Project

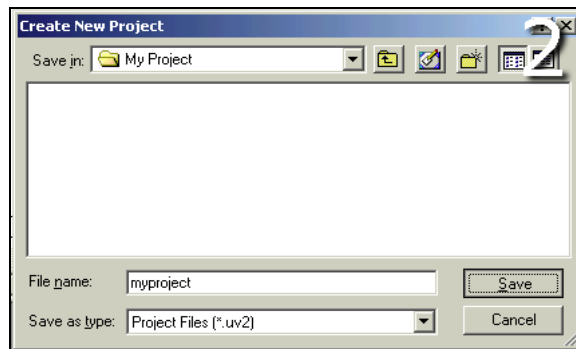
First open the program by clicking the associated icon.



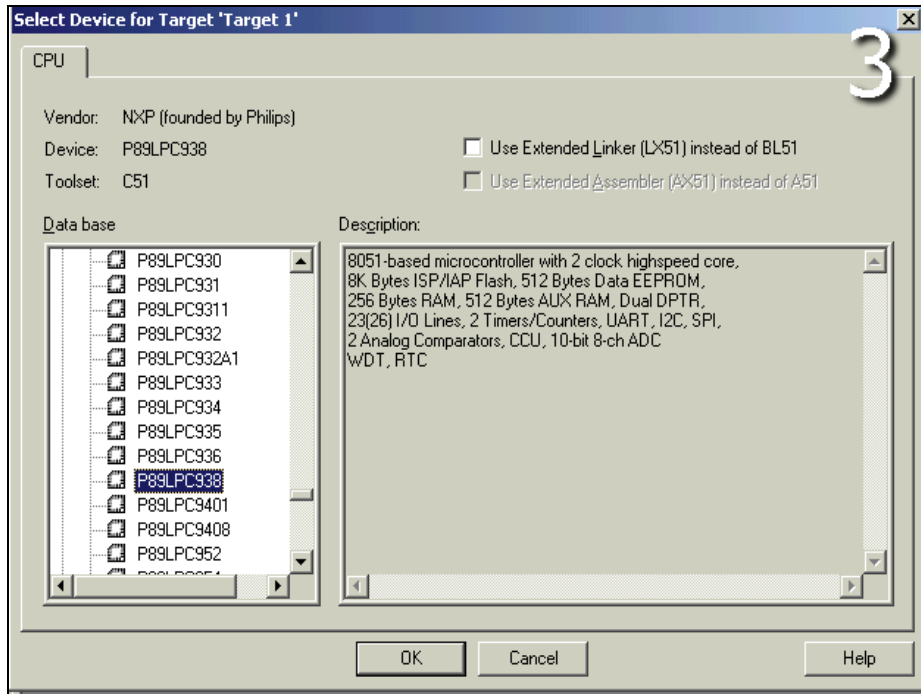
- 1- To start a new project click on the “**P**roject” button on the top bar and select “New μ Vision Project” menu item.



- 2- When the dialog box pops up, browse to the folder you want, type the name of your choosing for the project and click “**S**ave”



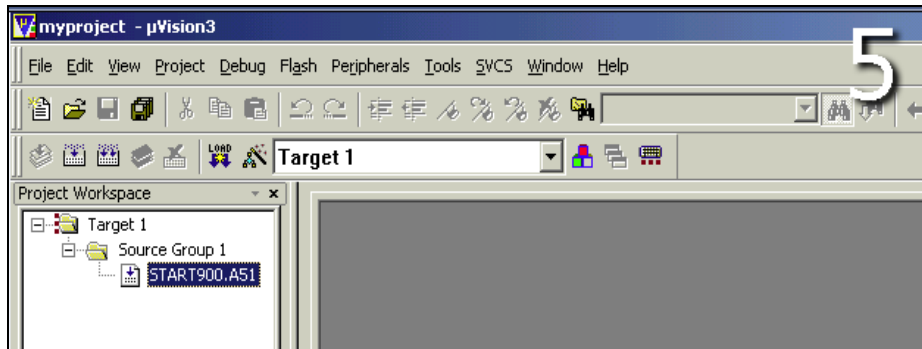
- 3- The next pop-up window will ask for the microcontroller you want to program. Browse among the vendors' names and find to select the microcontroller you are interested. Then click "OK"



- 4- The final pop-up box will ask if you want to Keil μ Vision to copy your microcontroller's startup code files to your project folder and include it to your project as part of your source code. Click "Yes".

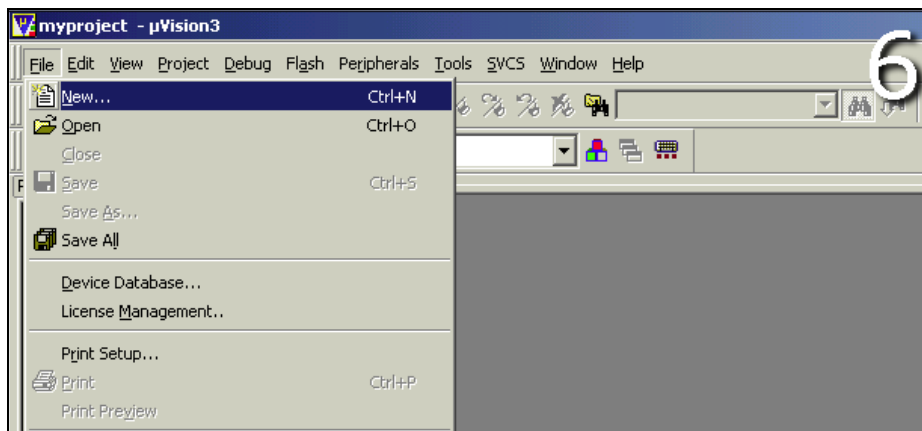


- 5- You can see in your "Project Workspace" section that a startup code named like "Start900.A51" is added. Note that this section only shows codes that are incorporated to your project, not all the files inside your project folder.



II- Starting to Write the C Code and Incorporating it

- 1- Next you want to start writing a new or copying your existed C based code for the project. Click on the "File" button on the top bar and select "New..." menu item.



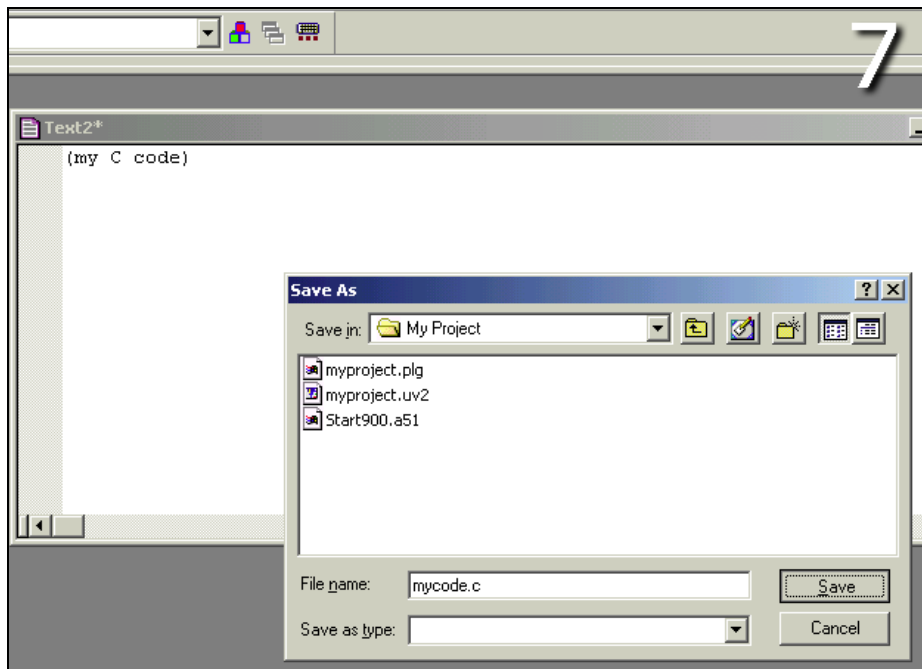
2- When you click “**N**ew...” a usual text editor window will appear in the main program window.

- a. Write a new C code or copy your existing ones inside the text editor.
- b. Make sure you include your microcontroller’s special register function identifier list file and other relevant “.h” files in the beginning of your code.

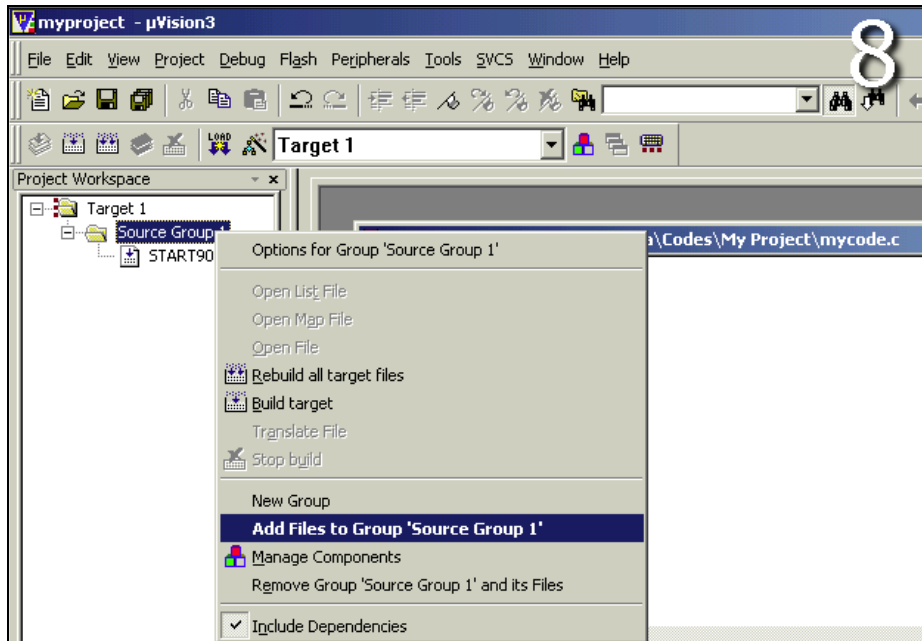
Example:

```
#include <reg938.h>
#include <stdio.h>
```

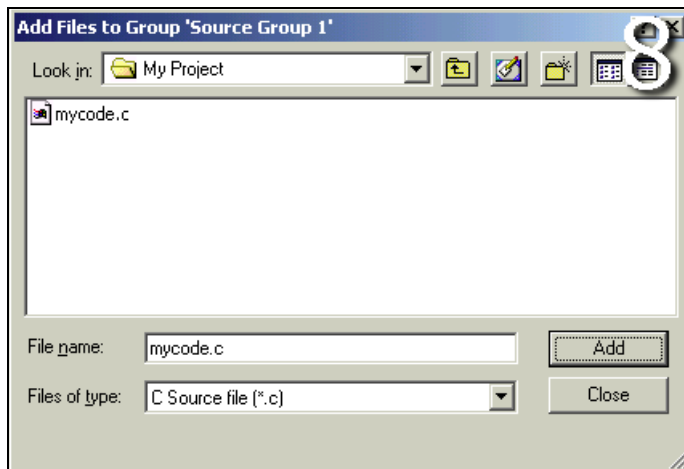
- c. After you are satisfied with your code, click on the “**F**ile” button on the top bar again and select “**S**ave **A**s...” menu item.
- d. Then type the name of your choosing for the code. Make sure you include the extension “.c” after the code name. The file should be saved where your main project file i.e. “.uv2” resides.



- 3- Next you need to incorporate your ".c" file into your project like the startup code which was incorporated when you first created the project. In your "Project Workspace" section on the left you will notice a folder tree structure. Browse and right click to the "Source Group 1" folder and select "Add Files to Group 'Source Group 1'" menu item.

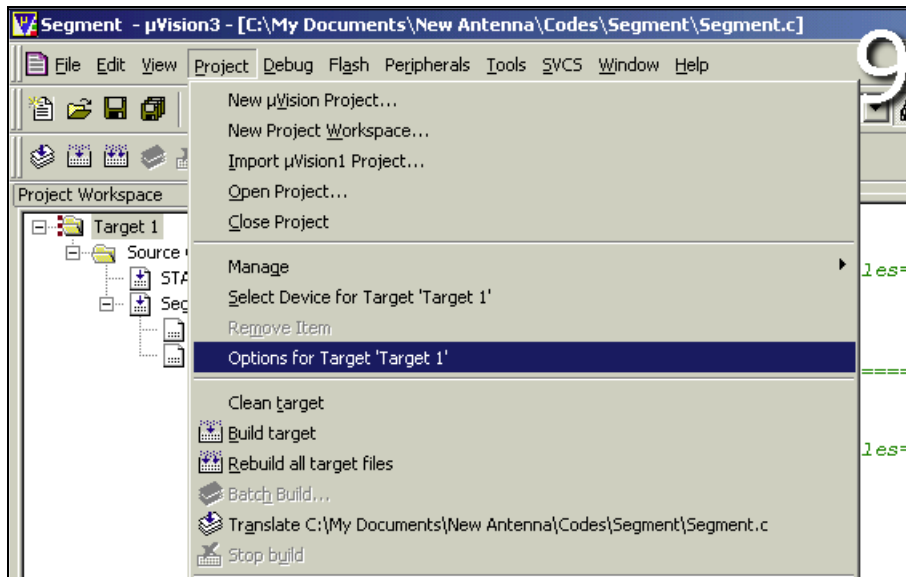


- 4- Choose the ".c" code you wish to be incorporated and click "Add".



III- Compiling the Project

- 1- In order to compile the project correctly, some parameters have to be entered correctly. Click on the “**Project**” button on the top bar and select “**Options for Target ‘Target 1’**” menu item. Note that the name “**Target 1**” is a default name which can be different depending on your project. Name of the project in this case is “**Segment**”.



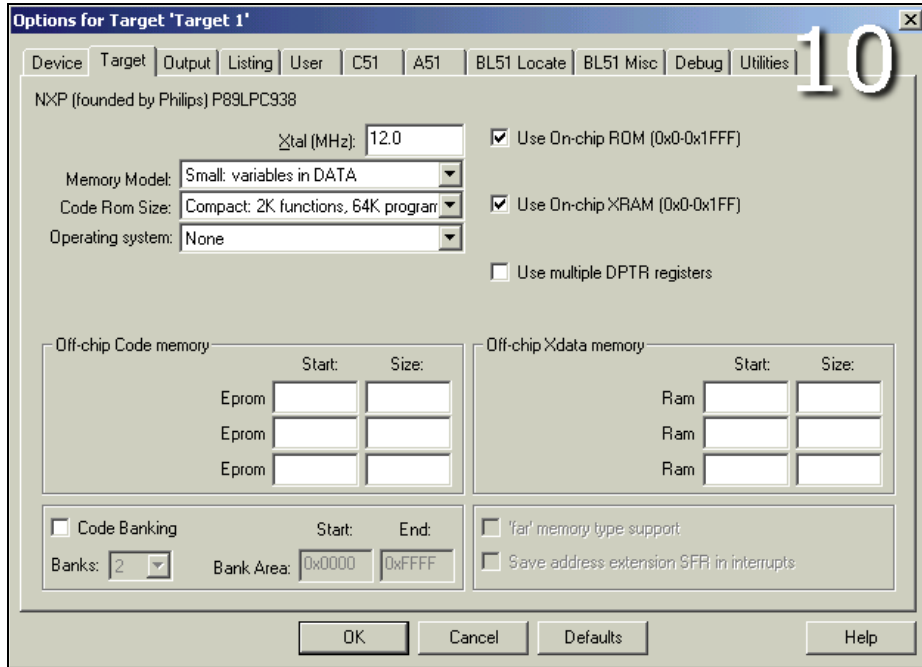
- 2- After clicking, a pop-up window with many tabs will appear. The first tab is the “**Device**” tab. You can check that tab if the correct microcontroller is selected, which you choose when you first created the project. The other tabs we are interested in are:
 - **Target**
 - **Output**
 - **Utilities**

The other tabs can be left as default.

In the “**Target**” tab, make sure that:

“ Xtal(MHz) ”	= 12.0
“ Memory Model ”	= Small: variables in DATA
“ Code Rom Size ”	= Compact: 2K functions, 64K program
“ Operating System ”	= None

Also “**Use On-chip Rom**” and “**Use On-chip XRAM**” should be checked.



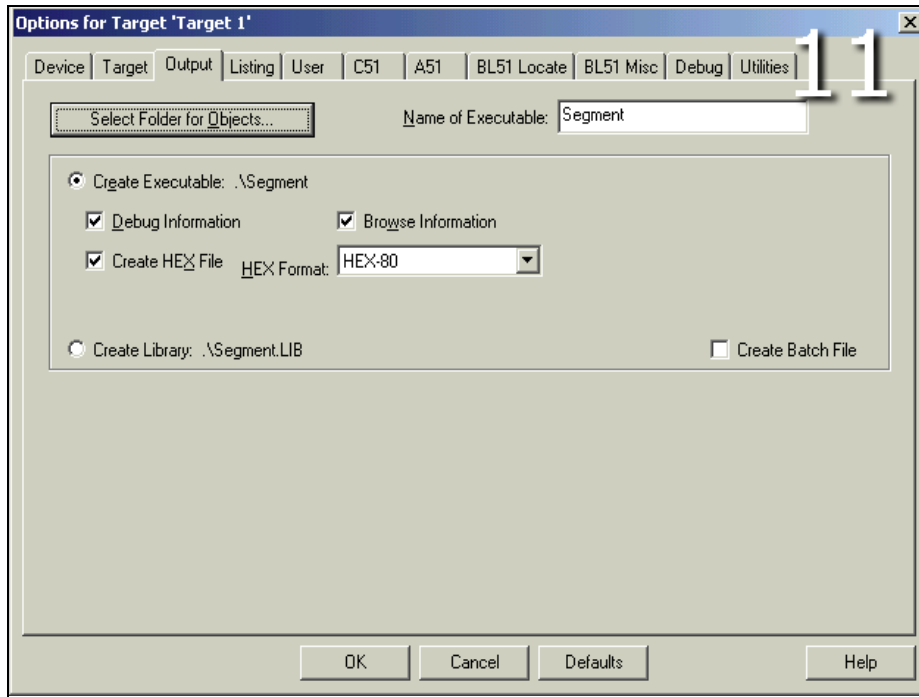
3- Then click on the “Output” tab.

In the “Name of the Executable” input field, enter the name of your choosing for the output “.hex” file, which will be downloaded into the microcontroller.

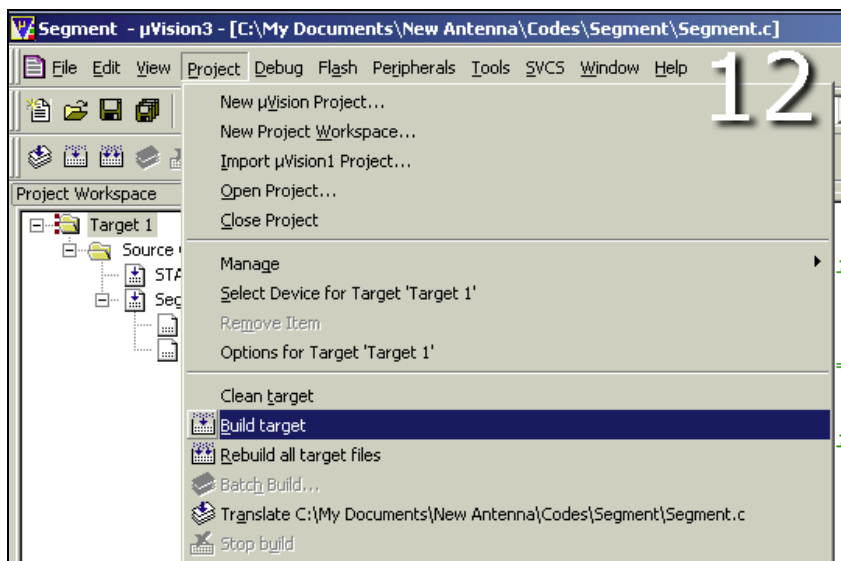
Then make sure the following radio buttons and checkboxes are marked as selected:

- “Create Executable”
- “Debug Information”
- “Browse Information”
- “Create HEX File”

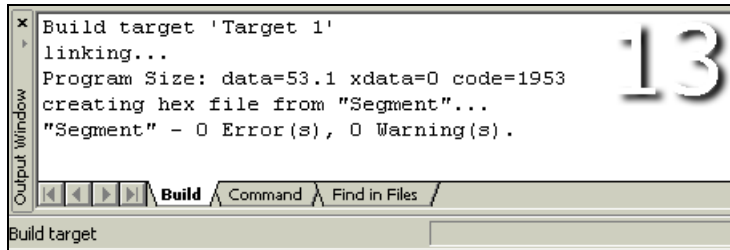
Also make sure that the “HEX Format” is “HEX-80”. (See the screenshot on the next page)



- 4- As far as compiling is concerned the last tab “Utilities” is not relevant. So click “OK” to close the window. To start compiling click on the “Project” button on the top bar and select “Build target” menu item.

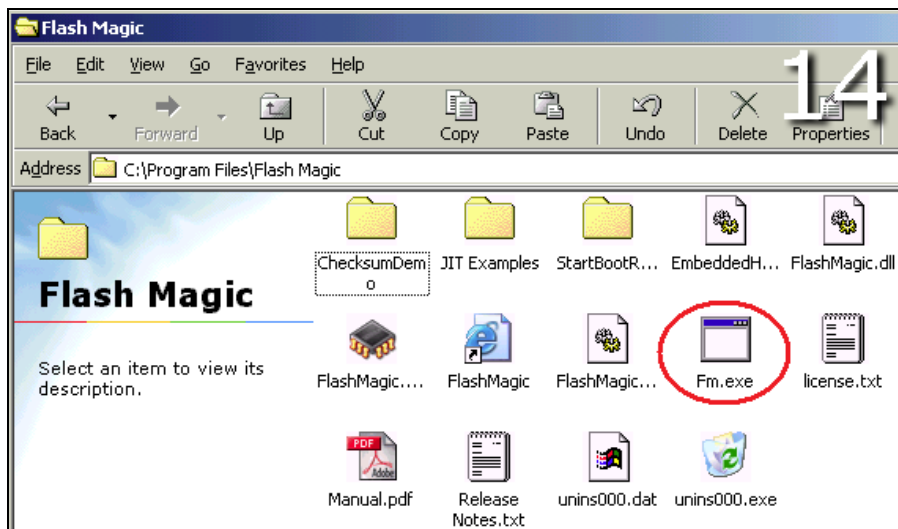


- 5- At this point you should see compilation messages at the bottom in the "Output Window" of Keil μ Vision. Check if the messages include any errors or warnings about your code. If there aren't, the compilation (creation of ".hex" file) is completed.



IV- Downloading program to the Microcontroller

- 1- To download the project to the microcontroller after compiling you need to have software called "FlashMagic" installed in your computer. You can download the latest version from <http://www.flashmagictool.com/>
- 2- Keil μ Vision uses the "FlashMagic" software as an external source to download the compiled ".hex" file into the microcontroller. You can do the downloading just using the Flashmagic's own graphical user interface (by executing "FlashMagic.exe"). But it is recommended to use μ Vision if you are unsure of the specific downloading parameters. Keil μ Vision uses Flashmagic as an intermediary via the "Fm.exe". You will need to provide the path of that executable file in Keil μ Vision next.



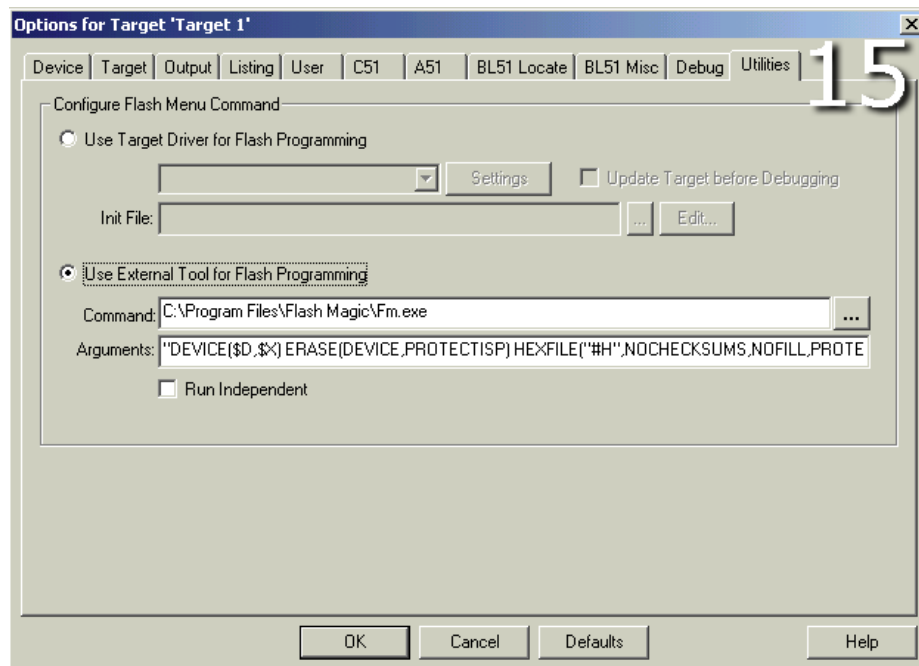
- 3- Now return to the Keil μ Vision; click on the “Project” button on the top bar and select “Options for Target ‘Target 1’” menu item again. When the options windows appears, go straight to the “Utilities” tab. Select the radio button saying “Use External Tool Flash Programming”. In the “Command” input field, enter the path of the “FlashMagic” software you installed. In this case the path is:

C:\Program Files\Flash Magic\Fm.exe

Now for the “Arguments” input field, enter the following line:

```
"DEVICE($D,$X) ERASE(DEVICE,PROTECTISP)  
HEXFILE("#H",NOCHECKSUMS,NOFILL,PROTECTISP) COM(2,9600) HARDWARE(KEILMCB900)"
```

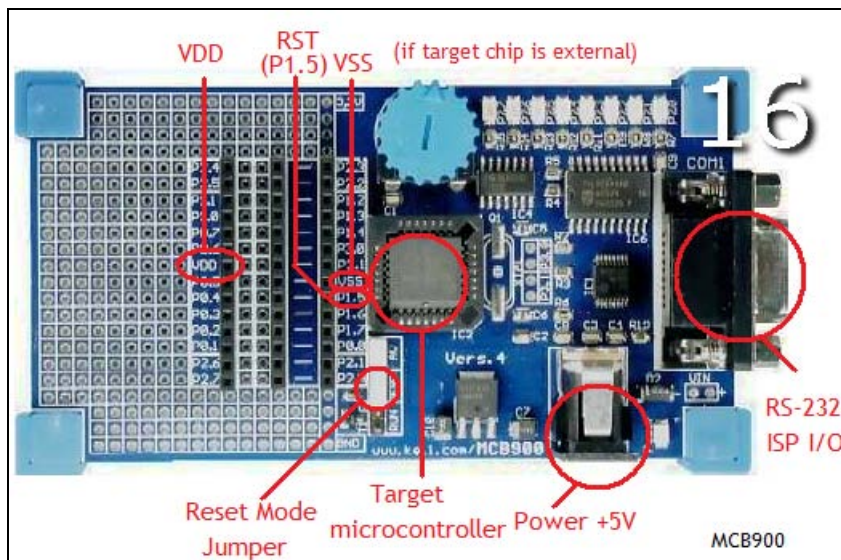
Notice the code fragment “[...]COM(2,9600)[...]”. This indicates that the download is going to be through COM port 2 with a baud rate of 9600bps. If you plan to use another COM port, change the number accordingly. Next click “OK” to close the options window.



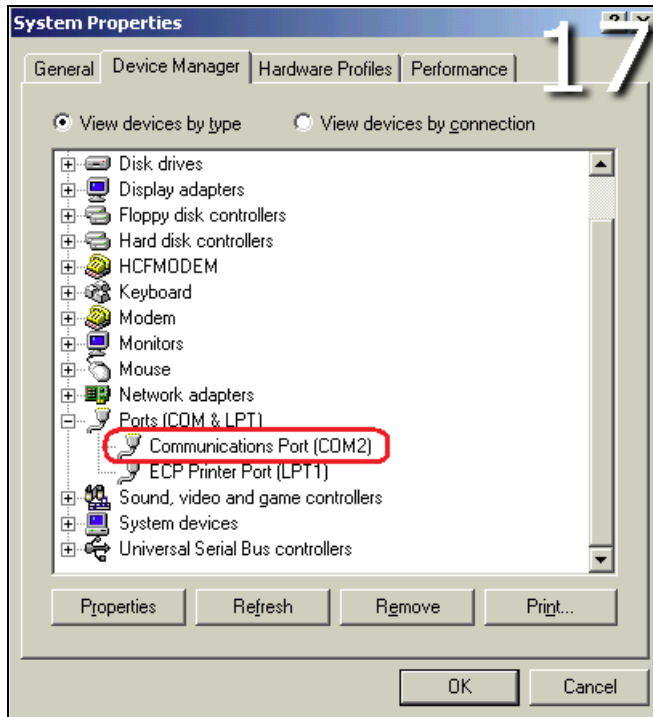
4- Now before starting to download, make sure that:

- The evaluation board (MCB900) is getting at least 5 Volts (max 9V) and 150mA (the shining red LED does guarantee appropriate power supply).
- The evaluation board is in reset mode, meaning that the jumper is in the middle (bridging the 3rd and 4th pins).
- The microcontroller (P89LPC938) is appropriately placed into the evaluation board's PLCC socket. If the microcontroller is externally connected, make sure its "RST" (P1.5), "VDD" and "VSS" pins are wired to the evaluation board's corresponding pins.
- The evaluation board is properly connected to the PC via a RS-232 serial cable. Check if your serial connection is assigned to the correct COM port number, which you specified in the "Arguments" input field in Keil μ Vision options window.

If you need more information about the MCB900 evaluation board, go to the URL: <http://www.keil.com/support/man/docs/mcb900/>

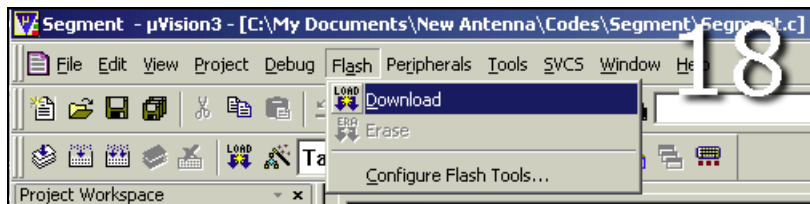


- 5- You can generally see which COM ports are active in Windows by inspecting the “Device Manager” window. It is usually reachable through the control panel.
If your computer does not have a COM port, there exist USB-Serial adapters you can buy which will act as a COM port.



- 6- To start downloading click on the “Flash” button on the top bar and select “Download” menu item. A few seconds later the program should be downloaded. When the process is completed, you will see a message at the “Output Window” saying:

```
Erase complete (DEVICE)  
Hex file programming complete
```



Appendix K

Technology Readiness Levels

- The following page defines a set of technology readiness levels that is applicable to our project.
- There are other definitions but the most used ones created by NASA and DOD.
- The following set of definitions are based on from NASA's TRL guide [31]
- The following page is taken from the *Los Alamos National Laboratory* web site. http://www.lanl.gov/orgs/tt/arpa-e/pdf/TRL_definitions.pdf

Definition Of Technology Readiness Levels

TRL 1 Basic principles observed and reported: Transition from scientific research to applied research. Essential characteristics and behaviors of systems and architectures. Descriptive tools are mathematical formulations or algorithms.

TRL 2 Technology concept and/or application formulated: Applied research. Theory and scientific principles are focused on specific application area to define the concept. Characteristics of the application are described. Analytical tools are developed for simulation or analysis of the application.

TRL 3 Analytical and experimental critical function and/or characteristic proof-of-concept: Proof of concept validation. Active Research and Development (R&D) is initiated with analytical and laboratory studies. Demonstration of technical feasibility using breadboard or brassboard implementations that are exercised with representative data.

TRL 4 Component/subsystem validation in laboratory environment: Standalone prototyping implementation and test. Integration of technology elements. Experiments with full-scale problems or data sets.

TRL 5 System/subsystem/component validation in relevant environment: Thorough testing of prototyping in representative environment. Basic technology elements integrated with reasonably realistic supporting elements. Prototyping implementations conform to target environment and interfaces.

TRL 6 System/subsystem model or prototyping demonstration in a relevant end-to-end environment (ground or space): Prototyping implementations on full-scale realistic problems. Partially integrated with existing systems. Limited documentation available. Engineering feasibility fully demonstrated in actual system application.

TRL 7 System prototyping demonstration in an operational environment (ground or space): System prototyping demonstration in operational environment. System is at or near scale of the operational system, with most functions available for demonstration and test. Well integrated with collateral and ancillary systems. Limited documentation available.

TRL 8 Actual system completed and "mission qualified" through test and demonstration in an operational environment (ground or space): End of system development. Fully integrated with operational hardware and software systems. Most user documentation, training documentation, and maintenance documentation completed. All functionality tested in simulated and operational scenarios. Verification and Validation (V&V) completed.

TRL 9 Actual system "mission proven" through successful mission operations (ground or space): Fully integrated with operational hardware/software systems. Actual system has been thoroughly demonstrated and tested in its operational environment. All documentation completed. Successful operational experience. Sustaining engineering support in place.

Vita

Alican Demir was born in Istanbul, Turkey on May 11, 1984. In 2007 he received his B.S. degree in Mechanical Engineering with a robotics concentration from the Johns Hopkins University Whiting School of Engineering, where he also started his MSE program, at Baltimore, Maryland. During his undergraduate and graduate studies he received the Provost Undergraduate Research Award in 2006, the ASME Senior Design Award in 2007 and the Creel Family Teaching Assistant Award in 2008. Since 2004, he has been working with the Locomotion in Mechanical and Biological Systems (LIMBS) Laboratory, where he developed a keen interest in bio-inspired robotics. Alican intends to stay in the field both as a researcher and developer whether it is in industry or academia.